Fall 2018

Thermodynamically Consistent Hydrodynamic Phase Field Models and Numerical Approximation for Multi-Component Compressible Viscous Fluid Mixtures

Xueping Zhao
University of South Carolina - Columbia

Thermodynamically Consistent Hydrodynamic Phase Field Models and Numerical Approximation for Multi-Component Compressible Viscous Fluid Mixtures

by

Xueping Zhao

Bachelor of Science
Qufu Normal University 2010

Master of Science
Nankai University 2013

Submitted in Partial Fulfillment of the Requirements

for the Degree of Doctor of Philosophy in

Mathematics

College of Arts and Sciences

University of South Carolina

2018

Accepted by:

Qi Wang, Major Professor

Xiaofeng Yang, Committee Member

Xinfeng Liu, Committee Member

Yi Sun, Committee Member

Guiren Wang, Committee Member

Cheryl L. Addy, Vice Provost and Dean of the Graduate School

Dedication

This dissertation is dedicated to my parents.

Acknowledgments

I would like to express my sincere gratitude to my adviser Dr. Qi Wang, who has guided me through the transition from classroom to research. His guidance helped me in all the time of research and writing of this thesis. I could not have imagined having a better advisor and mentor for my Ph.D study.

I also would like to thank Dr. Yi Sun, Dr. Xinfeng Liu, Dr. Xiaofeng Yang, and Dr. Guiren Wang for volunteering their time to be on my Dissertation Committee, also for their insightful comments and encouragement.

My sincere thanks also goes to USC Math faculty, fellow graduate students, and the staff. Together, we had a lot of fun in the last five years and went through all the ups and downs in both life and research.

Last but not the least, I would like to thank my parents Yongxi Zhao and Lanrong Zhao, and my husband Zhiping Mao for supporting and guiding me to become better and better in both life and work.

Abstract

Material systems comprising of multi-component, some of which are compressible, are ubiquitous in nature and industrial applications. In the compressible fluid flow, the material compressibility comes from two sources. One is the material compressibility itself and another is the mass-generating source. For example, the compressibility in the binary fluid flows of non-hydrocarbon (e.g. Carbon dioxide) and hydrocarbons encountered in the enhanced oil recovery (EOR) process, comes from the compressibility of the gas-liquid mixture itself. Another example of the mixture of compressible fluids is growing tissue, in which cell proliferation and cell migration make the material volume changes so that it cannot be described as incompressible.

We present a systematic derivation of thermodynamically consistent hydrodynamic phase field models for compressible viscous fluid mixtures using the generalized Onsager principle along with the one fluid multi-component formulation. By maintaining momentum conservation while enforcing mass conservation at different levels, we obtain two compressible models. When the fluid components in the mixture are incompressible, we show that one compressible model reduces to the quasi-incompressible model via a Lagrange multiplier approach. Several different approaches to arriving at the quasi-incompressible model are discussed. Then, we conduct a linear stability analysis on all the binary models derived in the thesis and show the differences of the models in near equilibrium dynamics.

We present a linear, second order fully discrete numerical scheme on a staggered grid for a thermodynamically consistent hydrodynamic phase field model of binary compressible flows of fluid mixtures derived from the generalized Onsager Principle.

The hydrodynamic model not only possesses the variational structure, but also warrants the mass, linear momentum conservation as well as energy dissipation. We first reformulate the model in an equivalent form using the energy quadratization method and then discretize the reformulated model to obtain a semi-discrete partial differential equation system using the Crank-Nicolson method in time. The numerical scheme so derived preserves the mass conservation and energy dissipation law at the semi-discrete level. Then, we discretize the semi-discrete PDE system on a staggered grid in space to arrive at a fully discrete scheme using the 2nd order finite difference method, which respects a discrete energy dissipation law. We prove the unique solvability of the linear system resulting from the fully discrete scheme. Mesh refinements are presented to show the convergence property of the new scheme.

In the compressible polymer mixtures, we first construct a Flory-Huggins type of free energy and explore the phase separation phenomena due to spinodal decomposition. We investigate the phase separation with and without hydrodynamics, respectively. It tells us that hydrodynamics indeed changes local densities, the path of phase evolution and even the final energy steady states of fluid mixtures. This is alarming, indicating that hydrodynamic effects are instrumental in determining the correct spatial phase diagram for the binary fluid mixture.

Finally, we study the interface dynamics and investigate the mass adsorption phenomena of one component at the interface, to show the performance of our model and the numerical scheme in simulating hydrodynamics of the hydrocarbon mixtures.

Table of Contents

List of Tables

List of Figures

Chapter 1

Introduction

1.1 Flows of fluid mixtures

Compressible flows of fluid mixtures

Material systems comprising of multi-components, some of which are compressible while others are incompressible, are ubiquitous in nature and industrial applications. The compressibility of the materials come from two sources. One is the volume changes of the materials themselves, such as the gases. Another is the mass-generating/loss processes, such as cell proliferation and apoptosis in tissues, and chemical reactions which produce new constituents in the system.

Studying the properties of compressible materials can help one to improve the yield and quantity of the products in industry, and solve problems in biological systems. For example, in the enhanced oil recovery (EOR) process, gas injection offers considerable potential benefits to oil recovery and is attracting the most new market interest since 1972. Properties (viscosity, density profiles et al.) of multi-component compressible mixtures of non-hydrocarbons and hydrocarbons have been studied by a number of investigators [13, 37, 45]. In developing tissues or cancerous tumors, cell proliferation and apoptosis introduce the fluidization and compressibility of the system [30, 49]. Studying the properties of the compressible tissues could provide us insights for the underlying mechanisms and treatment methods for challenging diseases.

Quasi-incompressible and incompressible flows of fluid mixtures

In some fluid mixtures, when each fluid component is incompressible with a constant specific density, the fluid mixture may not be incompressible when the densities are not equal. This fluid mixture was named a quasi-incompressible fluid and its thermodynamically consistent model has been derived and applied to various multi-phase fluid flows [25, 26, 35, 41]. The fluid mixture is truly incompressible only when all the fluid components are of the same specific density.

1.2 Mathematical models for flows of fluid mixtures

Models for multi-phase and multi-component materials

There are two general approaches to describe multi-phase and multi-component materials. One uses multi-fluid formulation to describe the density and velocity for each phase explicitly [4,16,22,23,27,28]. Another one uses an average velocity [33,62], normally the mass average velocity, together with chemical potentials to describe kinematics for each phase or component. In the latter approach, the average velocity is a measurable hydrodynamic quantity in fluids. For this reason, we choose this approach to formulate our phase field model for multi-phase and multi-component fluid flows.

Sharp interface models versus diffuse interface models

For interfacial dynamics problems, there are two kinds of mathematical models totally. One is the classical sharp interface approach, which requires an explicit tracking of interfaces during their evolution, such as grow, migrate and change topology. The surface tracking can be demanding and needs automatic adaptive mesh gener-

ation to trace the large or rapid shape modifications. As an alternative, methods that regularize the interface, such as level-set method, phase field approach (diffuse interface model), have been highly successful in treating deforming interfaces. Phase field model is a kind of physically motivated level set methods [63], which utilize a set of partial differential equations to describe the evolution of the whole system, thus avoiding the explicit treatment of the boundary conditions at the interface.

For immiscible fluid mixtures, sharp interface models and phase field models can both be used to describe fluid motions. While for miscible fluid mixtures, sharp interface models are no longer applicable. So, the phase field model becomes a primary platform to describe the fluid motion in the mixture.

Phase field models

Phase field method has been used successfully to formulate models for fluid mixtures in many applications like in life sciences [51, 52, 59, 65, 75] (cell biology [32, 43, 51, 69, 76, 77], biofilms [64–66], cell adhesion and motility [8, 39, 43, 44, 51], cell membrane [2, 21, 57, 60], tumor growth [59]), materials science [3, 7, 9], fluid dynamics [18, 40, 41, 56, 73], image processing [6, 36], etc. The most widely studied phase field model for binary fluid mixtures is the one for fluid mixtures of two incompressible fluids of identical densities [1, 38]. While modeling binary fluid mixtures using phase field models, one commonly uses a labeling or a phase variable (a volume fraction or a mass fraction) ϕ to distinguish between distinct material phases. For instance $\phi = 1$ indicates one fluid phase while $\phi = 0$ denotes the other fluid phase in the binary fluid mixture. For fluid mixtures, the interfacial region is tracked by $0 < \phi < 1$. A transport equation for the phase variable ϕ along with the conservation equations of momentum, the continuity equation together with necessary constitutive equations constitute the governing system of equations for the binary fluid mixture.

In the compressible fluid flow, we use the mass density ρ_i or molar density n_i in place of volume fraction ϕ_i $(i = 1, 2)$, to represent the distribution of each compressible component in the fluid mixture. In general, the transport equation for the mass density of each component is given by

$$\frac{\partial \rho_i}{\partial t} + \nabla \cdot (\rho_i \mathbf{v}_i) = j_i, \qquad i = 1, \cdots, N, \tag{1.2.1}$$

or

$$\frac{\partial n_i}{\partial t} + \nabla \cdot (n_i \mathbf{v}_i) = j_i, \qquad i = 1, \cdots, N, \tag{1.2.2}$$

where $\mathbf{v}_i$ is the velocity of the ith component, j_i is the mass source or molar source of the ith component. The transport equations for the mass or molar densities along with the conservation laws of mass and momentum constitute the governing equations of the hydrodynamic phase field models of the compressible fluid mixtures.

Non-Equilibrium Thermodynamics

Historically, there have been several theoretical frameworks for one to derive thermodynamical and hydrodynamical models for time dependent dynamics. The generalized Onsager principle, consisting of the Onsager linear response theory and positive entropy production rule [46,47], is the one we adopt in this thesis. The Onsager maximum entropy production principle based on the Onsager-Machlup action potential is another approach to deriving models for Hamiltonian and dissipative systems [17,46]. The Hamilton least action principle is a classical one for Hamiltonian or conservative systems. The Hamilton-Rayleigh principle is another incarnation of the Onsager maximum entropy principle [4, 16, 22, 23, 27, 28]. There is also a more elaborate approach to develop a general equation for the non-equilibrium reversible-irreversible coupling (abbreviated as GENERIC) for non-equilibrium theories [5,14,15,29]. These

formulations share the commonality in that the non-equilibrium models have a unified mathematical structure consisting of a reversible (hyperbolic) and irreversible (parabolic, dissipative) component in the evolutionary equations. Some of these equations represent conservation laws for the material system such as mass, momentum and energy conservation while others serve as constitutive equations pertinent to the material properties of the material system that the equations describe. The different methods may differ however in how they handle the boundary conditions as well as if one use the dissipation functional or the mobility (or the friction coefficient) to derive the constitutive equations.

The models in this thesis

Distinguishing properties of the compressible hydrodynamic phase field models include that the density of each compressible material component is a variable, the mass average velocity of the fluid flow is most likely not solenoidal, and the pressure is determined by the equation of state or the free energy of the mixture system (at least in the isothermal case). In [41], Truskinovsky and Lowengrub derived the Navier−Stokes−Cahn−Hilliard (NSCH) system for a binary mixture of two incompressible fluid flows with unmatched densities in the fluid components, in which the mass concentration of one fluid component in the binary fluid flow is used as the phase variable. They termed the hydrodynamic phase field model quasi-incompressible. In [33, 34], Sun et al. propose a general diffuse interface model with a given equation of state (e.g. Peng-Robinson equation of state) to describe the multi-component fluid flow based on the principles of the NVT-based framework.

In this thesis, we formulate the hydrodynamic phase field model for compressible fluid of N-fluid components ($N > 1$) using the one fluid multi-component formulation [5]. We derive thermodynamically consistent compressible phase field model for

multi-component fluid mixtures systematically through a variational approach coupled with the generalized Onsager principle [62]. As it is already demonstrated that hydrodynamic models obeys conservation laws do not necessarily satisfy the second law of thermodynamics if the constitutive equations are not derived in a thermodynamically consistent way. The second law or equivalently the Onsager entropy production requirement is thus an additional condition that a well-posed model should satisfy to ensure its well-posedness mathematically. It does not yield additional governing equations for the model. Instead, it does impose an additional constraint on the model and dictates how entropy is produced during the transient dynamical process when the system approaches the steady state.

In this thesis, we first derive two classes hydrodynamic phase field models for compressible fluid mixtures using the Onsager principle. After we obtain the "general" compressible models for multi-component fluid mixtures, we hierarchically impose additional "conservation" and/or "incompressibility" conditions to the material system to arrive at constrained, quasi-incompressible theories to show the hierarchical relationship between the compressible model and the constrained models for multi-component fluid mixtures. Through this systematic approach, we demonstrate how one can derive constrained theories via a Lagrange multiplier approach coupled with the generalized Onsager principle, extending the method applied to single phase materials to multi-component material mixtures in the context of one fluid multi-component framework. In the more general compressible model, we enforce global mass conservation so that the model can be used to describe material systems undergoing mass conversion among different components. We then study near equilibrium dynamics of the general models and their various limits through a linear stability analysis. Note that we derive the models for viscous fluid components in this thesis. However, this approach can be readily extended to complex fluids to account for viscoelastic effects induced by mesoscopic structures in the complex fluid [62].

1.3 Energy stable numerical schemes

The hydrodynamic phase field model is nonlinear, exemplified in its free energy, mobility coefficients and the advection in the transport equations. Higher order approximation, unconditional energy stability as well as computational efficiency are desired properties to attain in developing its numerical approximation. To preserve the energy dissipation property, several time-marching approaches have been developed in the past: convex splitting method [10, 12, 19, 20], stabilization method [54, 74], and energy quadratization (EQ, including SAV) approach [26,26,68,71].The convex splitting method has been used to obtain a series of first order energy stable schemes for various PDE models exhibiting energy dissipation properties. However, the convex-splitting scheme is usually nonlinear and therefore can be expensive to solve from time to time. On the other hand, even though it is possible to construct a second order convex splitting scheme in some cases, it was usually done on a case by case basis and a general formulation is not yet available. The stabilization method is another method for obtaining energy stable numerical approximations, which is equivalent to a convex splitting method in some cases. By adding a linear, stablizing operator in the order of the truncation error, one can obtain an energy stable algorithm. In general, a second order stabilizing scheme can be derived, it preserves the discrete energy decay but not the dissipation rate. The energy quadratization(EQ), also known as the invariant energy quadratization(IEQ), method was proposed recently [61] and well developed in various gradient flows and hydrodynamic phase field models [26, 68, 71]. By introducing intermediate variables, one can rewrite the nonlinear free energy functional into a quadratic from, from which a linear second order or even higher order numerical scheme can be constructed [24, 67, 70].

Recently, Sun et al. [33, 34] used the convex splitting approach and the scalar auxiliary variable method [55], which is developed based on the EQ strategy, to solve binary compressible hydrodynamic phase field models, respectively. They obtained

some first order semi-discrete schemes. In this thesis, we develop a linear, second order, fully discrete numerical scheme for the hydrodynamic phase field model for binary fluid mixtures based on the energy quadratization strategy. We will show that this scheme is unconditionally energy stable and the linear system resulting from the second order numerical scheme is uniquely solvable. At each time step, the linear algebraic system is solved with a linear pre-conditioner. Two examples on phase separation dynamics in viscous polymeric blends and interface evolution in gas-liquid mixtures are presented to show the usefulness of the new scheme in some practical applications.

1.4 A brief review of the thesis

The thesis is organized as follows. In Chapter 2, we firstly formulate two classes of hydrodynamic phase field models for the fluid mixture of compressible fluids with different mass conservation constraints. Then, via the Lagrange Multiplier approach, we reduce the compressible model with local total mass conservation law into a quasi-incompressible model for the fluid mixture of two incompressible fluids. In addition, we generalize the derivation to fluid mixtures of N components. The non-dimensionalization of the models is carried out correspondingly. In Chapter 3, we discuss near-equilibrium dynamics of the models using a linear stability analysis. In Chapter 4, we reformulate the model using the energy quadratization method. The fully discrete numerical scheme, where we use second order finite difference in space and "linearized" Crank-Nicolson method in time, is given in where the unique solvability of the scheme and the property of energy dissipation are proved as well. In Chapter 5, 6, we show several numerical experiments that validate the accuracy, stability and efficiency of the numerical scheme. We give concluding remarks in Chapter 7.

Chapter 2

A general framework of hydrodynamic phase field models for compressible viscous fluid flows

2.1 Hydrodynamic phase field models for binary fluid flows

We present a systematic derivation of thermodynamically consistent hydrodynamic phase field models for binary compressible fluid flows with respect to various conditions on mass conservation and incompressibility following the generalized Onsager principle [62].

2.1.1 Compressible model with the global mass conservation law

We first consider a mixture of two compressible viscous fluids with density and velocity pairs $(\rho_1, \mathbf{v}_1)$ and $(\rho_2, \mathbf{v}_2)$, respectively. We define the total mass of the fluid mixture as $\rho = \rho_1 + \rho_2$ and the mass average velocity as $\mathbf{v} = \frac{1}{\rho}(\rho_1\mathbf{v}_1 + \rho_2\mathbf{v}_2)$. We allow the mass of fluid components to change via conversion, generation, or annihilation at specified rates. In this general framework, the mass balance equation for each fluid component is given respectively by

$$\frac{\partial \rho_i}{\partial t} + \nabla \cdot (\rho_i \mathbf{v}_i) = r_i, \quad i = 1, 2, \tag{2.1.1}$$

where r_i is the mass conversion/generation/annihilation rate for the ith component. The corresponding momentum conservation equations are given by

$$\frac{\partial (\rho_i \mathbf{v}_i)}{\partial t} + \nabla \cdot (\rho_i \mathbf{v}_i \mathbf{v}_i) = \nabla \cdot \sigma_i + \mathbf{F}_{i,e} + r_i \mathbf{v}_i, \quad i = 1, 2, \tag{2.1.2}$$

where σ_i is the viscous stress of the ith fluid component, $\mathbf{F}_{i,e}$ the extra force of the ith fluid component including the friction force between different fluid components and some elastic forces, and $r_i\mathbf{v}_i$ the force due to mass conversion/generation/annihilation in the ith fluid component.

We rewrite the mass conservation equations using the average velocity as follows

$$\frac{\partial \rho_i}{\partial t} + \nabla \cdot (\rho_i \mathbf{v}) = j_i, \quad i = 1, 2, \tag{2.1.3}$$

where $j_i = \nabla \cdot (\rho_i(\mathbf{v} - \mathbf{v}_i)) + r_i$ is the excessive production rate of the ith fluid component.

If we add the mass balance equations (2.1.3) and linear momentum equations (2.1.2) of all the components, respectively, we obtain the total mass balance equation and total linear momentum balance equation as follows

$$\begin{aligned} &\frac{\partial \rho}{\partial t} + \nabla \cdot (\rho \mathbf{v}) = \textstyle\sum_{i=1}^{2} j_i = \sum_{i=1}^{2} r_i, \\ &\frac{\partial (\rho \mathbf{v})}{\partial t} + \nabla \cdot (\rho \mathbf{v}\mathbf{v}) = \nabla \cdot \sigma^s + \mathbf{F}_e, \end{aligned} \tag{2.1.4}$$

where $\mathbf{F}_e = \sum_{i=1}^{i=2}(\mathbf{F}_{i,e} + r_i\mathbf{v}_i)$ and $\sigma^s = \sum_{i=1}^{i=2}(\sigma_i - \rho_i(\mathbf{v}_i - \mathbf{v})(\mathbf{v}_i - \mathbf{v}))$ is the stress tensor. The angular momentum balance implies the symmetry of σ^s. All j_i, i=1, 2, σ^s and $\mathbf{F}_e$ will be determined later through constitutive relations.

We assume the free energy of the system is given by

$$F = \textstyle\int_V f(\rho_1, \rho_2, \nabla\rho_1, \nabla\rho_2) d\mathbf{x}, \tag{2.1.5}$$

where f the free energy density function and V the domain in which the fluid mixture occupies. The total mechanical energy of the system is given by

$$E_{total} = \textstyle\int_V [\frac{1}{2}\rho||\mathbf{v}||^2 + f] d\mathbf{x}. \tag{2.1.6}$$

We next calculate the total energy dissipation rate as follows.

$$\begin{aligned} &\tfrac{dE_{total}}{dt} = \textstyle\int_V [-\sigma^s : \mathbf{D} + (\mathbf{F}_e + \rho_1\nabla\mu_1 + \rho_2\nabla\mu_2 - \frac{1}{2}(j_1 + j_2)\mathbf{v}) \cdot \mathbf{v} \\ &+\mu_1(j_1) + \mu_2(j_2)] d\mathbf{x} + \textstyle\int_{\partial V} [(\sigma^s \cdot \mathbf{v}) - \frac{1}{2}(\rho\mathbf{v}\|\mathbf{v}\|^2) \\ &+(-\mu_1\rho_1\mathbf{v} - \mu_2\rho_2\mathbf{v} + \tfrac{\partial f}{\partial(\nabla\rho_1)}\tfrac{\partial \rho_1}{\partial t} + \tfrac{\partial f}{\partial(\nabla\rho_2)}\tfrac{\partial \rho_2}{\partial t})] \cdot \mathbf{n} dS. \end{aligned} \tag{2.1.7}$$

where $\mu_1 = \frac{\partial f}{\partial \rho_1} - \nabla \cdot \frac{\partial f}{\partial \nabla \rho_1}$, $\mu_2 = \frac{\partial f}{\partial \rho_2} - \nabla \cdot \frac{\partial f}{\partial \nabla \rho_2}$ are the chemical potentials with respect to ρ_1 and ρ_2, respectively, $\mathbf{D} = \frac{1}{2}(\nabla \mathbf{v} + \nabla \mathbf{v}^T)$ is the rate of strain tensor. We define the elastic force as

$$\mathbf{F}_e = -\rho_1 \nabla \mu_1 - \rho_2 \nabla \mu_2 + \tfrac{1}{2}(j_1 + j_2)\mathbf{v}. \tag{2.1.8}$$

This force does not contribute to the energy dissipation.

Using the Onsager principle, we propose

$$\begin{aligned} \sigma^s &= 2\eta \mathbf{D} + \nu tr(\mathbf{D})\mathbf{I}, \\ \begin{pmatrix} j_1 \\ j_2 \end{pmatrix} &= -\mathcal{M} \begin{pmatrix} \mu_1 \\ \mu_2 \end{pmatrix}, \end{aligned} \tag{2.1.9}$$

where η, ν are mass-average shear and volumetric viscosities, respectively, and $\mathcal{M}$ is an operator. The bulk energy dissipation rate reduces to

$$\tfrac{dE_{total}}{dt} = -\int_V [2\eta \mathbf{D} : \mathbf{D} + \nu tr(\mathbf{D})^2 + (\mu_1, \mu_2) \cdot \mathcal{M} \cdot (\mu_1, \mu_2)] d\mathbf{x}. \tag{2.1.10}$$

It is non-positive definite provided $\mathcal{M}$ is nonnegative definite and η, ν are non-negative. The constitutive relation gives a general compressible model for binary fluid flows.

In practice, the interesting scenarios are the following two:

1. $\int_V \sum_{i=1}^2 r_i = 0$; so, $\int_V \sum_{i=1}^2 j_i = 0$.

2. $r_i = 0, i = 1, 2$; so, $\sum_{i=1}^2 j_i = 0$.

The first condition yields the compressible model of global mass conservation law while the second one gives the compressible model of local mass conservation law. For the first case, a special choice of the mobility operator is the following

$$\begin{aligned} j_1 &= \nabla \cdot M_{11} \nabla \mu_1 + \nabla \cdot M_{12} \nabla \mu_2, \\ j_2 &= \nabla \cdot M_{21} \nabla \mu_1 + \nabla \cdot M_{22} \nabla \mu_2, \end{aligned} \tag{2.1.11}$$

where $M_{ij}, i, j = 1, 2$ are mobility coefficients. If we set

$$\mathbf{v}|_{\partial V} = 0, \qquad \mathbf{n} \cdot \frac{\partial f}{\partial(\nabla \rho_1)}|_{\partial V} = 0, \qquad \mathbf{n} \cdot \frac{\partial f}{\partial(\nabla \rho_2)}|_{\partial V} = 0, \tag{2.1.12}$$

on the boundary of the domain V, the surface terms vanish in the energy dissipation functional so that the energy dissipation rate reduces to

$$\frac{dE_{total}}{dt} = -\int_V [2\eta \mathbf{D} : \mathbf{D} + \nu tr(\mathbf{D})^2 + (\nabla \mu_1, \nabla \mu_2) \cdot \mathbf{M} \cdot (\nabla \mu_1, \nabla \mu_2)] d\mathbf{x}, \tag{2.1.13}$$

where $\mathbf{M} = (M_{ij})$. It is non-positive definite provided $\eta, \nu \geq 0$ and $\mathbf{M}$ is non-negative definite.

We summarize the governing system of equations in the hydrodynamic model for binary compressible fluids with a global mass conservation law as follows:

$$\begin{cases} \frac{\partial \rho_1}{\partial t} + \nabla \cdot (\rho_1 \mathbf{v}) = j_1 = \nabla \cdot M_{11} \cdot \nabla \mu_1 + \nabla \cdot M_{12} \cdot \nabla \mu_2, \\ \frac{\partial \rho_2}{\partial t} + \nabla \cdot (\rho_2 \mathbf{v}) = j_2 = \nabla \cdot M_{21} \cdot \nabla \mu_1 + \nabla \cdot M_{22} \cdot \nabla \mu_2, \\ \frac{\partial (\rho \mathbf{v})}{\partial t} + \nabla \cdot (\rho \mathbf{v}\mathbf{v}) - \frac{1}{2}(j_1 + j_2)\mathbf{v} = 2\nabla \cdot (\eta \mathbf{D}) + \nabla(\nu \nabla \cdot \mathbf{v}) \\ -\rho_1 \nabla \mu_1 - \rho_2 \nabla \mu_2. \end{cases} \tag{2.1.14}$$

We denote the shear viscosities of the fluid component 1 and 2 as η_1, η_2, and the volumetric viscosities of the two components as ν_1, ν_2, respectively. There are several options of defining average viscosity coefficients in the binary model.

- Viscosity coefficients are interpolated using mass fractions and given by

$$\eta = \frac{\rho_1}{\rho}\eta_1 + \frac{\rho_2}{\rho}\eta_2, \qquad \nu = \frac{\rho_1}{\rho}\nu_1 + \frac{\rho_2}{\rho}\nu_2. \tag{2.1.15}$$

- Viscosity coefficients are interpolated through volume fractions ϕ and $(1 - \phi)$ in quasi-incompressible models (presented later) and given by

$$\eta = \phi\eta_1 + (1 - \phi)\eta_2, \qquad \nu = \phi\nu_1 + (1 - \phi)\nu_2, \tag{2.1.16}$$

  where ϕ is the volume fraction of fluid 1.

- By the Krieger-Dougherty law, the shear viscosity η exhibits a strong non-linear dependence on the local solute concentration and is given by

$$\eta(x) = \eta_0(1-x)^{-\nu}, \tag{2.1.17}$$

in which x is the solute concentration (ρ_1 or ρ_2 in this model), η_0 is the viscosity of the pure solvent. For example in mixtures of CO_2 and n-decane, the solvent is n-decane and solute is CO_2. The volumetric viscosity is obtained analogously.

As a customary approximation, we assume the free energy density function f is composed of the conformational entropy, and the bulk energy h as follows

$$\begin{aligned} &f(\rho_1, \rho_2, \nabla\rho_1, \nabla\rho_2) = h(\rho_1, \rho_2, T) \\ &+\tfrac{1}{2}(\kappa_{\rho_1\rho_1}(\nabla\rho_1)^2 + 2\kappa_{\rho_1\rho_2}(\nabla\rho_1, \nabla\rho_2) + \kappa_{\rho_2\rho_2}(\nabla\rho_2)^2). \end{aligned} \tag{2.1.18}$$

where T is the absolute temperature, $h(\rho_1, \rho_2, T)$ is the homogeneous bulk free energy density function, $\kappa_{\rho_1\rho_1}, \kappa_{\rho_1\rho_2}$ and $\kappa_{\rho_2\rho_2}$ are parameters parameterizing the conformational entropy, which are all functions of T. For example, for the partially miscible binary fluid mixture of n-decane and CO_2, where n-decane is denoted as fluid 1 and CO_2 as fluid 2, the Peng-Robinson bulk free energy density is defined by the following

$$\begin{aligned} &h(\rho_1, \rho_2, T) = \tfrac{r_m\rho_1+\rho_2}{m_2}\varphi(T) - \tfrac{r_m\rho_1+\rho_2}{m_2}RTln(\tfrac{m_2}{r_m\rho_1+\rho_2} - b) - \\ &\tfrac{r_m\rho_1+\rho_2}{m_2}\tfrac{a}{2\sqrt{2}b}ln[\tfrac{m_2+(r_m\rho_1+\rho_2)b(1+\sqrt{2})}{m_2+(r_m\rho_1+\rho_2)b(1-\sqrt{2})}] \\ &+\tfrac{r_m\rho_1+\rho_2}{m_2}RT[\tfrac{r_m\rho_1}{r_m\rho_1+\rho_2}ln\tfrac{r_m\rho_1}{r_m\rho_1+\rho_2} + \tfrac{\rho_2}{r_m\rho_1+\rho_2}ln\tfrac{\rho_2}{r_m\rho_1+\rho_2}]. \end{aligned} \tag{2.1.19}$$

where R is the ideal gas constant, $\varphi(T) = -RT(1 - log(\lambda^3))$ is a temperature-dependent function, λ is the thermal wavelength of a massive particle, m_i is the molar mass of component i for $i = 1, 2$, respectively, $r_m = m_2/m_1$ is the ratio of the molar mass of carbon dioxide m_2 to the molar mass of n-decane m_1, $b(\rho_1, \rho_2)$ is a volume parameter and $a(\rho_1, \rho_2, T)$ is an interaction parameter. This free energy was proposed to extend that of the Van der Waals' to describe the deviation away from the ideal gas model.

Another example of the bulk free energy density for polymeric liquids is given by the Flory-Huggins mixing energy density

$$h(\rho_1, \rho_2, T) = \frac{k_B T}{m}[\frac{\rho_1}{N_1} ln \frac{\rho_1}{\rho} + \frac{\rho_2}{N_2} ln \frac{\rho_2}{\rho} + \chi \frac{\rho_1 \rho_2}{\rho}], \tag{2.1.20}$$

where m is the mass of an average molecule in the mixture and $N_{1,2}$ are two polymerization indices.

Notice that $j_i, i = 1, 2$ in (2.1.14) are obtained from the constitutive equation and if $\sum_{i=1}^{2} j_i \neq 0$, this model does not necessarily conserve mass locally. However, $\int_V (\rho_1 + \rho_2) d\mathbf{x}$ is a constant. So, the mass of the system is conserved globally. This model describes a binary viscous compressible fluid systems in which mass is conserved globally but not locally. In this model, the exact physical meaning of the velocity is lost due to the lack of local mass conservation. It is no long a mass average velocity! Therefore, what does the momentum equation stands for becomes fuzzy physically. The applicability of this model needs to be scrutinized further. A more general model can be built from (2.1.9) by specifying a more general mobility operator $\mathcal{M}$. However, we will not pursue it in this study.

Next, we impose the local mass conservation constraint to arrive at the model that conserves mass locally.

2.1.2 Compressible model with local mass conservation law

If $j_1 + j_2 = 0$, the total mass of the system is conserved locally, i.e.,

$$\frac{\partial \rho}{\partial t} + \nabla \cdot (\rho \mathbf{v}) = 0, \tag{2.1.21}$$

which imposes an constraint on the mass fluxes:

$$\sum_{i=1}^{2} \sum_{j=1}^{2} \nabla \cdot M_{ij} \cdot \nabla \mu_j = 0. \tag{2.1.22}$$

We obtain the governing system of equations for the compressible fluid mixture as follows

$$\begin{cases} \frac{\partial \rho}{\partial t} + \nabla \cdot (\rho \mathbf{v}) = 0, \\ \frac{\partial \rho_i}{\partial t} + \nabla \cdot (\rho_i \mathbf{v}) = \nabla \cdot M_{i1} \cdot \nabla \mu_1 + \nabla \cdot M_{i2} \cdot \nabla \mu_2, \quad i = 1, 2, \\ \frac{\partial (\rho \mathbf{v})}{\partial t} + \nabla \cdot (\rho \mathbf{v}\mathbf{v}) = 2\nabla \cdot (\eta \mathbf{D}) + \nabla(\nu \nabla \cdot \mathbf{v}) - \sum_{i=1}^{2} \rho_i \nabla \mu_i. \end{cases} \tag{2.1.23}$$

Notice that we could have used ρ, ρ_1 as the fundamental variables in the derivation of the thermodynamic model in lieu of ρ_1 and ρ_2 since $\rho = \rho_1 + \rho_2$. With these variables, we reformulate the free energy density function

$$\begin{aligned} &f(\rho_1, \rho_2, \nabla \rho_1, \nabla \rho_2) = f(\rho_1, \rho - \rho_1, \nabla \rho_1, \nabla(\rho - \rho_1)) = \tilde{f}(\rho_1, \rho, \nabla \rho_1, \nabla \rho) \\ &= \tilde{h}(\rho_1, \rho, T) + \tfrac{1}{2}(\tilde{\kappa}_{\rho_1 \rho_1}(\nabla \rho_1)^2 + 2\tilde{\kappa}_{\rho \rho_1}(\nabla \rho, \nabla \rho_1) + \tilde{\kappa}_{\rho \rho}(\nabla \rho)^2), \end{aligned} \tag{2.1.24}$$

where $\tilde{\kappa}_{\rho_1 \rho_1} = \kappa_{\rho_1 \rho_1} + \kappa_{\rho_2 \rho_2} - 2\kappa_{\rho_1 \rho_2}, \tilde{\kappa}_{\rho \rho_1} = \kappa_{\rho_1 \rho_2} - \kappa_{\rho_2 \rho_2}$, and $\tilde{\kappa}_{\rho \rho} = \kappa_{\rho_2 \rho_2}$, where $\kappa_{\rho_1 \rho_1}, \kappa_{\rho_1 \rho_2}, \kappa_{\rho_2 \rho_2}$ are the coefficients of the gradient terms in free energy (2.1.18). The corresponding chemical potentials are given by

$$\begin{aligned} &\tilde{\mu}_1 = \tfrac{\delta \tilde{f}}{\delta \rho_1} = \tfrac{\delta f}{\delta \rho_1} + \tfrac{\delta f}{\delta \rho_2} \tfrac{\partial \rho_2}{\partial \rho_1} = \mu_1 - \mu_2, \qquad \tilde{\mu} = \tfrac{\delta \tilde{f}}{\delta \rho} = \tfrac{\delta f}{\delta \rho_2} \tfrac{\partial \rho_2}{\partial \rho} = \mu_2. \\ &\mu_1 = \tilde{\mu}_1 + \tilde{\mu}, \qquad \mu_2 = \tilde{\mu}. \end{aligned} \tag{2.1.25}$$

System ((2.1.23)) reduces to

$$\begin{cases} \frac{\partial \rho}{\partial t} + \nabla \cdot (\rho \mathbf{v}) = 0, \\ \frac{\partial \rho_1}{\partial t} + \nabla \cdot (\rho_1 \mathbf{v}) = \nabla \cdot [M_{11} \cdot \nabla \tilde{\mu}_1 + (M_{11} + M_{12}) \cdot \nabla \tilde{\mu}], \\ \frac{\partial (\rho \mathbf{v})}{\partial t} + \nabla \cdot (\rho \mathbf{v}\mathbf{v}) = 2\nabla \cdot (\eta \mathbf{D}) + \nabla(\nu \nabla \cdot \mathbf{v}) - \rho_1 \nabla \tilde{\mu}_1 - \rho \nabla \tilde{\mu}. \end{cases} \tag{2.1.26}$$

If we assign

$$M_{12} = M_{21} = -M_{11}, \quad M_{22} = M_{11}, \tag{2.1.27}$$

system (2.1.23) reduces further to a special model

$$\begin{cases} \frac{\partial \rho}{\partial t} + \nabla \cdot (\rho \mathbf{v}) = 0, \\ \frac{\partial \rho_1}{\partial t} + \nabla \cdot (\rho_1 \mathbf{v}) = \nabla \cdot M_{11} \cdot \nabla \tilde{\mu}_1, \\ \frac{\partial (\rho \mathbf{v})}{\partial t} + \nabla \cdot (\rho \mathbf{v}\mathbf{v}) = 2\nabla \cdot (\eta \mathbf{D}) + \nabla(\nu \nabla \cdot \mathbf{v}) - \rho_1 \nabla \tilde{\mu}_1 - \rho \nabla \tilde{\mu}. \end{cases} \tag{2.1.28}$$

This is a special model for compressible binary fluid mixtures among infinitely many choices in the mobility matrix. Apparently, model (2.1.26) is more general.

The boundary conditions at a solid boundary are given by (2.1.12) except that the last one is replaced by $\mathbf{n} \cdot \frac{\partial f}{\partial \nabla \rho} = 0$ equivalently when ρ is used as a fundamental variable. The energy dissipation rate of the special model reduces to

$$\frac{dE_{total}}{dt} = -\int_V [2\eta \mathbf{D} : \mathbf{D} + \nu tr(\mathbf{D})^2 + \tilde{\mu}_1 M_{11} \tilde{\mu}_1] d\mathbf{x} \leq 0, \tag{2.1.29}$$

provided $\eta, \nu \geq 0$ and $M_{11} > 0$. This is a compressible binary fluid model that respects mass and momentum conservation. For the more general model (2.1.26), the energy dissipation property is warranted so long as the mobility matrix $\mathbf{M}$ is non-negative definite. So, this class of models is thermodynamically consistent.

We next show how this (special) model reduces to another class of compressible models when the two fluid components are incompressible, known as the quasi-incompressible model [35, 41]. For the more general compressible with a local mass conservation law, an analogous result can be obtained.

2.1.3 Quasi-incompressible model

When the fluid mixture is consisted of two incompressible viscous fluid components, where the specific densities $\hat{\rho}_1$ and $\hat{\rho}_2$ are constants, we denote the volume fraction of fluid component 1 as ϕ and the other by $1 - \phi$. Then, the densities of the two fluids in the mixture are given as follows

$$\rho_1 = \phi \hat{\rho}_1, \quad \rho_2 = (1 - \phi)\hat{\rho}_2. \tag{2.1.30}$$

The total density of the fluid mixture is given by

$$\rho = \phi \hat{\rho}_1 + (1 - \phi)\hat{\rho}_2. \tag{2.1.31}$$

If we use ρ_1 as a fundamental physical variable, ρ is represented by ρ_1 as follows,

$$\rho = \rho_1 + (1 - \frac{\rho_1}{\hat{\rho}_1})\hat{\rho}_2 = \hat{\rho}_2 + (1 - \frac{\hat{\rho}_2}{\hat{\rho}_1})\rho_1. \tag{2.1.32}$$

This means that the two variables ρ and ρ_1 are related linearly in this fluid mixture system. We view this as a special case of the fully compressible model subject to constraint (2.1.32). To accommodate the constraint, we augment the free energy density by $\pi(\hat{\rho}_2 + (1 - \frac{\hat{\rho}_2}{\hat{\rho}_1})\rho_1 - \rho)$, where π is a Lagrange multiplier. We denote the modified free energy density function as $\hat{f}$,

$$\hat{f} = \tilde{f}(\rho_1, \nabla\rho_1, \rho, \nabla\rho) + \pi[\hat{\rho}_2 + (1 - \frac{\hat{\rho}_2}{\hat{\rho}_1})\rho_1 - \rho]. \tag{2.1.33}$$

The corresponding chemical potentials and their relations to the chemical potentials in the compressible model are given as follows

$$\begin{aligned} &\hat{\mu}_1 = \frac{\delta\hat{f}}{\delta\rho_1} = \tilde{\mu}_1 + \pi(1 - \frac{\hat{\rho}_2}{\hat{\rho}_1}), \quad \hat{\mu} = \frac{\delta\hat{f}}{\delta\rho} = \tilde{\mu} - \pi, \quad \tilde{\mu}_1 = \frac{\delta\tilde{f}}{\delta\rho_1}|_\rho, \\ &\tilde{\mu} = \frac{\delta\tilde{f}}{\delta\rho}|_{\rho_1}, \quad \mu_\phi = \frac{\delta\hat{f}}{\delta\rho_1}|_\rho \frac{\delta\rho_1}{\delta\phi} + \frac{\delta\hat{f}}{\delta\rho}|_{\rho_1} \frac{\delta\rho}{\delta\phi} = \hat{\rho}_1\hat{\mu}_1 + (\hat{\rho}_1 - \hat{\rho}_2)\hat{\mu}. \end{aligned} \tag{2.1.34}$$

From the mass conservation of the mixture system (2.1.28)-1, we have

$$(\hat{\rho}_1 - \hat{\rho}_2)[\frac{\partial\phi}{\partial t} + \nabla\cdot(\phi\mathbf{v})] + \hat{\rho}_2\nabla\cdot\mathbf{v} = 0. \tag{2.1.35}$$

The transport equation of ρ_1 is rewritten into

$$\frac{\partial\phi}{\partial t} + \nabla\cdot(\phi\mathbf{v}) = \frac{1}{\hat{\rho}_1}(\nabla\cdot M_{11}\cdot\nabla)(\hat{\mu_1}). \tag{2.1.36}$$

The linear momentum conservation equation is rewritten into

$$\rho(\frac{\partial\mathbf{v}}{\partial t} + \mathbf{v}\cdot\nabla\mathbf{v}) = \nabla\cdot(2\eta\mathbf{D}) + \nabla(\nu\nabla\cdot\mathbf{v}) - \nabla\Pi - \phi\nabla\mu_\phi, \tag{2.1.37}$$

where η, ν are volume averaged viscosity coefficients and the hydrostatic pressure is defined by

$$\Pi = \hat{\rho}_2(\tilde{\mu} - \pi). \tag{2.1.38}$$

With this definition, the transport equation (2.1.36) for ϕ is written into

$$\frac{\partial\phi}{\partial t} + \nabla\cdot(\phi\mathbf{v}) = \frac{1}{\hat{\rho}_1^2}(\nabla\cdot M_{11}\cdot\nabla)(\mu_\phi + \Pi(1 - \frac{\hat{\rho}_1}{\hat{\rho}_2})). \tag{2.1.39}$$

Combining the mass conservation law (2.1.35) and transport equation (2.1.39) of the ϕ, we obtain

$$\nabla \cdot \mathbf{v} = (1 - \frac{\hat{\rho}_1}{\hat{\rho}_2})\frac{1}{\hat{\rho}_1^2}(\nabla \cdot M_{11} \cdot \nabla)(\mu_\phi + \Pi(1 - \frac{\hat{\rho}_1}{\hat{\rho}_2})). \tag{2.1.40}$$

We summarize the governing equations of the quasi-incompressible model as follows

$$\begin{cases} \nabla \cdot \mathbf{v} = (1 - \frac{\hat{\rho}_1}{\hat{\rho}_2})\frac{1}{\hat{\rho}_1^2}(\nabla \cdot M_{11} \cdot \nabla)(\mu_\phi + \Pi(1 - \frac{\hat{\rho}_1}{\hat{\rho}_2})), \\ \frac{\partial \phi}{\partial t} + \nabla \cdot (\phi \mathbf{v}) = \frac{1}{\hat{\rho}_1^2}(\nabla \cdot M_{11} \cdot \nabla)(\mu_\phi + \Pi(1 - \frac{\hat{\rho}_1}{\hat{\rho}_2})), \\ \rho[\frac{\partial \mathbf{v}}{\partial t} + \mathbf{v} \cdot \nabla \mathbf{v}] = \nabla \cdot (2\eta \mathbf{D}) + \nabla(\nu \nabla \cdot \mathbf{v}) - \nabla \Pi - \phi \nabla \mu_\phi. \end{cases} \tag{2.1.41}$$

The free energy density reduces to

$$\begin{aligned} &\tilde{f}(\rho_1, \rho, \nabla \rho_1, \nabla \rho) = \tilde{h}(\hat{\rho}_1 \phi, \hat{\rho}_1 \phi + \hat{\rho}_2(1 - \phi), T) \\ &+\frac{1}{2}(\tilde{\kappa}_{\rho_1 \rho_1}(\nabla \rho_1)^2 + 2\tilde{\kappa}_{\rho_1 \rho}(\nabla \rho_1, \nabla \rho) + \tilde{\kappa}_{\rho \rho}(\nabla \rho)^2) \\ &= \hat{h}(\phi) + \frac{1}{2}\hat{\kappa}_{\phi\phi}\|\nabla \phi\|^2, \end{aligned} \tag{2.1.42}$$

where $\hat{h}(\phi) = \tilde{h}(\hat{\rho}_1 \phi, (\hat{\rho}_1 - \hat{\rho}_2)\phi + \hat{\rho}_2, T)$, $\hat{\kappa}_{\phi\phi} = \tilde{\kappa}_{\rho_1 \rho_1}\hat{\rho}_1{}^2 + 2\tilde{\kappa}_{\rho_1 \rho}\hat{\rho}_1(\hat{\rho}_1 - \hat{\rho}_2) + \tilde{\kappa}_{\rho\rho}(\hat{\rho}_1 - \hat{\rho}_2)^2$. This is the equation system for quasi-incompressible binary fluids obtained in [35]. The upshot of the derivation shows that we can obtain the constrained theory from the unconstrained theory by augmenting the free energy with the algebraic constraint via a Lagrange multiplier.

The energy dissipation rate of the binary quasi-incompressible fluid flow (2.1.41) is given by

$$\frac{dE_{total}}{dt} = -\int_V [2\eta \mathbf{D} : \mathbf{D} + \nu tr(\mathbf{D})^2 + \nabla \hat{\mu}_1 \cdot M_{11} \cdot \nabla \hat{\mu}_1] d\mathbf{x} \leq 0, \tag{2.1.43}$$

provided $\eta, \nu \geq 0$, $M_{11} > 0$, where $\hat{\mu}_1 = \frac{1}{\hat{\rho}_1}(\mu_\phi + \Pi(1 - \frac{\hat{\rho}_1}{\hat{\rho}_2}))$.

When $\hat{\rho}_1 = \hat{\rho}_2 = \rho$, the system reduces to an incompressible model

$$\begin{cases} \nabla \cdot \mathbf{v} = 0, \\ \frac{\partial \phi}{\partial t} + \nabla \cdot (\phi \mathbf{v}) = \frac{1}{\rho^2}(\nabla \cdot M_{11} \cdot \nabla)\mu_\phi, \\ \rho[\frac{\partial \mathbf{v}}{\partial t} + \mathbf{v} \cdot \nabla \mathbf{v}] = \nabla \cdot (2\eta \mathbf{D}) + \nabla(\nu \nabla \cdot \mathbf{v}) - \nabla \Pi - \phi \nabla \mu_\phi. \end{cases} \tag{2.1.44}$$

This is the incompressible model derived by Halperin et al [31].

These derivations can be readily extended to account for multi-component fluid systems.

2.2 Hydrodynamic phase Field Models for N-component Multiphase Compressible Fluid Flows

When fluid mixtures are composed of N fluid components, we use $\rho_i, i = 1, 2, \cdots, N$ to denote the mass density of the ith component and assume the free energy of the fluid mixture is given by

$$F = \int_\Omega f(\rho_1, \nabla\rho_1, \cdots, \rho_N, \nabla\rho_N) d\mathbf{x}, \tag{2.2.1}$$

where f is the free energy density. The derivation of the hydrodynamic phase field models follows the procedures alluded to in the previous section. We present the results next.

2.2.1 Compressible model with the global mass conservation law

We choose $\rho_1, \cdots, \rho_N$ as the primitive variables. Following the procedure outlined in the previous section, we obtain the governing system of equations for the N-component multi-phase viscous fluid mixture as follows

$$\begin{cases} \frac{\partial \rho_i}{\partial t} + \nabla \cdot (\rho_i \mathbf{v}) = j_i = \sum_{j=1}^N \nabla \cdot M_{ij} \cdot \nabla \mu_j, \quad i = 1, 2, \cdots, N, \\ \frac{\partial (\rho \mathbf{v})}{\partial t} + \nabla \cdot (\rho \mathbf{v}\mathbf{v}) - \frac{1}{2}(\sum_{i=1}^N j_i)\mathbf{v} = 2\nabla \cdot (\eta \mathbf{D}) + \nabla(\nu \nabla \cdot \mathbf{v}) - \sum_{i=1}^N \rho_i \nabla \mu_i, \end{cases} \tag{2.2.2}$$

where M_{ij}, i, j = 1, ..., N, are the mobility coefficients, and $\eta = \sum_{i=1}^N \eta_i \frac{\rho_i}{\rho}, \nu = \sum_{i=1}^N \nu_i \frac{\rho_i}{\rho}$ are mass-average viscosities, respectively.

The energy dissipation rate is given by

$$\begin{aligned} &\frac{dE_{total}}{dt} = -\int_V [2\eta \mathbf{D} : \mathbf{D} + \nu tr(\mathbf{D})^2 \\ &+ (\nabla\mu_1, \nabla\mu_2, \cdots, \nabla\mu_N) \cdot \mathbf{M} \cdot (\nabla\mu_1, \nabla\mu_2, \cdots, \nabla\mu_N)] d\mathbf{x} \leq 0, \end{aligned} \tag{2.2.3}$$

provided $\eta, \nu \geq 0$, $\mathbf{M} = (M_{ij})_{ij=1}^{N}$ is a symmetric non-negative definite mobility coefficient matrix.

2.2.2 Compressible model with the local mass conservation law

If $\sum_{i=1}^{N} j_i = 0$, the total mass of the system is conserved locally, i.e.,

$$\frac{\partial \rho}{\partial t} + \nabla \cdot (\rho \mathbf{v}) = 0, \tag{2.2.4}$$

We obtain the governing system of equations as follows

$$\begin{cases} \frac{\partial \rho}{\partial t} + \nabla \cdot (\rho \mathbf{v}) = 0, \quad \text{or} \quad \sum_{i=1}^{N} \sum_{j=1}^{N} \nabla \cdot M_{ij} \cdot \nabla \mu_j = 0, \\ \frac{\partial \rho_i}{\partial t} + \nabla \cdot (\rho_i \mathbf{v}) = \sum_{j=1}^{N} \nabla \cdot M_{ij} \cdot \nabla \mu_j, \quad i = 1, 2, \cdots, N, \\ \frac{\partial (\rho \mathbf{v})}{\partial t} + \nabla \cdot (\rho \mathbf{v}\mathbf{v}) = 2\nabla \cdot (\eta \mathbf{D}) + \nabla(\nu \nabla \cdot \mathbf{v}) - \sum_{i=1}^{N} \rho_i \nabla \mu_i, \end{cases} \tag{2.2.5}$$

where η, ν are mass averaged shear and volumetric viscosities, $\mathbf{v}$ is the mass average velocity and $\mathbf{M} = (M_{ij})_{i,j=1}^{N}$ is the symmetric mobility coefficient matrix. In this case, the energy dissipation rate is given by

$$\begin{aligned} &\frac{dE_{total}}{dt} = -\int_V [2\eta \mathbf{D} : \mathbf{D} + \nu tr(\mathbf{D})^2 \\ &+ (\nabla \mu_1, \nabla \mu_2, \cdots, \nabla \mu_N) \cdot \mathbf{M} \cdot (\nabla \mu_1, \nabla \mu_2, \cdots, \nabla \mu_N)] d\mathbf{x} \leq 0, \end{aligned} \tag{2.2.6}$$

provided $\eta, \nu \geq 0$ and $\mathbf{M}$ is a symmetric non-negative definite mobility coefficient matrix subject to constraint $\sum_{i=1}^{N} \sum_{j=1}^{N} \nabla \cdot M_{ij} \cdot \nabla \mu_j = 0$.

Analogously, we choose $\rho_1, \cdots, \rho_{N-1}, \rho$ as the primitive variables, where $\rho = \sum_{i=1}^{N} \rho_i$. Then, we represent $\rho_N = \rho - \sum_{i=1}^{N-1} \rho_i$. The free energy density is written as

$$\begin{aligned} &f(\rho_1, \nabla \rho_1, \cdots, \rho_N, \nabla \rho_N) = f(\rho_1, \nabla \rho_1, \cdots, \rho - \textstyle\sum_{i=1}^{N-1} \rho_i, \nabla(\rho - \sum_{i=1}^{N-1} \rho_i)) \\ &= \tilde{f}(\rho_1, \nabla \rho_1, \cdots, \rho_{N-1}, \nabla \rho), \end{aligned} \tag{2.2.7}$$

The corresponding chemical potentials are given by

$$\begin{aligned} &\tilde{\mu}_i = \frac{\delta \tilde{f}}{\delta \rho_i} = \frac{\delta f}{\delta \rho_i} + \frac{\delta f}{\delta \rho_N} \frac{\delta \rho_N}{\delta \rho_i} = \mu_i - \mu_N, i = 1, \cdots, N-1, \tilde{\mu} = \frac{\delta \tilde{f}}{\delta \rho} = \frac{\delta f}{\delta \rho_N} \frac{\delta \rho_N}{\delta \rho} = \mu_N. \\ &\mu_i = \tilde{\mu}_i + \tilde{\mu}, \mu_N = \tilde{\mu}. \end{aligned} \tag{2.2.8}$$

The transport equation of the densities are given by

$$\frac{\partial \rho_i}{\partial t} + \nabla \cdot (\rho_i \mathbf{v}) = \sum_{j=1}^{N-1} \nabla \cdot M_{ij} \cdot \nabla \tilde{\mu}_j + (\sum_{j=1}^{N} \nabla \cdot M_{ij}) \tilde{\mu}, \quad i = 1, 2, \cdots, N-1. \tag{2.2.9}$$

The mass conservation equation implies

$$\sum_{i=1}^{N} \sum_{j=1}^{N-1} \nabla \cdot M_{ij} \cdot \nabla \tilde{\mu}_j + (\sum_{i,j=1}^{N} \nabla \cdot M_{ij} \cdot \nabla) \tilde{\mu} = 0. \tag{2.2.10}$$

The mobility coefficients must satisfy the above constraint. If we assign

$$M_{iN} = -\sum_{j=1}^{N-1} M_{ij} = M_{Ni}, \quad M_{NN} = -\sum_{i=1}^{N-1} M_{iN} = \sum_{i=1}^{N-1} \sum_{j=1}^{N-1} M_{ij}, \tag{2.2.11}$$

the constraint is satisfied and system (2.2.5) reduces to a special model

$$\begin{cases} \frac{\partial \rho}{\partial t} + \nabla \cdot (\rho \mathbf{v}) = 0, \\ \frac{\partial \rho_i}{\partial t} + \nabla \cdot (\rho_i \mathbf{v}) = \sum_{j=1}^{N-1} \nabla \cdot M_{ij} \cdot \nabla \tilde{\mu}_j, \quad i = 1, 2, \cdots, N-1, \\ \frac{\partial (\rho \mathbf{v})}{\partial t} + \nabla \cdot (\rho \mathbf{v} \mathbf{v}) = 2\nabla \cdot (\eta \mathbf{D}) + \nabla(\nu \nabla \cdot \mathbf{v}) - \sum_{i=1}^{N-1} \rho_i \nabla \tilde{\mu}_i - \rho \nabla \tilde{\mu}. \end{cases} \tag{2.2.12}$$

This is a special model for compressible fluid mixtures of N-components. The energy dissipation rate is given by

$$\begin{aligned} &\frac{dE_{total}}{dt} = -\int_V [2\eta \mathbf{D} : \mathbf{D} + \nu tr(\mathbf{D})^2 \\ &+ (\nabla \tilde{\mu}_1, \nabla \tilde{\mu}_2, \cdots, \nabla \tilde{\mu}_{N-1}) \cdot \mathbf{M} \cdot (\nabla \tilde{\mu}_1, \nabla \tilde{\mu}_2, \cdots, \nabla \tilde{\mu}_{N-1})] d\mathbf{x} \leq 0, \end{aligned} \tag{2.2.13}$$

provided $\eta, \nu \geq 0$ and $\mathbf{M} = (M_{ij})_{i,j=1}^{N-1}$ is a symmetric non-negative definite mobility coefficient matrix.

2.2.3 Quasi-incompressible model

When each of the fluid component is incompressible in the viscous fluid mixture, we denote the volume fraction of the ith component as ϕ_i and specific density as $\hat{\rho}_i$ for $i = 1, \cdots, N$, respectively. Then, $\sum_{i=1}^{N} \phi_i = 1$ and the total mass density in the mixture is given by

$$\rho = \sum_{i=1}^{N} \phi_i \hat{\rho}_i = \sum_{i=1}^{N-1} \phi_i \hat{\rho}_i + (1 - \sum_{i=1}^{N-1} \phi_i) \hat{\rho_N} = \sum_{i=1}^{N-1} \rho_i + (1 - \sum_{i=1}^{N-1} \frac{\rho_i}{\hat{\rho}_i}) \hat{\rho_N}. \tag{2.2.14}$$

We assume the volume fraction of the Noth component is nonzero. Then, the free energy density is a functional of the first $N-1$ volume fractions $(\phi_1, \cdots, \phi_{N-1})$. If we augment the free energy by $\pi(\sum_{i=1}^{N-1}\rho_i + (1-\sum_{i=1}^{N-1}\frac{\rho_i}{\hat{\rho}_i})\hat{\rho_N} - \rho)$, where π is a Lagrange multiplier, then, the modified free energy density function is given by

$$\begin{aligned}\hat{f} &= \tilde{f}(\rho_1, \nabla\rho_1, ..., \rho_{N-1}, \nabla\rho_{N-1}, \rho, \nabla\rho)\\ &+\pi[\textstyle\sum_{i=1}^{N-1}\rho_i + (1-\sum_{i=1}^{N-1}\frac{\rho_i}{\hat{\rho}_i})\hat{\rho_N} - \rho].\end{aligned} \tag{2.2.15}$$

Following the procedure alluded to in the previous section, we derive the following governing system of equations of the quasi-incompressible fluid from the special compressible model as follows

$$\begin{cases}\nabla\cdot\mathbf{v} = \sum_{i=1}^{N-1}\sum_{j=1}^{N-1}(1-\frac{\hat{\rho}_j}{\hat{\rho}_N})\frac{1}{\hat{\rho}_i\hat{\rho}_j}(\nabla\cdot M_{ij}\cdot\nabla)(\mu_{\phi_j} + \Pi(1-\frac{\hat{\rho}_j}{\hat{\rho}_N})),\\ \frac{\partial\phi_i}{\partial t} + \nabla\cdot(\phi_i\mathbf{v}) = \sum_{j=1}^{N-1}\frac{1}{\hat{\rho}_i\hat{\rho}_j}(\nabla\cdot M_{ij}\cdot\nabla)(\mu_{\phi_j} + \Pi(1-\frac{\hat{\rho}_j}{\hat{\rho}_N})),\\ i = 1, 2, \cdots, N-1,\\ \rho[\frac{\partial\mathbf{v}}{\partial t} + \mathbf{v}\cdot\nabla\mathbf{v}] = \nabla\cdot(2\eta\mathbf{D}) + \nabla(\nu\nabla\cdot\mathbf{v}) - \nabla\Pi - \sum_{i=1}^{N-1}\phi_i\nabla\mu_{\phi_i},\end{cases} \tag{2.2.16}$$

where

$$\begin{aligned}&\tilde{\mu}_i = \tfrac{\delta\tilde{f}}{\delta\rho_i}, \quad \tilde{\mu} = \tfrac{\delta\tilde{f}}{\delta\rho},\\ &\hat{\mu}_i = \tilde{\mu}_i + \pi(1-\tfrac{\hat{\rho}_N}{\hat{\rho}_i}), \quad i = 1, \cdots, N-1, \quad \hat{\mu} = \tilde{\mu} - \pi,\\ &\mu_{\phi_i} = \tfrac{\delta\hat{f}}{\delta\phi_i} = \tfrac{\delta\hat{f}}{\delta\rho_i}|_\rho\tfrac{\delta\rho_i}{\delta\phi_i} + \tfrac{\delta\hat{f}}{\delta\rho}|_{\rho_i}\tfrac{\delta\rho}{\delta\phi_i} = \hat{\rho}_i\hat{\mu}_i + (\hat{\rho}_i - \hat{\rho}_N)\hat{\mu},\\ &\Pi = -\hat{\rho}_N\pi + \hat{\rho}_N\mu,\end{aligned} \tag{2.2.17}$$

and Π serves as the hydrostatic pressure.

The energy dissipation rate is

$$\begin{aligned}\tfrac{dE_{total}}{dt} &= -\textstyle\int_V[2\eta\mathbf{D}:\mathbf{D} + \nu tr(\mathbf{D})^2\\ &+(\nabla\hat{\mu}_1, \nabla\hat{\mu}_2, \cdots, \nabla\hat{\mu}_{N-1})\cdot\mathbf{M}\cdot(\nabla\hat{\mu}_1, \nabla\hat{\mu}_2, \cdots, \nabla\hat{\mu}_{N-1})]d\mathbf{x} \le 0,\end{aligned} \tag{2.2.18}$$

provided $\eta, \nu \ge 0$, $\mathbf{M} = (M)_{i,j=1}^{N-1}$ is a symmetric non-negative definite matrix, where $\hat{\mu}_i = \frac{1}{\hat{\rho}_i}[\mu_{\phi_j} + \Pi(1-\frac{\hat{\rho}_j}{\hat{\rho}_N})]$. A more general model can be derived from the general compressible model by enforcing the incompressibility constraint. But, we will not present it here.

For a fluid mixture with $\hat{\rho}_i = \rho$, the system reduces to an incompressible model

$$\begin{cases} \nabla \cdot \mathbf{v} = 0, \\ \frac{\partial \phi_i}{\partial t} + \nabla \cdot (\phi_i \mathbf{v}) = \sum_{j=1}^{N-1} \frac{1}{\rho^2} (\nabla \cdot M_{ij} \cdot \nabla) \mu_{\phi_j}, \quad i = 1, 2, \cdots, N-1, \\ \rho[\frac{\partial \mathbf{v}}{\partial t} + \mathbf{v} \cdot \nabla \mathbf{v}] = \nabla \cdot (2\eta \mathbf{D}) + \nabla(\nu \nabla \cdot \mathbf{v}) - \nabla \Pi - \sum_{i=1}^{N-1} \phi_i \nabla \mu_{\phi_i}. \end{cases} \tag{2.2.19}$$

For phase field models of N components where $N \geq 2$, there exists a second way to derive the quasi-incompressible phase field model. We begin with a fully compressible model of $N+1$ components, each of which is of density $\rho_i, i = 1, \cdots, N$ and ρ. We assume the free energy density depends on $(\rho_1, \cdots, \rho_N, \rho)$. The second approach to derive the quasi-incompressible model is to augment the free energy by $\pi(\sum_{i=1}^{N} \rho_i - \rho) + B(\sum_{i=1}^{N} \frac{\rho_i}{\hat{\rho}_i} - 1)$, where π and B are two Lagrange multipliers. We define the modified free energy density function by

$$\hat{f} = f(\rho_1, \nabla \rho_1, \cdots, \rho_N, \nabla \rho_N) + \pi(\sum_{i=1}^{N} \rho_i - \rho) + B(\sum_{i=1}^{N} \frac{\rho_i}{\hat{\rho}_i} - 1). \tag{2.2.20}$$

The chemical potentials are given by

$$\begin{aligned} &\hat{\mu}_i = \frac{\delta \hat{f}}{\delta \rho_i} = \frac{\delta f}{\delta \rho_i} + \frac{1}{\hat{\rho}_i} B + \pi = \mu_i + \frac{1}{\hat{\rho}_i} B + \pi, \quad i = 1, \cdots, N, \\ &\hat{\mu} = \frac{\delta \hat{f}}{\delta \rho} = -\pi. \end{aligned} \tag{2.2.21}$$

The governing system of equations with N+1 components subject to the two constraints is given by

$$\begin{cases} \frac{\partial \rho}{\partial t} + \nabla \cdot (\rho \mathbf{v}) = 0, \\ \frac{\partial \rho_i}{\partial t} + \nabla \cdot (\rho_i \mathbf{v}) = \sum_{j=1}^{N} \nabla \cdot M_{ij} \cdot \nabla \hat{\mu}_j, \quad i = 1, 2, \cdots, N, \\ \frac{\partial (\rho \mathbf{v})}{\partial t} + \nabla \cdot (\rho \mathbf{v} \mathbf{v}) = 2\nabla \cdot (\eta \mathbf{D}) + \nabla(\nu \nabla \cdot \mathbf{v}) - \sum_{i=1}^{N} \rho_i \nabla \hat{\mu}_i - \rho \nabla \hat{\mu}, \end{cases} \tag{2.2.22}$$

where $\mathbf{M}$ is the symmetric mobility matrix, which satisfies $\sum_{i,j=1}^{N} \nabla \cdot M_{ij} \cdot \nabla \hat{\mu}_j = 0$. This is a more general quasi-incompressible model.

In fact, if we assign $M_{Ni} = M_{iN} = -\sum_{j=1}^{N-1} M_{ij}$ and apply the constraints $\sum_{i=1}^{N} \rho_i = \rho$, $\sum_{i=1}^{N} \phi_i = 1$ and $\rho_i = \phi_i \hat{\rho}_i$, we obtain the chemical potential with

respect to ϕ_i, i=1,2, $\cdots$, N-1, in the quasi-incompressible limit,

$$\begin{aligned}&\mu_{\phi_i} = \frac{\delta \hat{f}}{\delta \phi_i} = \frac{\delta \hat{f}}{\delta \rho_i}\frac{\partial \rho_i}{\partial \phi_i} + \frac{\delta \hat{f}}{\delta \rho}\frac{\partial \rho}{\partial \phi_i} + \frac{\delta \hat{f}}{\delta \rho_N}\frac{\partial \rho_N}{\partial \phi_i} = \hat{\mu}_i\hat{\rho}_i + \hat{\mu}(\hat{\rho}_i - \hat{\rho_N}) - \hat{\rho_N}\hat{\mu_N},\\ &i = 1, \cdots, N.\end{aligned} \tag{2.2.23}$$

If we define

$$\Pi = \hat{\rho_N}(\hat{\mu} + \hat{\mu}_N) = \hat{\rho_N}\mu_N + B, \tag{2.2.24}$$

The model in (2.2.22) reduces to

$$\begin{cases}\nabla \cdot \mathbf{v} = \sum_{i=1}^{N-1}\sum_{j=1}^{N-1}(1 - \frac{\hat{\rho}_j}{\hat{\rho}_N})\frac{1}{\hat{\rho}_i\hat{\rho}_j}(\nabla \cdot M_{ij} \cdot \nabla)(\mu_{\phi_j} + \Pi(1 - \frac{\hat{\rho}_j}{\hat{\rho}_N})),\\ \frac{\partial \phi_i}{\partial t} + \nabla \cdot (\phi_i \mathbf{v}) = \sum_{j=1}^{N-1}\frac{1}{\hat{\rho}_i\hat{\rho}_j}(\nabla \cdot M_{ij} \cdot \nabla)(\mu_{\phi_j} + \Pi(1 - \frac{\hat{\rho}_j}{\hat{\rho}_N})),\\ i = 1, 2, \cdots, N-1,\\ \rho[\frac{\partial \mathbf{v}}{\partial t} + \mathbf{v} \cdot \nabla \mathbf{v}] = \nabla \cdot (2\eta \mathbf{D}) + \nabla(\nu \nabla \cdot \mathbf{v}) - \nabla \Pi - \sum_{i=1}^{N-1}\phi_i \nabla \mu_{\phi_i},\end{cases} \tag{2.2.25}$$

which is exactly the quasi-incompressible model given in (2.2.16).

2.3 Non-dimensionalization

Next, we non-dimensionalize the binary model equations and compare their near equilibrium dynamics.

2.3.1 Compressible model with the global mass conservation law

In model (2.1.14), selecting characteristic time scale t_0, characteristic length scale l_0, and characteristic density scale ρ_0, we nondimensionalize the variables and parameters as follows

$$\begin{aligned}&\tilde{t} = \frac{t}{t_0}, \quad \tilde{x} = \frac{x}{l_0}, \quad \tilde{\rho}_1 = \frac{\rho_1}{\rho_0}, \quad \tilde{\rho}_2 = \frac{\rho_2}{\rho_0}, \quad \tilde{\mathbf{v}} = \frac{\mathbf{v}t_0}{l_0},\\ &\tilde{M}_{ij} = \frac{M_{ij}}{t_0\rho_0}, \quad i, j = 1, 2, \quad \frac{1}{Re_s} = \tilde{\eta} = \frac{t_0}{\rho_0 l_0^2}\eta, \quad \frac{1}{Re_v} = \tilde{\nu} = \frac{t_0}{\rho_0 l_0^2}\nu,\\ &\tilde{\mu}_1 = \frac{t_0^2}{l_0^2}\mu_1, \quad \tilde{\mu}_2 = \frac{t_0^2}{l_0^2}\mu_2, \quad J_i = \frac{j_i t_0}{\rho_0}, i = 1, 2,\end{aligned} \tag{2.3.1}$$

where Re_s, Re_v are the Reynolds number corresponding to the shear and volumetric stresses. The scaling of chemical potentials μ_1, μ results from the non-dimensionalization of the total energy. We summarize the governing equation with non-dimensional variables and parameters as follows, dropping the $\tilde{}$ for simplicity,

$$\begin{cases} \frac{\partial \rho_1}{\partial t} + \nabla \cdot (\rho_1 \mathbf{v}) = J_1 = \nabla \cdot M_{11} \cdot \nabla \mu_1 + \nabla \cdot M_{12} \cdot \nabla \mu_2, \\ \frac{\partial \rho_2}{\partial t} + \nabla \cdot (\rho_2 \mathbf{v}) = J_2 = \nabla \cdot M_{12} \cdot \nabla \mu_1 + \nabla \cdot M_{22} \cdot \nabla \mu_2, \\ \frac{\partial (\rho \mathbf{v})}{\partial t} + \nabla \cdot (\rho \mathbf{v} v) - \frac{1}{2}(J_1 + J_2)\mathbf{v} = 2\nabla \cdot (\frac{1}{Re_s}\mathbf{D}) + \nabla(\frac{1}{Re_v}\nabla \cdot \mathbf{v}) \\ -\rho_1 \nabla \mu_1 - \rho_2 \nabla \mu_2. \end{cases} \tag{2.3.2}$$

2.3.2 Compressible model with the local mass conservation law

Analogously, in model (2.1.28), we nondimensionalize the variables and parameters as above and in particular

$$\tilde{M}_{11} = \frac{M_{11}}{t_0 \rho_0}. \tag{2.3.3}$$

We summarize the governing equation with non-dimensional variables and parameters as follows, dropping the $\tilde{}$ for simplicity,

$$\begin{cases} \frac{\partial \rho}{\partial t} + \nabla \cdot (\rho \mathbf{v}) = 0, \\ \frac{\partial \rho_1}{\partial t} + \nabla \cdot (\rho_1 \mathbf{v}) = \nabla \cdot M_{11} \cdot \nabla \tilde{\mu}_1, \\ \frac{\partial (\rho \mathbf{v})}{\partial t} + \nabla \cdot (\rho \mathbf{v} v) = 2\nabla \cdot (\frac{1}{Re_s}\mathbf{D}) + \nabla(\frac{1}{Re_v}\nabla \cdot \mathbf{v}) - \rho_1 \nabla \tilde{\mu}_1 - \rho \nabla \tilde{\mu}. \end{cases} \tag{2.3.4}$$

2.3.3 Quasi-incompressible model

In model (2.1.41), in addition to the above, we nondimensionalize two new ones as follows:

$$\tilde{\mu}_\phi = \frac{t_0^2}{\rho_0 l_0^2}\mu_\phi, \quad \tilde{\Pi} = \Pi \frac{t_0^2}{\rho_0 l_0^2}. \tag{2.3.5}$$

Dropping the ˜ on the non-dimensionalized variables and parameters, the governing equation system of the quasi-incompressible fluid flows is written as follows,

$$\begin{cases} \nabla \cdot \mathbf{v} = (1 - \frac{\hat{\rho}_1}{\hat{\rho}_2}) \frac{1}{\hat{\rho}_1^2} (\nabla \cdot M_{11} \cdot \nabla)(\mu_\phi + \Pi(1 - \frac{\hat{\rho}_1}{\hat{\rho}_2})), \\ \frac{\partial \phi}{\partial t} + \nabla \cdot (\phi \mathbf{v}) = \frac{1}{\hat{\rho}_1^2} (\nabla \cdot M_{11} \cdot \nabla)(\mu_\phi + \Pi(1 - \frac{\hat{\rho}_1}{\hat{\rho}_2})), \\ \rho[\frac{\partial \mathbf{v}}{\partial t} + \mathbf{v} \cdot \nabla \mathbf{v}] = 2\nabla \cdot (\frac{1}{Re_s}\mathbf{D}) + \nabla(\frac{1}{Re_v}\nabla \cdot \mathbf{v}) - \nabla\Pi - \phi\nabla\mu_\phi. \end{cases} \tag{2.3.6}$$

Chapter 3

Comparison of models

We investigate near equilibrium dynamics by conducting a linear stability analysis of the models from each class about a constant steady state. Through analyzing the dispersion relations of the selected models, we would like to identify the intrinsic relation among compressible, quasi-incompressible and incompressible models, in particular, to reveal the consequence of the hierarchical reduction to linear stability. We focus on models of a binary fluid mixture only in this study.

3.1 Compressible model with the global mass conservation law

This compressible model admits one constant solution:

$$\mathbf{v} = \mathbf{0}, \quad \rho_1 = \rho_1^0, \quad \rho_2 = \rho_2^0, \tag{3.1.1}$$

where ρ_1^0, ρ_2^0 are constants. We perturb the constant solution with the normal mode as follows:

$$\mathbf{v} = \epsilon e^{\alpha t + i\mathbf{k}\cdot\mathbf{x}}\mathbf{v}^c, \quad \rho_1 = \rho_1^0 + \epsilon e^{\alpha t + i\mathbf{k}\cdot\mathbf{x}}{\rho_1}^c, \quad \rho_2 = \rho_2^0 + \epsilon e^{\alpha t + i\mathbf{k}\cdot\mathbf{x}}{\rho_2}^c. \tag{3.1.2}$$

where ϵ is a small parameter, representing the magnitude of the perturbation, and $\mathbf{v}^c, \rho_1^c, \rho_2^c$ are constants, α is the growth rate, $\mathbf{k}$ is the wave number of the perturbation. Without loss of generality, we limit our study to 1 dimensional perturbations in $\mathbf{k}$ in 2D models. Substituting these perturbations into the equations in (2.3.2) and truncate the equations at order $O(\epsilon)$, we obtain the linearized equations. The dispersion equation of the linearized equation systems is given by the algebraic equation of

α:

$$
\begin{aligned}
&(\tfrac{1}{Re_s}k^2+\alpha\rho^0)\{\alpha^3\rho_0+\alpha^2k^2[\tfrac{1}{Re}+\rho^0M_{11}(h_{\rho_1\rho_1}+\kappa_{\rho_1\rho_1}k^2)\\
&+\rho^0M_{22}(h_{\rho_2\rho_2}+\kappa_{\rho_2\rho_2}k^2)]+\alpha^2k^2[2\rho^0M_{12}(h_{\rho_1\rho_2}+\kappa_{\rho_1\rho_2}k^2)]\\
&+\alpha[\mathbf{p}^T\cdot\mathbf{C}\cdot\mathbf{p}+\mathbf{p}^T\cdot\mathbf{K}\cdot\mathbf{p}k^2]k^2+\alpha\tfrac{1}{Re}[M_{11}(h_{\rho_1\rho_1}+\kappa_{\rho_1\rho_1}k^2)\\
&+M_{22}(h_{\rho_2\rho_2}+\kappa_{\rho_2\rho_2}k^2)+2M_{12}(h_{\rho_1\rho_2}+\kappa_{\rho_1\rho_2}k^2)]k^4\\
&+\alpha\rho^0|\mathbf{M}|[(h_{\rho_1\rho_1}+\kappa_{\rho_1\rho_1}k^2)(h_{\rho_2\rho_2}+\kappa_{\rho_2\rho_2}k^2)-(h_{\rho_1\rho_2}+\kappa_{\rho_1\rho_2}k^2)^2]k^4\\
&+k^4(\tfrac{1}{Re}|\mathbf{M}|k^2+M_{22}(\rho_1^0)^2+M_{11}(\rho_2^0)^2-2M_{12}\rho_1^0\rho_2^0)\\
&[(h_{\rho_1\rho_1}+\kappa_{\rho_1\rho_1}k^2)(h_{\rho_2\rho_2}+\kappa_{\rho_2\rho_2}k^2)-(h_{\rho_1\rho_2}+\kappa_{\rho_1\rho_2}k^2)^2]\}=0.
\end{aligned}
\tag{3.1.3}
$$

where $\mathbf{p}=(\rho_1^0,\rho_2^0)^T$ and $\frac{1}{Re}=2\frac{1}{Re_s}+\frac{1}{Re_v}$. $|\mathbf{M}|$ is the determinant of the mobility coefficient matrix $\mathbf{M}=(M_{i,j})$, $\mathbf{K}$ is the coefficient matrix of the conformational entropy

$$
\mathbf{K}=\begin{pmatrix}\kappa_{\rho_1\rho_1} & \kappa_{\rho_1\rho_2}\\ \kappa_{\rho_1\rho_2} & \kappa_{\rho_2\rho_2}\end{pmatrix},
\tag{3.1.4}
$$

$\mathbf{C}$ is the Hessian of the bulk free energy $h(\rho_1,\rho_2,T)$ in (2.1.18) with respect to ρ_1 and ρ_2,

$$
\mathbf{C}=\begin{pmatrix}h_{\rho_1\rho_1} & h_{\rho_1\rho_2}\\ h_{\rho_1\rho_2} & h_{\rho_2\rho_2}\end{pmatrix},
\tag{3.1.5}
$$

where $h_{\rho_i\rho_j}$ represents the second order derivative of the bulk free energy density $h(\rho_1,\rho_2,T)$ with respect to ρ_i and ρ_j, i, j = 1, 2.

One root of equation (5.2.6) is given by

$$
\alpha_0=-\frac{1}{\rho^0Re_s}k^2.
\tag{3.1.6}
$$

This is the viscous mode associated to the viscous stress. The other three roots are governed by a cubic polynomial equation and their closed forms are essentially impenetrable. Instead, we present them using asymptotic formulae in long and short wave range and numerical calculations in the intermediate wave range.

The asymptotic expressions of the three growth rates at $|k| \ll 1$ are given by

$$\alpha_1 = x_1 k^2 + y_1 k^4 + O(k^5), \quad \alpha_{2,3} = x_{2,3} k + y_{2,3} k^2 + O(k^3), \tag{3.1.7}$$

where

$$x_1 = -\frac{g_1|\mathbf{C}|}{\mathbf{p}^T\cdot\mathbf{C}\cdot\mathbf{p}}, \quad x_{2,3} = \pm\sqrt{-\frac{\mathbf{p}^T\cdot\mathbf{C}\cdot\mathbf{p}}{\rho^0}},$$

$$\begin{aligned} y_1 = &-\frac{1}{\mathbf{p}^T\cdot\mathbf{C}\cdot\mathbf{p}}\Big[\frac{1}{Re}|\mathbf{M}||\mathbf{C}| + dg_1\Big] - \frac{1}{\mathbf{p}^T\cdot\mathbf{C}\cdot\mathbf{p}}\Big[\rho^0 x_1^3 + x_1^2(\frac{1}{Re} + \rho^0\mathbf{M}:\mathbf{C}) + \\ &x_1(\rho^0|\mathbf{M}||\mathbf{C}| + \frac{1}{Re}\mathbf{M}:\mathbf{C} + \mathbf{p}^T\cdot\mathbf{K}\cdot\mathbf{p})\Big], \end{aligned} \tag{3.1.8}$$

$$y_{2,3} = -\frac{1}{2\rho^0 Re} - \frac{1}{2\mathbf{p}^T\cdot\mathbf{C}\cdot\mathbf{p}}[M_{11}(\rho_1^0 h_{\rho_1\rho_1} + \rho_2^0 h_{\rho_1\rho_2})^2 + M_{22}(\rho_1^0 h_{\rho_1\rho_2} + \rho_2^0 h_{\rho_2\rho_2})^2].$$

where $d = h_{\rho_1\rho_1}\kappa_{\rho_2\rho_2} + h_{\rho_2\rho_2}\kappa_{\rho_1\rho_1} - 2h_{\rho_1\rho_2}\kappa_{\rho_1\rho_2}$ and $g_1 = M_{22}(\rho_1^0)^2 + M_{11}(\rho_2^0)^2 - 2M_{12}\rho_1^0\rho_2^0 \geq 0$, since $\mathbf{M} \geq 0$ and at least one of its eigenvalues is positive.

When $|k| \gg 1$, the three growth rates are given by

$$\alpha_{1,2} = x_{1,2} k^4 + y_{1,2} k^2 + O(k), \quad \alpha_3 = x_3 k^2 + y_3 + O(\tfrac{1}{k}), \tag{3.1.9}$$

where

$$x_{1,2} = -\frac{\mathbf{M}:\mathbf{K}}{2} \pm \frac{1}{2\rho^0}\sqrt{(\mathbf{M}:\mathbf{K}\rho^0)^2 - 4[\frac{1}{Re}\mathbf{M}:\mathbf{K} + \rho^0|\mathbf{M}||\mathbf{K}|]}, \quad x_3 = -\frac{1}{\rho^0 Re},$$

$$y_{1,2} = \frac{-\frac{1}{Re}|\mathbf{M}||\mathbf{K}| - x_{1,2}^2(\frac{1}{Re} + \rho^0\mathbf{M}:\mathbf{C}) - x_{1,2}(\frac{1}{Re}\mathbf{M}:\mathbf{K} + \rho^0|\mathbf{M}|d)}{3x_{1,2}^2\rho^0 + 2x_{1,2}\rho^0(\mathbf{M}:\mathbf{K}) + \rho^0|\mathbf{M}||\mathbf{K}|}, \tag{3.1.10}$$

$$y_3 = -\frac{1}{\rho^0|\mathbf{M}||\mathbf{K}|}\Big[x_3^2(\rho^0\mathbf{M}:\mathbf{K}) + x_3(\rho^0|\mathbf{M}|d + \frac{1}{Re}\mathbf{M}:\mathbf{K}) + |\mathbf{M}|\frac{1}{Re}d + g_1|\mathbf{K}|\Big].$$

The thermodynamic mode α_1 is related to the mobility matrix and hessian matrix of the bulk free energy exclusively. The rest two eigenvalues $\alpha_{2,3}$ are coupled with hydrodynamics.

Obviously, α_0 is negative so the viscous mode is stable. From the asymptotic expansions of α at $|k| \gg 1$, we observe that all three eigenvalues $\alpha_{1,2,3}$ are negative (3.1.9) since $\mathbf{K} > 0, \mathbf{M} \geq 0$ and viscosity coefficients positive. This indicates that

Table 3.1 Sign of the eigenvalues when $|k| \ll 1$ in different regimes of $\mathbf{C}$. Negative sign indicates stability while positive sign indicates instability.

	α_0	α_1	α_2	α_3
$\mathbf{C} > 0$	-	-	-	-
$\mathbf{C} < 0$	-	+	+	-
$\mathbf{C}$ is indefinite	-	$\mathbf{p}^T \cdot \mathbf{C} \cdot \mathbf{p}$ has the same sign with $\lvert\mathbf{C}\rvert$: -; Otherwise, +.	If $\mathbf{p}^T \cdot \mathbf{C} \cdot \mathbf{p} > 0$: -; If $\mathbf{p}^T \cdot \mathbf{C} \cdot \mathbf{p} < 0$: +.	-

the model does not have any short-wave instability near its steady states, which is physically meaningful.

When $|k| \ll 1$, we notice that the leading term in α_1 is determined by the combination of mobility coefficient matrix $\mathbf{M}$ and hessian matrix $\mathbf{C}$ of the bulk free energy. We assume that $\mathbf{M} \geq 0$ and has at least one positive eigenvalue, so $g_1 > 0$. We discuss the dependence of the leading order term of α_1 on $\mathbf{C}$.

- When $\mathbf{C} > 0$, the leading term $-\frac{g_1|\mathbf{C}|}{\mathbf{p}^T \cdot \mathbf{C} \cdot \mathbf{p}} k^2 < 0$, then $\alpha_1 < 0$. So, this mode is stable.

- When $\mathbf{C} < 0$, the leading term $-\frac{g_1|\mathbf{C}|}{\mathbf{p}^T \cdot \mathbf{C} \cdot \mathbf{p}} k^2 > 0$, then $\alpha_1 > 0$. This instability is due to the spinodal decomposition in the coupled Cahn-Hilliard type equations of ρ_1 and ρ_2.

- When $\mathbf{C}$ is indefinite and $\mathbf{p}^T \cdot \mathbf{C} \cdot \mathbf{p}$ has the same sign with $|\mathbf{C}|$, the property of α_1 is the same as the case where $\mathbf{C} > 0$; Otherwise, the property of α_1 is the same as the case of $\mathbf{C} < 0$.

$\alpha_{2,3}$ represent the two coupled modes. Their signs depend on the model parameters. Since the leading term is determined by the properties of the hessian matrix $\mathbf{C}$, we discuss their dependence on $\mathbf{C}$ below.

- When $\mathbf{C} > 0$, $\sqrt{(-\frac{1}{\rho^0}\mathbf{p}^T \cdot \mathbf{C} \cdot \mathbf{p})}$ is imaginary. In this situation, the leading order growth rate in $\alpha_{2,3}$ is the quadratic term $(-\frac{1}{Re}\frac{1}{2\rho^0} - \frac{1}{2\mathbf{p}^T \cdot \mathbf{C} \cdot \mathbf{p}}(M_{11}(\rho_1^0 h_{\rho_1\rho_1} +$

$\rho_2^0 h_{\rho_1\rho_2})^2 + M_{22}(\rho_1^0 h_{\rho_1\rho_2} + \rho_2^0 h_{\rho_2\rho_2})^2))k^2 \leq 0$. So, the two modes are stable.

- When $\mathbf{C} < 0$, the leading term is given by $\pm\sqrt{(-\frac{1}{\rho^0}\mathbf{p}^T \cdot \mathbf{C} \cdot \mathbf{p})}k$, indicating there exists an unstable mode. This verified the fact that the steady state at a concave free energy surface is unstable.

- When $\mathbf{C}$ is indefinite and $\mathbf{p}^T \cdot \mathbf{C} \cdot \mathbf{p} > 0$, the property of $\alpha_{2,3}$ is the same as the case where $\mathbf{C} > 0$. Similarly, the property of $\alpha_{2,3}$ is the same as the case of $\mathbf{C} < 0$ when $\mathbf{p}^T \cdot \mathbf{C} \cdot \mathbf{p} < 0$.

The stability property of the model with respect to $\mathbf{C}$ in the long wave regime is summarized in Table (3.1). For the intermediate wave regime, we have to compute the growth rate numerically, which can only be done for specific free energy density functions.

3.2 Compressible model with the local mass conservation law

Notice that the compressible model with the local mass conservation law also admits the same constant solution (5.2.4). We repeat the same normal mode analysis analogous to the previous model and obtain the dispersion equation as follows:

$$(\alpha\rho^0 + \tfrac{1}{Re_s}k^2)\{\alpha^3\rho^0 + \alpha^2[\rho^0 k^2 M_{11}(\tilde{h}_{\rho_1\rho_1} + \tilde{\kappa}_{\rho_1\rho_1}k^2) + \tfrac{1}{Re}k^2] + \alpha[k^2 M_{11}(\tilde{h}_{\rho_1\rho_1} + \tilde{\kappa}_{\rho_1\rho_1}k^2)\tfrac{1}{Re}k^2 + \mathbf{p}^T \cdot \mathbf{C} \cdot \mathbf{p}k^2 + \mathbf{p}^T \cdot \mathbf{K} \cdot \mathbf{p}k^4))] + k^4 M_{11}(\rho^0)^2((\tilde{h}_{\rho_1\rho_1} + k^2\tilde{\kappa}_{\rho_1\rho_1})(\tilde{h}_{\rho\rho} + \tilde{\kappa}_{\rho\rho}k^2) - (\tilde{h}_{\rho\rho_1} + k^2\tilde{\kappa}_{\rho\rho_1})^2)\} = 0. \tag{3.2.1}$$

Again, $\alpha_0 = -\frac{1}{\rho^0}\frac{1}{Re_s}k^2$ is a root of this algebraic equation. We present the rest asymptotically.

When $|k| \ll 1$, we have

$$\alpha_1 = -\frac{M_{11}(\rho^0)^2|\mathbf{C}|}{\mathbf{p}^T\cdot\mathbf{C}\cdot\mathbf{p}}k^2 + (-\frac{x_0^3\rho^0+x_0^2[\rho^0 M_{11}\tilde{h}_{\rho_1\rho_1}+\frac{1}{Re}]+x_0[\mathbf{p}^T\cdot\mathbf{K}\cdot\mathbf{p}+\tilde{h}_{\rho_1\rho_1}M_{11}\frac{1}{Re}]}{\mathbf{p}^T\cdot\mathbf{C}\cdot\mathbf{p}}$$

$$-\frac{M_{11}(\rho^0)^2[\tilde{h}_{\rho_1\rho_1}\tilde{\kappa}_{\rho\rho}+\tilde{h}_{\rho\rho}\tilde{\kappa}_{\rho_1\rho_1}-2\tilde{h}_{\rho\rho_1}\tilde{\kappa}_{\rho\rho_1}]}{\mathbf{p}^T\cdot\mathbf{C}\cdot\mathbf{p}})k^4 + O(k^5), \tag{3.2.2}$$

$$\alpha_{2,3} = \pm\sqrt{(-\frac{1}{\rho^0}\mathbf{p}^T\cdot\mathbf{C}\cdot\mathbf{p})}k - (\frac{1}{Re}\frac{1}{2\rho^0} + \frac{M_{11}}{2\mathbf{p}^T\cdot\mathbf{C}\cdot\mathbf{p}}(\rho_1^0\tilde{h}_{\rho_1\rho_1}+\rho^0\tilde{h}_{\rho\rho_1})^2)k^2 + O(k^3),$$

where $x_0 = -\frac{M_{11}(\rho^0)^2|\mathbf{C}|}{\mathbf{p}^T\cdot\mathbf{C}\cdot\mathbf{p}}$. When $|k| \gg 1$,

$$\alpha_1 = -M_{11}\tilde{\kappa}_{\rho_1\rho_1}k^4 - M_{11}\tilde{h}_{\rho_1\rho_1}k^2 + O(k),$$

$$\alpha_{2,3} = \frac{-\frac{1}{Re}\pm\sqrt{(\frac{1}{Re})^2-4\tilde{\kappa}_{\rho_1\rho_1}^{-1}(\rho^0)^3|\mathbf{K}|}}{2\rho^0}k^2 + \frac{-M_{11}(\rho^0)^2[\tilde{h}_{\rho_1\rho_1}\tilde{\kappa}_{\rho\rho}+\tilde{h}_{\rho\rho}\tilde{\kappa}_{\rho_1\rho_1}-2\tilde{h}_{\rho\rho_1}\tilde{\kappa}_{\rho\rho_1}]}{2x_{2,3}\rho^0 M_{11}\tilde{\kappa}_{\rho_1\rho_1}+M_{11}\tilde{\kappa}_{\rho_1\rho_1}\frac{1}{Re}} \tag{3.2.3}$$

$$-\frac{x_{2,3}^3\rho^0+x_{2,3}^2[\rho^0 M_{11}\tilde{h}_{\rho_1\rho_1}+\frac{1}{Re}]+x_{2,3}[M_{11}\tilde{h}_{\rho_1\rho_1}\frac{1}{Re}+\mathbf{p}^T\cdot\mathbf{K}\cdot\mathbf{p}]}{2x_{2,3}\rho^0 M_{11}\tilde{\kappa}_{\rho_1\rho_1}+M_{11}\tilde{\kappa}_{\rho_1\rho_1}\frac{1}{Re}} + O(\frac{1}{k}),$$

where $x_{2,3} = \frac{-\frac{1}{Re}\pm\sqrt{(\frac{1}{Re})^2-4\tilde{\kappa}_{\rho_1\rho_1}^{-1}(\rho^0)^3|\mathbf{K}|}}{2\rho^0}$,

$$\mathbf{C} = \begin{pmatrix} \tilde{h}_{\rho\rho} & \tilde{h}_{\rho\rho_1} \\ \tilde{h}_{\rho\rho_1} & \tilde{h}_{\rho_1\rho_1} \end{pmatrix} \tag{3.2.4}$$

is the hessian matrix of the bulk free energy density function h with respect to ρ and ρ_1 and evaluated at the constant steady state, and

$$\mathbf{K} = \begin{pmatrix} \tilde{\kappa}_{\rho\rho} & \tilde{\kappa}_{\rho\rho_1} \\ \tilde{\kappa}_{\rho\rho_1} & \tilde{\kappa}_{\rho_1\rho_1} \end{pmatrix} \tag{3.2.5}$$

is the coefficient matrix of the quadratic conformational entropy term in the free energy density function (2.1.24).

Like in the previous model, the first growth rate α_0 is the viscous mode associated to the viscous stress exclusively; the second growth rate α_1 is a thermodynamic mode, related to the transport equation of density ρ_1 and dictated by the mobility matrix and hessian matrix of the bulk free energy. The rest two growth rates $\alpha_{2,3}$ are coupled modes.

Obviously, α_0 is negative so the viscous mode is stable. For the other three modes, we adopt the same strategy combining asymptotic analysis with numerical computations. From asymptotic expansions (3.2.3) of α at $|k| \gg 1$, we observe that all three eigenvalues $\alpha_{1,2,3}$ are negative, given that $\mathbf{K}$ and the mobility coefficients are both positive definite. This indicates that the model does not have any short-wave instability near its steady states. The properties of the three modes in the long wave regime are identical to the cases discussed in the previous section for the more general compressible model and summarized in Table 3.1.

For the intermediate wave regime, we have to compute the growth rate using a specific free energy density function numerically. We use the Peng-Robinson bulk free energy as an example here [48], which is given by

$$\begin{aligned}
&\tilde{h}(\rho_1,\rho,T) = \tfrac{r_m\rho_1+(\rho-\rho_1)}{m_2}\varphi(T) - \tfrac{r_m\rho_1+(\rho-\rho_1)}{m_2}RTln(\tfrac{m_2}{r_m\rho_1+(\rho-\rho_1)} - b)\\
&-\tfrac{r_m\rho_1+(\rho-\rho_1)}{m_2}\tfrac{a}{2\sqrt{2}b}ln[\tfrac{m_2+(r_m\rho_1+(\rho-\rho_1))b(1+\sqrt{2})}{m_2+(r_m\rho_1+(\rho-\rho_1))b(1-\sqrt{2})}]\\
&+\tfrac{r_m\rho_1+(\rho-\rho_1)}{m_2}RT[\tfrac{r_m\rho_1}{r_m\rho_1+(\rho-\rho_1)}ln\tfrac{r_m\rho_1}{r_m\rho_1+(\rho-\rho_1)} + \tfrac{\rho_2}{r_m\rho_1+(\rho-\rho_1)}ln\tfrac{(\rho-\rho_1)}{r_m\rho_1+(\rho-\rho_1)}].
\end{aligned} \tag{3.2.6}$$

This is obtained by replacing ρ_1, ρ_2 in the free energy density given in (2.1.19) by $\rho_1, \rho_2 = \rho - \rho_1$. This free energy density is either positive definite or indefinite in its entire physical domain. The positive definite domain and indefinite domain are shown in Figure 3.1 in (ρ_1, ρ) space. *N*otice that in this example, when $\mathbf{C}$ is indefinite, we always have $|\mathbf{C}| < 0$, it is impossible to have two unstable modes α_1 and α_2 exist simultaneously according to table (3.1). We then search the parameter space to sample all the possible instabilities associated to the compressible model with this free energy.

As an example, we choose the steady state given by $(\rho^0, \rho_1^0, \mathbf{v}_0) = (400, 2, 0, 0)$ to show the positive grow in α_1. To show positive growth in the coupled mode α_2, we choose $(\rho^0, \rho_1^0, \mathbf{v}_0) = (1000, 0.025, 0, 0)$. Figure 3.2 plots the three growth rates $\alpha_{1,2,3}$ with $\alpha_1 > 0$ at the first constant solution. The corresponding eigenvector to α_1 of the linearized system is $(0, 1, 0, 0)$, indicating the unstable variable in the linear regime is

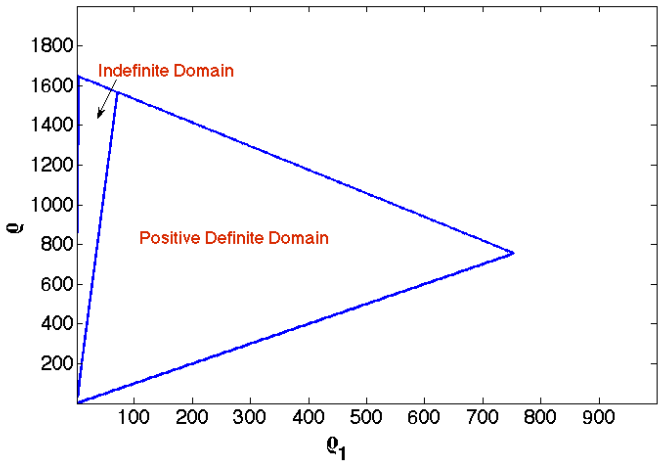

Figure 3.1 Domain of concavity of the Peng-Robinson free energy.

ρ_1. The three growth rates $\alpha_{1,2,3}$ with the coupled mode $\alpha_2 > 0$ at the second solution are plotted in Figure 3.3. The corresponding eigenvector to α_2 is $(0, 1, 0, 0)$ as well, indicating the instability is still associated with ρ_1. When $\mathbf{C} > 0$, the corresponding constant solution is stable. We choose constant solution $(\rho^0, \rho_1^0, \mathbf{v}_0) = (400, 200, 0, 0)$ as an example. The three growth rates $\alpha_{1,2,3}$ of negative real parts are shown in Figure 3.4. The numerical results show that the asymptotic analysis is accurate in their respective wave number range of applicability.

From the linear analysis above, we conclude that linear dynamics of compressible model (2.3.2) and (2.3.4) are qualitatively the same. Next, we investigate the near equilibrium dynamics of the quasi-incompressible model.

3.3 Quasi-incompressible model

The quasi-incompressible fluid flow model equations admit a constant solution:

$$\mathbf{v} = \mathbf{0}, \quad \phi = \phi^0, \quad \Pi = \Pi_0, \tag{3.3.1}$$

where ϕ^0, Π_0 are constants. We perturb the constant solution as follows:

$$\mathbf{v} = \epsilon e^{\alpha t + i\mathbf{k}\cdot\mathbf{x}}\mathbf{v}^c, \quad \phi = \phi^0 + \epsilon e^{\alpha t + i\mathbf{k}\cdot\mathbf{x}}\phi^c, \quad \Pi = \Pi_0 + \epsilon e^{\alpha t + i\mathbf{k}\cdot\mathbf{x}}\Pi^c, \tag{3.3.2}$$

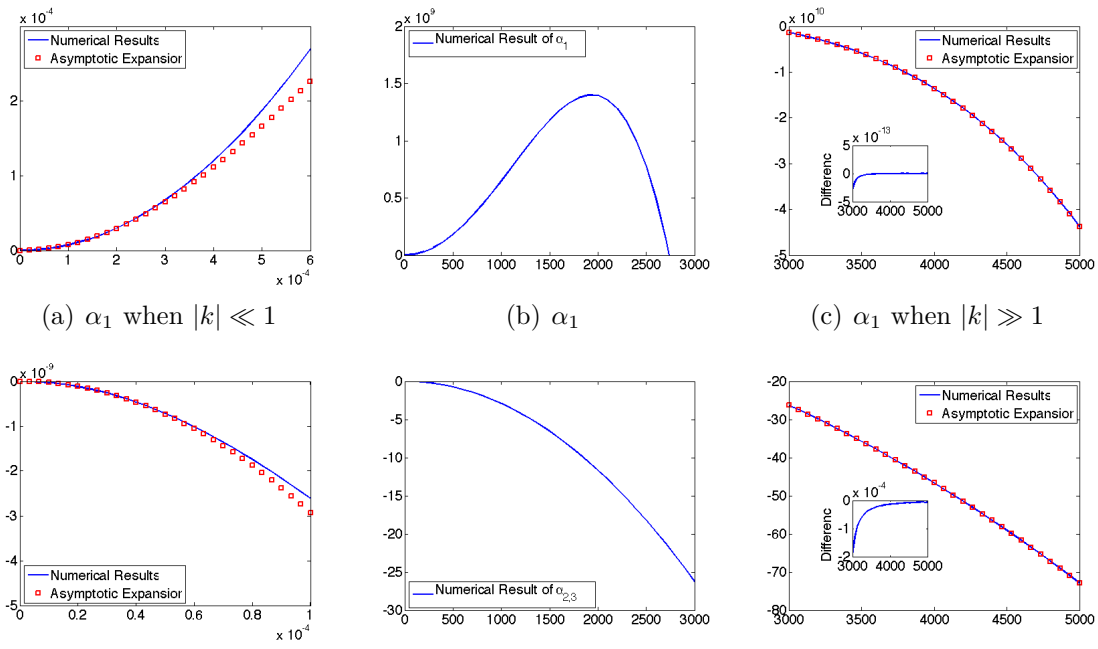

(a) α_1 when $|k| \ll 1$ (b) α_1 (c) α_1 when $|k| \gg 1$

(d) $\alpha_{2,3}$ when $|k| \ll 1$ (e) $\alpha_{2,3}$ (f) $\alpha_{2,3}$ when $|k| \gg 1$

Figure 3.2 Numerical growth rates and the corresponding asymptotic expansions. It tells us that $\alpha_1 > 0$ and all other eigen-modes are negative in compressible model (2.3.4) at constant state $(\rho^0, \rho_1^0, \mathbf{v}) = (400, 2, 0, 0)$ with the Peng-Robinson free energy. The vertical axis is the growth rate and the horizontal one is the wave number. (a). α_1 in the long wave range. (b). α_1 in the intermediate wave range. (c). α_1 in the short wave range. (d). $\alpha_{2,3}$ in the short wave range. (e). $\alpha_{2,3}$ in the intermediate wave range. (f). $\alpha_{2,3}$ in the short wave range. The parameter values used are: $M_{11} = 0.0001$, $Re_s = 1$, $Re_v = 3$, $\tilde{\kappa}_{\rho\rho} = 0.000106$, $\tilde{\kappa}_{\rho_1\rho_1} = 0.0001$, $\tilde{\kappa}_{\rho\rho_1} = 0$.

where ϵ is a small perturbation, and $\mathbf{v}^c, \phi^c, \Pi^c$ are constants.

The dispersion equation is a factorable, third order polynomial in α

$$(\tfrac{1}{Re_s}k^2 + \alpha\rho^0)(\alpha^2(1-\tfrac{\hat{\rho_1}}{\hat{\rho_2}})^2\tfrac{1}{\hat{\rho_1}^2}M_{11}k^2\rho^0 + \alpha[k^2 + \tfrac{1}{Re}(1-\tfrac{\hat{\rho_1}}{\hat{\rho_2}})^2\tfrac{1}{\hat{\rho_1}^2}M_{11}k^4] \tag{3.3.3}$$

$$+k^4M_{11}(\hat{h}_{\phi\phi} + k^2\hat{\kappa}_{\phi\phi})\tfrac{1}{\hat{\rho_1}^2}[1-(1-\tfrac{\hat{\rho_1}}{\hat{\rho_2}})\phi_0]^2) = 0.$$

i.e.

$$(\tfrac{1}{Re_s}k^2 + \alpha\rho^0)[(1-\tfrac{\hat{\rho_1}}{\hat{\rho_2}})^2\tfrac{1}{\hat{\rho_1}^2}M_{11}k^2](\alpha^2\rho^0 + \alpha[[(1-\tfrac{\hat{\rho_1}}{\hat{\rho_2}})^2\tfrac{1}{\hat{\rho_1}^2}M_{11}]^{-1} + \tfrac{1}{Re}k^2] \tag{3.3.4}$$

$$+k^2(\hat{h}_{\phi\phi} + k^2\hat{\kappa}_{\phi\phi})[\phi_0 - \tfrac{\hat{\rho_2}}{\hat{\rho_2}-\hat{\rho_1}}]^2) = 0.$$

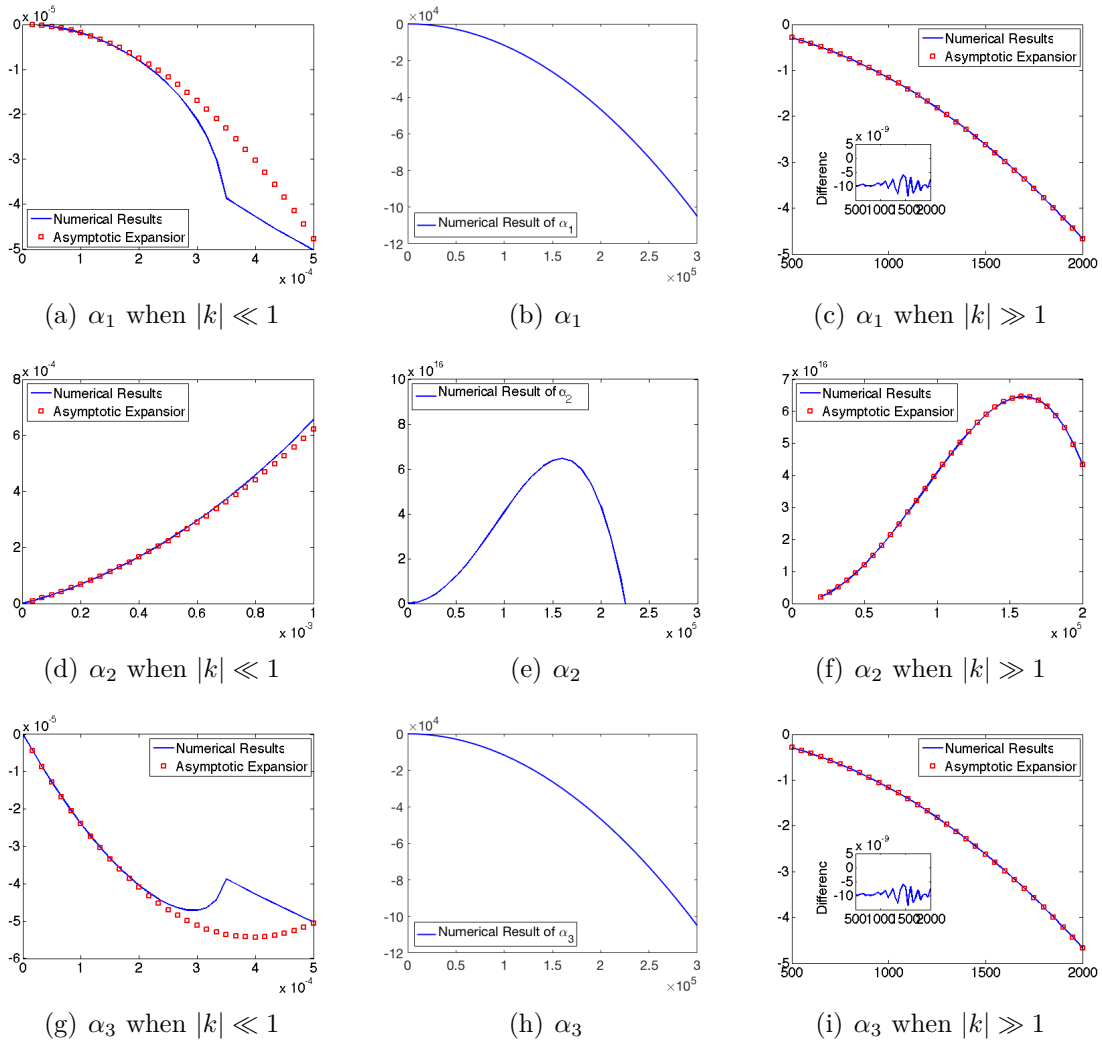

(a) α_1 when $|k| \ll 1$ (b) α_1 (c) α_1 when $|k| \gg 1$

(d) α_2 when $|k| \ll 1$ (e) α_2 (f) α_2 when $|k| \gg 1$

(g) α_3 when $|k| \ll 1$ (h) α_3 (i) α_3 when $|k| \gg 1$

Figure 3.3 Numerical growth rates and the corresponding asymptotic expansions. It shows that $\alpha_2 > 0$ while the other eigen-modes are negative compressible model (2.3.4) at constant state $(\rho^0, \rho_1^0, \mathbf{v}) = (1000, 0.025, 0, 0)$ with the Peng-robinson free energy. The vertical axis is the growth rate and the horizontal one is the wave number. (a). (d). (g). Growth rates in the short wave range. (b). (e). (h). Growth rates in the intermediate wave range. (c). (f). (j). Growth rates in the short wave range. The parameter values used are: $M_{11} = 0.0001$, $Re_s = 1$, $Re_v = 3$, $\tilde{\kappa}_{\rho\rho} = 0.000106$, $\tilde{\kappa}_{\rho_1\rho_1} = 0.0001$, $\tilde{\kappa}_{\rho\rho_1} = 0$.

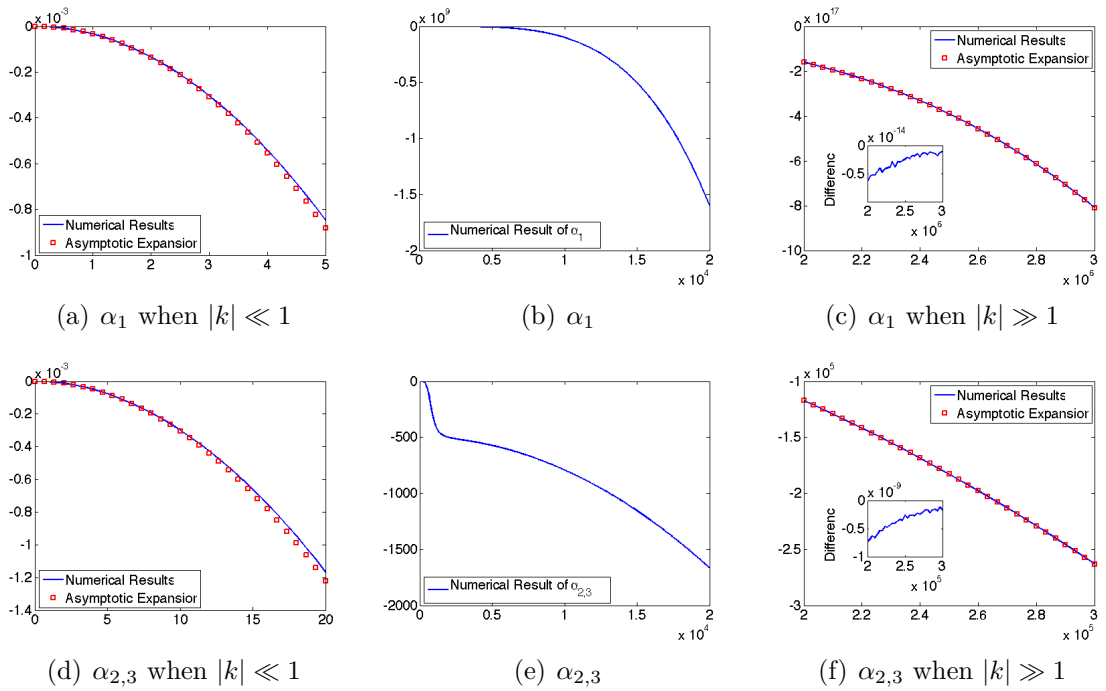

(a) α_1 when $|k| \ll 1$ (b) α_1 (c) α_1 when $|k| \gg 1$

(d) $\alpha_{2,3}$ when $|k| \ll 1$ (e) $\alpha_{2,3}$ (f) $\alpha_{2,3}$ when $|k| \gg 1$

Figure 3.4 Numerical growth rates and the corresponding asymptotic expansions. In this example, we observe that there are no unstable modes in compressible model (2.3.4) at constant state $(\rho^0, \rho_1^0, \mathbf{v}) = (400, 200, 0, 0)$ with the Peng-Robinson free energy. (a). and (d). Growth rates in the short wave range. (b). and (e). Growth rates in the intermediate wave range. (c). and (f). Growth rates in the short wave range. The parameter values used are: $M_{11} = 0.0001$, $Re_s = 10^6$, $Re_v = 3 \times 10^6$, $\tilde{\kappa}_{\rho\rho} = 0.000106$, $\tilde{\kappa}_{\rho_1\rho_1} = 0.0001$, $\tilde{\kappa}_{\rho\rho_1} = 0$.

The growth rates are given explicitly by

$$\alpha_0 = -\frac{1}{Re_s}\frac{1}{\rho^0}k^2,$$

$$\alpha_1 = \frac{-2k^2(\hat{h}_{\phi\phi}+k^2\hat{\kappa}_{\phi\phi})Q^2}{[(\frac{1}{Re}k^2+A)+\sqrt{(\frac{1}{Re}k^2+A)^2-4\rho^0k^2(\hat{h}_{\phi\phi}+k^2\hat{\kappa}_{\phi\phi})Q^2}]}, \tag{3.3.5}$$

$$\alpha_2 = \frac{-(\frac{1}{Re}k^2+A)-\sqrt{(\frac{1}{Re}k^2+A)^2-4\rho^0k^2(\hat{h}_{\phi\phi}+k^2\hat{\kappa}_{\phi\phi})Q^2}}{2\rho^0},$$

where

$$Q = \phi^0 - \frac{\hat{\rho}_2}{\hat{\rho}_2-\hat{\rho}_1}, \quad \frac{1}{Re} = 2\frac{1}{Re_s} + \frac{1}{Re_v} > 0, \quad A = [(1-\frac{\hat{\rho}_1}{\hat{\rho}_2})^2\frac{1}{(\hat{\rho}_1)^2}M_{11}]^{-1} > 0. \tag{3.3.6}$$

The stable hydrodynamic mode remains in α_0. The thermodynamic modes are now

given by $\alpha_{1,2}$. $Re(\alpha_1)$ can be positive only when $\hat{h}_{\phi\phi} < 0$, in which $Re(\alpha_1) > 0$ when $0 \leq k \leq \sqrt{-\frac{\hat{h}_{\phi\phi}}{\kappa_{\phi\phi}}}$. This instability is due to the spinodal decomposition in the coupled Cahn-Hilliard equation of ϕ. Given that the viscosity and mobility coefficients are all positive, $Re(\alpha_2) < 0$. So, the second coupled mode is a stable mode. In the long wave range ($|k| \ll 1$), $\alpha_1 \approx -\frac{M_{11}\hat{h}_{\phi\phi}}{\hat{\rho_1}^2\hat{\rho_2}^2}(\hat{\rho_1} + (\hat{\rho_1} - \hat{\rho_2})\phi^0)^2 k^2$.

When $\hat{\rho_1} = \hat{\rho_2}$, the model reduces to an incompressible model with the following two growth rates

$$\begin{aligned} \alpha_0 &= -\tfrac{1}{Re_s}\tfrac{1}{\rho^0}k^2, \\ \alpha_1 &= -\tfrac{1}{\hat{\rho_2}^2}M_{11}\hat{h}_{\phi\phi}k^2 - \tfrac{1}{\hat{\rho_1}^2}\hat{\kappa}_{\phi\phi}M_{11}k^4. \end{aligned} \tag{3.3.7}$$

The thermodynamic mode decouples from the hydrodynamic mode completely in the linear regime. The possible instability only lies in the spinodal mode of the Cahn-Hilliard equation. In fact, $A, Q \to \infty$ in this limit. So, the growth rate associated with α_2 in the quasi-incompressible model is lost.

3.4 Summary of linear stability results

In compressible phase field models, there are four modes in the 1D perturbation analysis: α_0 is the hydrodynamic mode dictated by the viscous stress, α_1 is the thermodynamic mode dominated by the mobility and the bulk free energy, the rest two modes $\alpha_{2,3}$ are coupled, which couples dynamics of phase behavior with hydrodynamics and may be unstable depending on the composition of the fluid mixture. When the Hessian matrix of the bulk free energy $\mathbf{C} > 0$, $\sqrt{(-\frac{1}{\rho^0}\mathbf{p}^T \cdot \mathbf{C} \cdot \mathbf{p})}$ is imaginary. So $\pm\sqrt{(-\frac{1}{\rho^0}\mathbf{p}^T \cdot \mathbf{C} \cdot \mathbf{p})}k$ represents a wave that does not contribute to the amplitude change in growth rates of the linearized system. The scenario on stability of the steady state is tabulated in table (3.1).

When the quasi-incompressible constraint is added, i.e. $\rho_1 = \hat{\rho_1}\phi, \rho_2 = \hat{\rho_2}(1-\phi)$.

The positive definite matrix $\mathbf{C}$ reduces to a singular matrix

$$\mathbf{C} = h_{\phi\phi} \begin{pmatrix} \frac{1}{\hat{\rho_1}\hat{\rho_1}} & -\frac{1}{\hat{\rho_1}\hat{\rho_2}} \\ -\frac{1}{\hat{\rho_1}\hat{\rho_2}} & \frac{1}{\hat{\rho_2}\hat{\rho_2}} \end{pmatrix} \tag{3.4.1}$$

Obviously, $|\mathbf{C}| = 0$ and $\mathbf{p}^T \cdot \mathbf{C} \cdot \mathbf{p} = (2\phi - 1)^2$ for $\rho_1^0 = \phi\hat{\rho_1}$, $\rho_2^0 = (1-\phi)\hat{\rho_2}$. The growth rates reduce to two modes labeled as $\alpha_{1,2}$. They are not necessary related to the $\alpha_{1,2}$ in the compressible model. Furthermore, when the quasi-incompressible mode reduces to the incompressible model, the coupled hydrodynamic modes vanishes, leading to one mode in α_1.

The analysis shows that the more constraints we have on the composition of the fluid mixture, the less coupled the equations are in the linear regime. In 3D models, the total number of growth rates will increase as the number of equations increases. But, the number of unstable modes will not change. In addition, the 1D perturbation analysis in wave numbers applies to multi-dimensional case as well. We will not omit the details for simplicity.

Chapter 4

Numerical scheme

We solve the governing equations for the binary compressible viscous fluid flows with local mass conservation law:

$$\begin{cases} \frac{\partial \rho_1}{\partial t} + \nabla \cdot (\rho_1 \mathbf{v}) = \nabla \cdot M_1 \cdot \nabla \mu_1 - \nabla \cdot M_1 \cdot \nabla \mu_2, \\ \frac{\partial \rho_2}{\partial t} + \nabla \cdot (\rho_2 \mathbf{v}) = -\nabla \cdot M_1 \cdot \nabla \mu_1 + \nabla \cdot M_1 \cdot \nabla \mu_2, \\ \frac{\partial (\rho \mathbf{v})}{\partial t} + \nabla \cdot (\rho \mathbf{v} v) = 2\nabla \cdot (\frac{1}{Re_s}\mathbf{D}) + \nabla(\frac{1}{Re_v}\nabla \cdot \mathbf{v}) - \rho_1 \nabla \mu_1 - \rho_2 \nabla \mu_2. \end{cases} \tag{4.0.1}$$

where

$$\begin{aligned} &\mu_1 = \frac{\delta f}{\delta \rho_1} = \frac{\partial f}{\partial \rho_1} - \kappa_{\rho_1 \rho_1} \Delta \rho_1 - \kappa_{\rho_1 \rho_2} \Delta \rho_2, \\ &\mu_2 = \frac{\delta f}{\delta \rho_2} = \frac{\partial f}{\partial \rho_2} - \kappa_{\rho_2 \rho_2} \Delta \rho_2 - \kappa_{\rho_1 \rho_2} \Delta \rho_1, \\ &\mathbf{D} = \tfrac{1}{2}(\nabla \mathbf{v} + (\nabla \mathbf{v})^T), \quad \frac{1}{Re_s} = \frac{\rho_1}{\rho}\frac{1}{Re_{s1}} + \frac{\rho_2}{\rho}\frac{1}{Re_{s2}}, \quad \frac{1}{Re_v} = \frac{\rho_1}{\rho}\frac{1}{Re_{v1}} + \frac{\rho_2}{\rho}\frac{1}{Re_{v2}}. \end{aligned} \tag{4.0.2}$$

4.1 Reformulation of the Model using Energy Quadratization

In order to use the Energy Quadratization (EQ) method to design numerical schemes, we need to reformulate the model equations. We first transform the energy of the system into a quadratic form

$$E_{total} = \int_V [\tfrac{1}{2}\rho \mathbf{v}^T \mathbf{v} + f] d\mathbf{x} = \int_V [\tfrac{1}{2}\mathbf{u}^T \mathbf{u} + q_1^2 + \tfrac{1}{2}\mathbf{p}^T \cdot \mathbf{K} \cdot \mathbf{p} - A] d\mathbf{x}. \tag{4.1.1}$$

where $\mathbf{u} = \sqrt{\rho}\mathbf{v}$, $q_1 = \sqrt{h(\rho_1, \rho_2, T) + A}$ and A is a constant such that $h(\rho_1, \rho_2, T) + A > 0$. We note that we can always find a constant A if the bulk free energy density function is bounded below. In addition, $\mathbf{p} = (\nabla \rho_1, \nabla \rho_2)^T$ and $\mathbf{K}$ is the coefficient

matrix of the conformational entropy

$$\mathbf{K} = \begin{pmatrix} \kappa_{\rho_1\rho_1} & \kappa_{\rho_1\rho_2} \\ \kappa_{\rho_1\rho_2} & \kappa_{\rho_2\rho_2} \end{pmatrix} > 0. \tag{4.1.2}$$

Using identity

$$\frac{\partial(\sqrt{\rho}\mathbf{u})}{\partial t} = \frac{1}{2\sqrt{\rho}}\frac{\partial \rho}{\partial t}\mathbf{u} + \sqrt{\rho}\frac{\partial \mathbf{u}}{\partial t} = -\frac{1}{2\sqrt{\rho}}\nabla\cdot(\sqrt{\rho}\mathbf{u})\mathbf{u} + \sqrt{\rho}\frac{\partial \mathbf{u}}{\partial t}, \tag{4.1.3}$$

we rewrite the governing equations into

$$\begin{cases} \frac{\partial \rho_1}{\partial t} + \nabla\cdot(\frac{\rho_1}{\sqrt{\rho}}\mathbf{u}) = \nabla\cdot M_1\cdot\nabla(\mu_1-\mu_2), \\ \frac{\partial \rho_2}{\partial t} + \nabla\cdot(\frac{\rho_2}{\sqrt{\rho}}\mathbf{u}) = -\nabla\cdot M_1\cdot\nabla(\mu_1-\mu_2), \\ \frac{\partial \mathbf{u}}{\partial t} + \frac{1}{2}(\frac{1}{\sqrt{\rho}}\nabla\cdot(\mathbf{u}\mathbf{u}) + \mathbf{u}\cdot\nabla\frac{\mathbf{u}}{\sqrt{\rho}}) = \frac{1}{\sqrt{\rho}}\nabla\cdot\sigma, \\ \frac{\partial q_1}{\partial t} = \frac{\partial q_1}{\partial \rho_1}\frac{\partial \rho_1}{\partial t} + \frac{\partial q_1}{\partial \rho_2}\frac{\partial \rho_2}{\partial t}, \end{cases} \tag{4.1.4}$$

where

$$\begin{aligned} &\sigma = \sigma^s + \sigma^e, \quad \sigma^s = 2\frac{1}{Re_s}\mathbf{D} + \frac{1}{Re_v}(\nabla\cdot\frac{\mathbf{u}}{\sqrt{\rho}})\mathbf{I}, \\ &\sigma^e = (f-\rho_1\mu_1-\rho_2\mu_2)\mathbf{I} - \frac{\partial f}{\partial\nabla\rho_1}\nabla\rho_1 - \frac{\partial f}{\partial\nabla\rho_2}\nabla\rho_2, \\ &\nabla\cdot\sigma = \nabla\cdot(\sigma^s+\sigma^e) = 2\nabla\cdot(\frac{1}{Re_s}\mathbf{D}) + \nabla(\frac{1}{Re_v}\nabla\cdot\frac{\mathbf{u}}{\sqrt{\rho}}) - \rho_1\nabla\mu_1 - \rho_2\nabla\mu_2, \\ &\mu_1 = \frac{\delta f}{\delta\rho_1} = \frac{\partial f}{\partial\rho_1} - \nabla\cdot\frac{\partial f}{\partial\nabla\rho_1} = 2q_1\frac{\partial q_1}{\partial\rho_1} - \kappa_{\rho_1\rho_1}\Delta\rho_1 - \kappa_{\rho_1\rho_2}\Delta\rho_2, \\ &\mu_2 = \frac{\delta f}{\delta\rho_2} = \frac{\partial f}{\partial\rho_2} - \nabla\cdot\frac{\partial f}{\partial\nabla\rho_2} = 2q_1\frac{\partial q_1}{\partial\rho_2} - \kappa_{\rho_2\rho_2}\Delta\rho_2 - \kappa_{\rho_1\rho_2}\Delta\rho_1, \\ &\mathbf{D} = \frac{1}{2}(\nabla\frac{\mathbf{u}}{\sqrt{\rho}} + (\nabla\frac{\mathbf{u}}{\sqrt{\rho}})^T), \quad \frac{1}{Re_s} = \frac{\rho_1}{\rho}\frac{1}{Re_{s1}} + \frac{\rho_2}{\rho}\frac{1}{Re_{s2}}, \quad \frac{1}{Re_v} = \frac{\rho_1}{\rho}\frac{1}{Re_{v1}} + \frac{\rho_2}{\rho}\frac{1}{Re_{v2}}. \end{aligned} \tag{4.1.5}$$

Remark 4.1.1. We define the inner product of two functions f and g as follows:

$$(f,g) = \int_V fg d\mathbf{x}. \tag{4.1.6}$$

Theorem 4.1.1. *System (4.1.4) is dissipative, and the corresponding energy dissipation rate is given by*

$$\begin{aligned} &\frac{\partial E}{\partial t} = -2(\frac{1}{Re_s}, \mathbf{D}:\mathbf{D}) - (\frac{1}{Re_v}\nabla\cdot\frac{\mathbf{u}}{\sqrt{\rho}}, \nabla\cdot\frac{\mathbf{u}}{\sqrt{\rho}}) \\ &-(\nabla\mu_1, \nabla\mu_2)\cdot\mathcal{M}\cdot(\nabla\mu_1,\nabla\mu_2)^T \le 0, \end{aligned} \tag{4.1.7}$$

where $Re_s, Re_v \geq 0, \mathcal{M} = \begin{pmatrix} M_1 & -M_1 \\ -M_1 & M_1 \end{pmatrix} \geq 0.$

Proof: By the definition of E, we have

$$\frac{\partial E}{\partial t} = \int_V \left[\mathbf{u}^T \frac{\partial \mathbf{u}}{\partial t} + 2q_1 \frac{\partial q_1}{\partial t} + (\nabla \rho_1, \nabla \rho_2) \cdot \mathbf{K} \cdot (\nabla \frac{\partial \rho_1}{\partial t}, \nabla \frac{\partial \rho_2}{\partial t})^T \right] d\mathbf{x}. \tag{4.1.8}$$

Taking the inner product of (4.1.4-3) with $\mathbf{u}$ and using integration by parts, we obtain

$$(\mathbf{u}, \frac{\partial \mathbf{u}}{\partial t}) = -2(\frac{1}{Re_s}, \mathbf{D} : \mathbf{D}) - (\frac{1}{Re_v} \nabla \cdot \frac{\mathbf{u}}{\sqrt{\rho}}, \nabla \cdot \frac{\mathbf{u}}{\sqrt{\rho}}) - (\mathbf{u}, \rho_1 \frac{1}{\sqrt{\rho}} \nabla \mu_1 + \rho_2 \frac{1}{\sqrt{\rho}} \nabla \mu_2). \tag{4.1.9}$$

Taking the inner product of (4.1.4-4) with $2q_1$, using the identities of μ_i, i= 1,2, and performing integration by parts, we obtain

$$\begin{aligned} &(2q_1, \frac{\partial q_1}{\partial t}) = -(\nabla \mu_1, \nabla \mu_2) \cdot \mathcal{M} \cdot (\nabla \mu_1, \nabla \mu_2)^T + (\frac{\rho_1}{\sqrt{\rho}} \mathbf{u}, \nabla \mu_1) + (\frac{\rho_2}{\sqrt{\rho}} \mathbf{u}, \nabla \mu_2) \\ &-(\nabla \rho_1, \nabla \rho_2) \cdot \mathbf{K} \cdot (\nabla \frac{\partial \rho_1}{\partial t}, \nabla \frac{\partial \rho_2}{\partial t})^T. \end{aligned} \tag{4.1.10}$$

Combining (4.1.9) and (4.1.10), we obtain

$$\begin{aligned} &\frac{\partial E}{\partial t} = -2(\frac{1}{Re_s}, \mathbf{D} : \mathbf{D}) - (\frac{1}{Re_v} \nabla \cdot \frac{\mathbf{u}}{\sqrt{\rho}}, \nabla \cdot \frac{\mathbf{u}}{\sqrt{\rho}}) \\ &-(\nabla \mu_1, \nabla \mu_2) \cdot \mathcal{M} \cdot (\nabla \mu_1, \nabla \mu_2)^T \leq 0 \end{aligned} \tag{4.1.11}$$

provided $\mathcal{M} \geq 0$.

We next design a second order energy stable numerical scheme based on the reformulated governing system of equations.

4.2 Linear, Second Order Energy Stable Numerical Scheme

4.2.1 Notations and Useful Lemmas

We first introduce some notations, finite difference operators and useful lemmas. Here, we follow the notations in [11, 53, 58]. Let $\Omega = [0, L_x] \times [0, L_y]$ be the computational domain with $L_x = h_x \times N_x$, $L_y = h_y \times N_y$, where N_x, N_y are positive integers, and h_x, h_y are spatial step sizes in the x and y direction, respectively. We define three

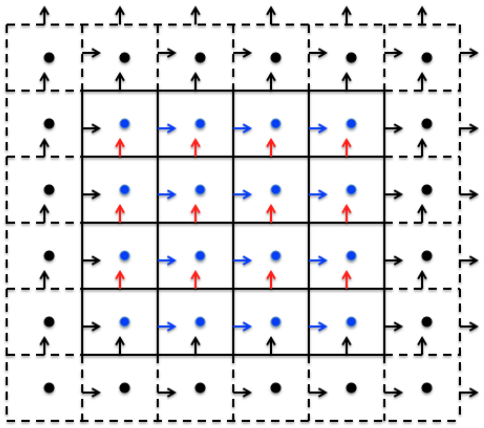

Figure 4.1 Staggered grid in 2D space.

sets for the grid points as follows

$$\begin{aligned} E_x &:= \{x_{i+1/2} = i \cdot h \quad | \quad i = 0, 1, \cdots, N_x\}, \\ C_x &:= \{x_i = (i - \tfrac{1}{2}) \cdot h \quad | \quad i = 1, \cdots, N_x\}, \\ C_{\overline{x}} &:= \{x_i = (i - \tfrac{1}{2}) \cdot h \quad | \quad i = 0, 1, \cdots, N_x, N_x + 1\}, \end{aligned} \tag{4.2.1}$$

where E_x is a uniform partition of $[0, L_x]$ of size N_x in the x-direction and its elements are called edge-centered points. The elements of C_x and $C_{\overline{x}}$ are called cell-centered points. The two points belonging to $C_{\overline{x}} \backslash C_x$ are called ghost points. Analogously, we define E_y as the uniform partition of $[0, L_y]$ of size N_y, called edge-centered points in the y-direction, and $C_y, C_{\overline{y}}$ the cell-centered points of the interval $[0, L_y]$. In Figure 4.1, we show the staggered grid in 2D space. In this paper, we discretize the variables with the Neumann boundary conditions at the cell-center and the ones with the Dirichlet boundary conditions at the edge-center. We define the corresponding

discrete function space on this staggered grid as follows

$$\begin{aligned}
&\mathcal{C}_{x\times y} := \{\phi : C_x \times C_y \to \mathcal{R}\}, \quad \mathcal{C}_{\overline{x}\times y} := \{\phi : C_{\overline{x}} \times C_y \to \mathcal{R}\},\\
&\mathcal{C}_{x\times \overline{y}} := \{\phi : C_x \times C_{\overline{y}} \to \mathcal{R}\}, \quad \mathcal{C}_{\overline{x}\times \overline{y}} := \{\phi : C_{\overline{x}} \times C_{\overline{y}} \to \mathcal{R}\},\\
&\mathcal{E}^{ew}_{x\times y} := \{\phi : E_x \times C_y \to \mathcal{R}\}, \quad \mathcal{E}^{ew}_{x\times \overline{y}} := \{\phi : E_x \times C_{\overline{y}} \to \mathcal{R}\},\\
&\mathcal{E}^{ns}_{x\times y} := \{\phi : C_x \times E_y \to \mathcal{R}\}, \quad \mathcal{E}^{ns}_{\overline{x}\times y} := \{\phi : C_{\overline{x}} \times E_y \to \mathcal{R}\},\\
&\mathcal{V}_{x\times y} := \{\phi : E_x \times E_y \to \mathcal{R}\}.
\end{aligned} \tag{4.2.2}$$

$\mathcal{C}_{x\times y}, \mathcal{C}_{\overline{x}\times y}, \mathcal{C}_{x\times \overline{y}}$ and $\mathcal{C}_{\overline{x}\times \overline{y}}$ are the sets for discrete cell-centered functions, and $\mathcal{E}^{ew}_{x\times y}, \mathcal{E}^{ns}_{x\times y}$ east-west and north-south edge-centered functions, respectively.

Average and Difference Operators

Assume $u, r \in \mathcal{E}^{ew}_{x\times y} \cup \mathcal{E}^{ew}_{x\times \overline{y}}$, $v, w \in \mathcal{E}^{ns}_{x\times y} \cup \mathcal{E}^{ns}_{\overline{x}\times y}$, $\phi, \psi \in \mathcal{C}_{x\times y} \cup \mathcal{C}_{\overline{x}\times y} \cup \mathcal{C}_{x\times \overline{y}} \cup \mathcal{C}_{\overline{x}\times \overline{y}}$ and $f \in \mathcal{V}_{x\times y}$, we define the east-west-edge-to-center average and difference operator as $a_x, d_x : \mathcal{E}^{ew}_{x\times \overline{y}} \cup \mathcal{V}_{x\times y} \to \mathcal{C}_{x\times \overline{y}} \cup \mathcal{E}^{ns}_{x\times y}$ component-wise as follows

$$\begin{aligned}
&a_x u_{i,j} := \tfrac{1}{2}(u_{i+\frac{1}{2},j} + u_{i-\frac{1}{2},j}), \quad d_x u_{i,j} := \tfrac{1}{h_x}(u_{i+\frac{1}{2},j} - u_{i-\frac{1}{2},j}),\\
&a_x f_{i,j+\frac{1}{2}} := \tfrac{1}{2}(f_{i+\frac{1}{2},j+\frac{1}{2}} + f_{i-\frac{1}{2},j+\frac{1}{2}}), \quad d_x f_{i,j+\frac{1}{2}} := \tfrac{1}{h_x}(f_{i+\frac{1}{2},j+\frac{1}{2}} - f_{i-\frac{1}{2},j+\frac{1}{2}}).
\end{aligned} \tag{4.2.3}$$

The north-south-edge-to-center average and difference operators are defined as $a_y, d_y : \mathcal{E}^{ns}_{\overline{x}\times y} \cup \mathcal{V}_{x\times y} \to \mathcal{C}_{\overline{x}\times y} \cup \mathcal{E}^{ew}_{x\times y}$ component-wise as follows

$$\begin{aligned}
&a_y v_{i,j} := \tfrac{1}{2}(v_{i,j+\frac{1}{2}} + v_{i,j-\frac{1}{2}}), \quad d_y v_{i,j} := \tfrac{1}{h_y}(v_{i,j+\frac{1}{2}} - v_{i,j-\frac{1}{2}}),\\
&a_y f_{i+\frac{1}{2},j} := \tfrac{1}{2}(f_{i+\frac{1}{2},j+\frac{1}{2}} + f_{i+\frac{1}{2},j-\frac{1}{2}}), \quad d_y f_{i+\frac{1}{2},j} := \tfrac{1}{h_y}(f_{i+\frac{1}{2},j+\frac{1}{2}} - f_{i+\frac{1}{2},j-\frac{1}{2}}).
\end{aligned} \tag{4.2.4}$$

We denote the center-to-east-west-edge average and difference operators as $A_x, D_x : \mathcal{C}_{\overline{x}\times \overline{y}} \cup \mathcal{E}^{ns}_{\overline{x}\times y} \to \mathcal{E}^{ew}_{x\times \overline{y}} \cup \mathcal{V}_{x\times y}$ in component-wise forms:

$$\begin{aligned}
&A_x \phi_{i+\frac{1}{2},j} := \tfrac{1}{2}(\phi_{i+1,j} + \phi_{i,j}), \quad D_x \phi_{i+\frac{1}{2},j} := \tfrac{1}{h_x}(\phi_{i+1,j} - \phi_{i,j}),\\
&A_x v_{i+\frac{1}{2},j+\frac{1}{2}} := \tfrac{1}{2}(v_{i+1,j+\frac{1}{2}} + v_{i,j+\frac{1}{2}}), \quad D_x v_{i+\frac{1}{2},j+\frac{1}{2}} := \tfrac{1}{h_x}(v_{i+1,j+\frac{1}{2}} - v_{i,j+\frac{1}{2}}).
\end{aligned} \tag{4.2.5}$$

Analogously, the center-to-north-south-edge average and difference operator are defined as $A_y, D_y : \mathcal{C}_{\overline{x}\times \overline{y}} \cup \mathcal{E}^{ew}_{x\times \overline{y}} \to \mathcal{E}^{ns}_{\overline{x}\times y} \cup \mathcal{V}_{x\times y}$ in component-wise forms:

$$\begin{aligned}
&A_y \phi_{i,j+\frac{1}{2}} := \tfrac{1}{2}(\phi_{i,j+1} + \phi_{i,j}), \quad D_y \phi_{i,j+\frac{1}{2}} := \tfrac{1}{h_y}(\phi_{i,j+1} - \phi_{i,j}),\\
&A_y u_{i+\frac{1}{2},j+\frac{1}{2}} := \tfrac{1}{2}(u_{i+\frac{1}{2},j+1} + u_{i+\frac{1}{2},j}), \quad D_y u_{i+\frac{1}{2},j+\frac{1}{2}} := \tfrac{1}{h_y}(u_{i+\frac{1}{2},j+1} - u_{i+\frac{1}{2},j}).
\end{aligned} \tag{4.2.6}$$

The standard 2D discrete Laplacian operator is defined as $\Delta_h : \mathcal{E}^{ew}_{x\times\overline{y}} \cup \mathcal{E}^{ns}_{\overline{x}\times y} \cup \mathcal{C}_{\overline{x}\times\overline{y}} \to \mathcal{E}^{ew}_{x\times y} \cup \mathcal{E}^{ns}_{x\times y} \cup \mathcal{C}_{x\times y}$:

$$\begin{aligned} &\Delta_h u := D_x(d_x u) + d_y(D_y u), \quad \Delta_h v := d_x(D_x v) + D_y(d_y v), \\ &\Delta_h \phi := d_x(D_x \phi) + d_y(D_y \phi). \end{aligned} \tag{4.2.7}$$

Boundary Conditions

The homogenous Neumann boundary conditions are discretized as follows

$$\begin{aligned} &\phi_{0,j} = \phi_{1,j}, \quad \phi_{N_x,j} = \phi_{N_x+1,j}, \quad j = 0, 1, 2, \cdots, N_y + 1, \\ &\phi_{i,0} = \phi_{i,1}, \quad \phi_{i,N_y} = \phi_{i,N_y+1}, \quad i = 0, 1, 2, \cdots, N_x + 1. \end{aligned} \tag{4.2.8}$$

We denote it as $\mathbf{n} \cdot \nabla_h \phi|_{\partial V} = 0$.

The homogeneously Dirichlet boundary conditions are discretized as follows

$$\begin{aligned} &u_{\frac{1}{2},j} = u_{N_x+\frac{1}{2},j} = 0, \quad j = 1, 2, \cdots, N_y, \\ &A_y u_{i+\frac{1}{2},\frac{1}{2}} = A_y u_{i+\frac{1}{2},N_y+\frac{1}{2}} = 0, \quad i = 0, 1, 2, \cdots, N_x, \\ &v_{i,\frac{1}{2}} = v_{i,N_y+\frac{1}{2}} = 0, \quad j = 1, 2, \cdots, N_x, \\ &A_x v_{\frac{1}{2},j+\frac{1}{2}} = A_x v_{N_x+\frac{1}{2},j+\frac{1}{2}} = 0, \quad j = 0, 1, 2, \cdots, N_y, \end{aligned} \tag{4.2.9}$$

We denote it as $u_h|_{\partial V} = 0$ and $v_h|_{\partial V} = 0$.

If $f \in \mathcal{V}_{x\times y}$ satisfies homogenous Dirichelet boundary condition, we have

$$f_{\frac{1}{2},j+\frac{1}{2}} = f_{N_x+\frac{1}{2},j+\frac{1}{2}} = f_{i+\frac{1}{2},\frac{1}{2}} = f_{i+\frac{1}{2},N_y+\frac{1}{2}} = 0. \tag{4.2.10}$$

where $i = 0, 1, 2, \cdots, N_x, j = 0, 1, 2, \cdots, N_y$. We denote is as $f_h|_{\partial V} = 0$.

Inner products and norms

We defined the following inner products for discrete functions

$$\begin{aligned} &(\phi, \psi)_2 := h_x h_y \textstyle\sum_{i=1}^{N_x} \sum_{j=1}^{N_y} \phi_{i,j} \psi_{i,j}, \quad [u, r]_{ew} := (a_x(ur), 1)_2, \\ &[v, w]_{ns} := (a_y(uw), 1)_2, \quad (f, g)_{vc} := (a_x(a_y(fg)), 1)_2, \\ &(\nabla\phi, \nabla\psi)_h := [D_x(\phi), D_x(\psi)]_{ew} + [D_y(\phi), D_y(\psi)]_{ns}, \end{aligned} \tag{4.2.11}$$

The corresponding norms are defined as follows

$$\begin{aligned} \|\phi\|_2 &:= (\phi,\phi)_2^{\frac{1}{2}}, \quad \|u\|_{ew} := [u,u]_{ew}^{\frac{1}{2}}, \\ \|v\|_{ns} &:= [v,v]_{ns}^{\frac{1}{2}}, \quad \|f\|_{vc} := (f,f)_{vc}^{\frac{1}{2}}. \end{aligned} \tag{4.2.12}$$

For $\phi = \mathcal{C}_{\overline{x}\times\overline{y}}$, we define $\|\nabla\phi\|_2$ as

$$\|\nabla\phi\|_2 := \sqrt{\|D_x\phi\|_{ew}^2 + \|D_y\phi\|_{ns}^2}, \tag{4.2.13}$$

For the edge-centered velocity vector $\mathbf{v} = (u,v)$, $u \in \mathcal{E}_{x\times\overline{y}}^{ew}, v \in \mathcal{E}_{\overline{x}\times y}^{ns}$, we define $\|\mathbf{v}\|_2, \|\nabla\mathbf{v}\|_2$ as

$$\begin{aligned} &\|\mathbf{v}\|_2 := \sqrt{\|u\|_{ew}^2 + \|v\|_{ns}^2}, \quad \|\nabla\mathbf{v}\|_2 := \sqrt{\|d_x u\|_2^2 + \|D_y u\|_{vc}^2 + \|D_x v\|_{vc}^2 + \|d_y v\|_2^2}, \\ &\|\mathbf{D}\|_2 := \sqrt{\|d_x u\|_2^2 + \tfrac{1}{2}\|D_y u\|_{vc}^2 + \tfrac{1}{2}\|D_x v\|_{vc}^2 + (D_y u, D_x v)_{vc} + \|d_y v\|_2^2}, \\ &(\phi, \mathbf{D}:\mathbf{D})_2 := \sqrt{(\phi,(d_x u)^2)_2 + (\phi,(d_y v)^2)_2 + A_0}, \\ &A_0 = \tfrac{1}{2}(A_x(A_y\phi),(D_y u)^2)_{vc} + \tfrac{1}{2}(A_x(A_y\phi),(D_x v)^2)_{vc} + (A_x(A_y\phi)D_y u, D_x v)_{vc}. \end{aligned} \tag{4.2.14}$$

Where $\mathbf{D} = \frac{1}{2}(\nabla\mathbf{v} + \nabla\mathbf{v}^T)$. From these definitions, we obtain the following lemmas [25]:

Lemma 4.2.1. *(Summation by parts): If $\phi \in \mathcal{C}_{\overline{x}\times\overline{y}}$, $u \in \mathcal{E}_{x\times y}^{ew}$, $v \in \mathcal{E}_{x\times y}^{ns}$, and $u_h|_{\partial V} = 0$ and $v_h|_{\partial V} = 0$, then*

$$\begin{aligned} &[A_x\phi, u]_{ew} = (\phi, a_x u)_2, \quad [A_y\phi, v]_{ns} = (\phi, a_y v)_2, \\ &[D_x\phi, u]_{ew} + (\phi, d_x u)_2 = 0, \quad [D_y\phi, v]_{ns} + (\phi, d_y v)_2 = 0, \end{aligned} \tag{4.2.15}$$

Lemma 4.2.2. *If $f \in \mathcal{V}_{x\times y}$, and $f_h|_{\partial V} = 0$, $u \in \mathcal{E}_{x\times\overline{y}}^{ew}$, $v \in \mathcal{E}_{\overline{x}\times y}^{ns}$, then*

$$[a_y f, u]_{ew} = (f, A_y u)_{vc}, \quad [a_x f, v]_{ns} = (f, A_x v)_{vc}. \tag{4.2.16}$$

Lemma 4.2.3. *If $f \in \mathcal{V}_{x\times y}$, $u \in \mathcal{E}_{x\times\overline{y}}^{ew}$, $v \in \mathcal{E}_{\overline{x}\times y}^{ns}$, and $u_h|_{\partial V} = 0$ and $v_h|_{\partial V} = 0$, then*

$$[d_y f, u]_{ew} + (f, D_y u)_{vc} = 0, \quad [d_x f, v]_{ns} + (f, D_x v)_{vc} = 0. \tag{4.2.17}$$

With these notations and lemmas, we are ready to introduce the fully-discrete numerical scheme in the following section.

4.2.2 Semi-discrete scheme in time

First, we discretize the governing equations using Crank-Nicolson method in time. We denote

$$\delta_t(\cdot)^{n+1/2} = \frac{1}{\Delta t}((\cdot)^{n+1} - (\cdot)^n), \qquad \overline{(\cdot)}^{n+1/2} = \frac{1}{2}(3(\cdot)^n - (\cdot)^{n-1}). \tag{4.2.18}$$

and

$$\begin{aligned}
&\mu_1^{n+1/2} = 2q_1^{n+1/2}\overline{\frac{\partial q_1}{\partial \rho_1}}^{n+1/2} - \kappa_{\rho_1\rho_1}\Delta\rho_1^{n+1/2} - \kappa_{\rho_1\rho_2}\Delta\rho_2^{n+1/2},\\
&\mu_2^{n+1/2} = 2q_1^{n+1/2}\overline{\frac{\partial q_1}{\partial \rho_2}}^{n+1/2} - \kappa_{\rho_1\rho_2}\Delta\rho_1^{n+1/2} - \kappa_{\rho_2\rho_2}\Delta\rho_2^{n+1/2},\\
&\mathbf{D}^{n+1/2} = \frac{1}{2}(\nabla(\overline{\frac{1}{\sqrt{\rho}}}^{n+1/2}\mathbf{u}^{n+1/2}) + \nabla(\overline{\frac{1}{\sqrt{\rho}}}^{n+1/2}\mathbf{u}^{n+1/2})^T),\\
&\frac{1}{Re_s} = \overline{\frac{\rho_1}{\rho}}^{n+1/2}\frac{1}{Re_{s1}} + \overline{\frac{\rho_2}{\rho}}^{n+1/2}\frac{1}{Re_{s2}},\\
&\frac{1}{Re_v} = \overline{\frac{\rho_1}{\rho}}^{n+1/2}\frac{1}{Re_{v1}} + \overline{\frac{\rho_2}{\rho}}^{n+1/2}\frac{1}{Re_{v2}}.
\end{aligned} \tag{4.2.19}$$

The second order algorithm is given below.

Algorithm 1.

$$\begin{cases}
\delta_t\rho_1^{n+1/2} + \nabla\cdot(\overline{\rho_1}^{n+1/2}\overline{\frac{1}{\sqrt{\rho}}}^{n+1/2}\mathbf{u}^{n+1/2})\\
= \nabla\cdot M_1\cdot\nabla\mu_1^{n+1/2} - \nabla\cdot M_1\cdot\nabla\mu_2^{n+1/2},\\
\delta_t\rho_2^{n+1/2} + \nabla\cdot(\overline{\rho_2}^{n+1/2}\overline{\frac{1}{\sqrt{\rho}}}^{n+1/2}\mathbf{u}^{n+1/2})\\
= -\nabla\cdot M_1\cdot\nabla\mu_1^{n+1/2} + \nabla\cdot M_1\cdot\nabla\mu_2^{n+1/2},\\
\delta_t\mathbf{u}^{n+1/2} + \frac{1}{2}(\overline{\frac{1}{\sqrt{\rho}}}^{n+1/2}\nabla\cdot(\overline{\mathbf{u}}^{n+1/2}\mathbf{u}^{n+1/2})\\
+\overline{\mathbf{u}}^{n+1/2}\cdot\nabla(\overline{\frac{1}{\sqrt{\rho}}}^{n+1/2}\mathbf{u}^{n+1/2})) =\\
\overline{\frac{1}{\sqrt{\rho}}}^{n+1/2}(2\nabla\cdot(\frac{1}{Re_s}\mathbf{D}^{n+1/2}) + \nabla(\frac{1}{Re_v}\nabla\cdot(\overline{\frac{1}{\sqrt{\rho}}}^{n+1/2}\mathbf{u}^{n+1/2}))\\
-\overline{\rho_1}^{n+1/2}\nabla\mu_1^{n+1/2} - \overline{\rho_2}^{n+1/2}\nabla{\mu_2}^{n+1/2}),\\
\delta_t q_1^{n+1/2} = \overline{\frac{\partial q_1}{\partial\rho_1}}^{n+1/2}\delta_t\rho_1^{n+1/2} + \overline{\frac{\partial q_1}{\partial\rho_2}}^{n+1/2}\delta_t\rho_2^{n+1/2},
\end{cases} \tag{4.2.20}$$

For the scheme, we have the following theorem.

Theorem 4.2.1. *Scheme* (4.2.20) *is unconditional energy stable, and satisfies the following discrete energy identity*

$$\begin{aligned}
&\tfrac{E^{n+1}-E^n}{\Delta t} = -2(\tfrac{1}{Re_s}, \boldsymbol{D}^{n+1/2} : \boldsymbol{D}^{n+1/2}) \\
&-(\tfrac{1}{Re_v}\nabla\cdot(\overline{\tfrac{1}{\sqrt{\rho}}}^{n+1/2}\boldsymbol{u}^{n+1/2}), \nabla\cdot(\overline{\tfrac{1}{\sqrt{\rho}}}^{n+1/2}\boldsymbol{u}^{n+1/2})) \\
&-(\nabla\mu_1^{n+1/2}, \nabla\mu_2^{n+1/2})\cdot\mathcal{M}\cdot(\nabla\mu_1^{n+1/2}, \nabla\mu_2^{n+1/2})^T < 0,
\end{aligned} \tag{4.2.21}$$

Where

$$E^n = \textstyle\int_V [\frac{1}{2}||\boldsymbol{u}^n||^2 + (q_1^n)^2 + \frac{1}{2}(\boldsymbol{p}^n)^T\cdot\boldsymbol{K}^n\cdot\boldsymbol{p}^n - A]d\boldsymbol{x}. \tag{4.2.22}$$

and $\mathbf{p}^n = (\nabla\rho_1^n, \nabla\rho_2^n)$.

Remark 4.2.1. We note that a useful identity in the proof of the theorem.

$$(\mathbf{u}^{n+1/2}, \tfrac{1}{2}(\overline{\tfrac{1}{\sqrt{\rho}}}^{n+1/2}\nabla\cdot(\overline{\mathbf{u}}^{n+1/2}\mathbf{u}^{n+1/2}) + \overline{\mathbf{u}}^{n+1/2}\cdot\nabla(\overline{\tfrac{1}{\sqrt{\rho}}}^{n+1/2}\mathbf{u}^{n+1/2}))) = 0. \tag{4.2.23}$$

Proof: By the definition of E^n, we have

$$\begin{aligned}
&\tfrac{E^{n+1}-E^n}{\Delta t} = \textstyle\int_V \mathbf{u}^{n+1/2}\delta_t\mathbf{u}^{n+1/2} + 2q_1^{n+1/2}\delta_t q_1^{n+1/2} + \kappa_{\rho_1\rho_1}\nabla\rho^{n+1/2}\delta_t\nabla\rho_1^{n+1/2} \\
&+\kappa_{\rho_2\rho_2}\nabla\rho_2^{n+1/2}\delta_t\nabla\rho_2^{n+1/2} + \kappa_{\rho_1\rho_2}[\nabla\rho_1^{n+1/2}\delta_t\nabla\rho_2^{n+1/2} + \nabla\rho_2^{n+1/2}\delta_t\nabla\rho_1^{n+1/2}]d\mathbf{x},
\end{aligned} \tag{4.2.24}$$

Taking the inner product of (4.2.20)-3 with $\mathbf{u}^{n+1/2}$, using identity (4.2.23), and performing integration by parts, we obtain

$$\begin{aligned}
&(\mathbf{u}^{n+1/2}, \delta_t\mathbf{u}^{n+1/2}) = -2(\tfrac{1}{Re_s}\mathbf{D}^{n+1/2} : \mathbf{D}^{n+1/2}) \\
&-(\tfrac{1}{Re_v}\nabla\cdot(\overline{\tfrac{1}{\sqrt{\rho}}}^{n+1/2}\mathbf{u}^{n+1/2}), \nabla\cdot(\overline{\tfrac{1}{\sqrt{\rho}}}^{n+1/2}\mathbf{u}^{n+1/2})) \\
&-(\mathbf{u}^{n+1/2}, \overline{\tfrac{1}{\sqrt{\rho}}}^{n+1/2}\overline{\rho_1}^{n+1/2}\nabla\mu_1^{n+1/2} + \overline{\tfrac{1}{\sqrt{\rho}}}^{n+1/2}\overline{\rho_2}^{n+1/2}\nabla{\mu_2}^{n+1/2})).
\end{aligned} \tag{4.2.25}$$

Taking the inner product of (4.2.20-4) with $2q_1^{n+\frac{1}{2}}$, using (4.2.20-1,2), and performing integration by parts, we obtain

$$\begin{aligned}
&2(q_1^{n+1/2}, \delta_t q_1^{n+1/2}) = (\overline{\tfrac{1}{\sqrt{\rho}}}^{n+1/2}\overline{\rho_1}^{n+1/2}, \nabla{\mu_1}^{n+1/2}) + (\overline{\rho_2}^{n+1/2}\overline{\tfrac{1}{\sqrt{\rho}}}^{n+1/2}, \nabla{\mu_2}^{n+1/2}) \\
&-\kappa_{\rho_1\rho_1}\nabla\rho_1^{n+1/2}\delta_t\nabla\rho_1^{n+1/2} - \kappa_{\rho_2\rho_2}\nabla\rho_2^{n+1/2}\delta_t\nabla\rho_2^{n+1/2} \\
&-\kappa_{\rho_1\rho_2}[\nabla\rho_1^{n+1/2}\delta_t\nabla\rho_2^{n+1/2} + \nabla\rho_2^{n+1/2}\delta_t\nabla\rho_1^{n+1/2}] \\
&-(\nabla\mu_1^{n+1/2}, \nabla\mu_2^{n+1/2})\cdot\mathcal{M}\cdot(\nabla\mu_1^{n+1/2}, \nabla\mu_2^{n+1/2})^T.
\end{aligned} \tag{4.2.26}$$

Utilizing (4.2.24), (4.2.25) and (4.2.26), we arrive at the conclusion

$$\begin{aligned}
&\tfrac{E^{n+1}-E^n}{\Delta t} = -2(\tfrac{1}{Re_s}\mathbf{D}^{n+1/2} : \mathbf{D}^{n+1/2}) \\
&-(\tfrac{1}{Re_v}\nabla\cdot(\overline{\tfrac{1}{\sqrt{\rho}}}^{n+1/2}\mathbf{u}^{n+1/2}), \nabla\cdot(\overline{\tfrac{1}{\sqrt{\rho}}}^{n+1/2}\mathbf{u}^{n+1/2})) \\
&-(\nabla\mu_1^{n+1/2}, \nabla\mu_2^{n+1/2})\cdot\mathcal{M}\cdot(\nabla\mu_1^{n+1/2}, \nabla\mu_2^{n+1/2})^T \le 0
\end{aligned} \tag{4.2.27}$$

provided $\mathcal{M} \ge 0$.

4.2.3 Fully Discrete Numerical Scheme

Firstly, let's introduce two denotations as follows

$$\begin{aligned}
g_{v1} &= A_x(\overline{\tfrac{1}{\sqrt{\rho}}}^{n+1/2})(2D_x(\tfrac{1}{Re_s^{n+1/2}}d_x(A_x(\overline{\tfrac{1}{\sqrt{\rho}}}^{n+1/2})u^{n+1/2})) \\
&+d_y(A_x(A_y\tfrac{1}{Re_s^{n+1/2}})D_y(A_x(\overline{\tfrac{1}{\sqrt{\rho}}}^{n+1/2})u^{n+1/2}))) \\
&+A_x(\overline{\tfrac{1}{\sqrt{\rho}}}^{n+1/2})d_y(A_x(A_y\tfrac{1}{Re_s^{n+1/2}})D_x(A_y(\overline{\tfrac{1}{\sqrt{\rho}}}^{n+1/2})v^{n+1/2})) \\
&+A_x(\overline{\tfrac{1}{\sqrt{\rho}}}^{n+1/2})D_x(\tfrac{1}{Re_v^{n+1/2}}d_x(A_x(\overline{\tfrac{1}{\sqrt{\rho}}}^{n+1/2})u^{n+1/2})) \\
&+A_x(\overline{\tfrac{1}{\sqrt{\rho}}}^{n+1/2})D_x(\tfrac{1}{Re_v^{n+1/2}}d_y(A_y(\overline{\tfrac{1}{\sqrt{\rho}}}^{n+1/2})v^{n+1/2})) \\
&-A_x(\overline{\rho_1}^{n+1/2}\overline{\tfrac{1}{\sqrt{\rho}}}^{n+1/2})D_x(\mu_1^{n+1/2}) - A_x(\overline{\rho_2}^{n+1/2}\overline{\tfrac{1}{\sqrt{\rho}}}^{n+1/2})D_x(\mu_2^{n+1/2}),
\end{aligned} \tag{4.2.28}$$

$$\begin{aligned}
g_{v2} &= A_y(\overline{\tfrac{1}{\sqrt{\rho}}}^{n+1/2})(d_x(A_x(A_y\tfrac{1}{Re_s^{n+1/2}})D_x(A_y(\overline{\tfrac{1}{\sqrt{\rho}}}^{n+1/2})v^{n+1/2})) \\
&+2D_y(\tfrac{1}{Re_s^{n+1/2}}d_y(A_y(\overline{\tfrac{1}{\sqrt{\rho}}}^{n+1/2})v^{n+1/2}))) \\
&+A_y(\overline{\tfrac{1}{\sqrt{\rho}}}^{n+1/2})d_x(A_x(A_y\tfrac{1}{Re_s^{n+1/2}})D_y(A_x(\overline{\tfrac{1}{\sqrt{\rho}}}^{n+1/2})u^{n+1/2})) \\
&+A_y(\overline{\tfrac{1}{\sqrt{\rho}}}^{n+1/2})D_y(\tfrac{1}{Re_v^{n+1/2}}d_x(A_x(\tfrac{1}{\sqrt{\rho}})u^{n+1/2})) \\
&+A_y(\overline{\tfrac{1}{\sqrt{\rho}}}^{n+1/2})D_y(\tfrac{1}{Re_v^{n+1/2}}d_y(A_y(\overline{\tfrac{1}{\sqrt{\rho}}}^{n+1/2})v^{n+1/2})) \\
&-A_y(\overline{\rho_1}^{n+1/2}\overline{\tfrac{1}{\sqrt{\rho}}}^{n+1/2})D_y(\mu_1^{n+1/2}) - A_y(\overline{\rho_2}^{n+1/2}\overline{\tfrac{1}{\sqrt{\rho}}}^{n+1/2})D_y(\mu_2^{n+1/2}).
\end{aligned} \tag{4.2.29}$$

Then, we discretize the semidiscrete equations in (4.2.20) using the second order finite difference discretization on staggered grids in space to obtain a fully discrete scheme as follows

Algorithm 2.

$$
\begin{cases}
\Big\{\delta_t\rho_1^{n+1/2} + d_x(A_x(\overline{\rho}_1^{n+1/2}\overline{\frac{1}{\sqrt{\rho}}}^{n+1/2})u^{n+1/2}) + d_y(A_y(\overline{\rho}_1^{n+1/2}\overline{\frac{1}{\sqrt{\rho}}}^{n+1/2})v^{n+1/2}) = \\
M_1\Delta_h\mu_1^{n+1/2} - M_1\Delta_h\mu_2^{n+1/2}\Big\}|_{i,j}, i = 1,\cdots,N_x, j = 1,\cdots,N_y, \\
\\
\Big\{\delta_t\rho_2^{n+1/2} + d_x(A_x(\overline{\rho}_2^{n+1/2}\overline{\frac{1}{\sqrt{\rho}}}^{n+1/2})u^{n+1/2}) + d_y(A_y(\overline{\rho}_2^{n+1/2}\overline{\frac{1}{\sqrt{\rho}}}^{n+1/2})v^{n+1/2}) = \\
-M_1\Delta_h\mu_1^{n+1/2} + M_1\Delta_h\mu_2^{n+1/2}\Big\}|_{i,j}, i = 1,\cdots,N_x, j = 1,\cdots,N_y, \\
\\
\Big\{\delta_t u^{n+1/2} + \frac{1}{2}(\overline{u}^{n+1/2}D_x(\overline{\frac{1}{\sqrt{\rho}}}^{n+1/2}a_x u^{n+1/2}) \\
+A_x(\overline{\frac{1}{\sqrt{\rho}}}^{n+1/2}d_x(\overline{u}^{n+1/2}u^{n+1/2}))) \\
+\frac{1}{2}(a_x(A_x\overline{v}^{n+1/2}D_y(A_x(\overline{\frac{1}{\sqrt{\rho}}}^{n+1/2})u^{n+1/2})) \\
+A_x(\overline{\frac{1}{\sqrt{\rho}}}^{n+1/2})d_y(A_y u^{n+1/2}A_x(\overline{v}^{n+1/2})) \\
= g_{v1}\Big\}|_{i+\frac{1}{2},j}, i = 1,\cdots,N_x-1, j = 1,\cdots,N_y, \\
\\
\Big\{\delta_t v^{n+1/2} + \frac{1}{2}(a_x(A_y\overline{u}^{n+1/2}D_x(A_y(\overline{\frac{1}{\sqrt{\rho}}}^{n+1/2})v^{n+1/2})) \\
+A_y(\overline{\frac{1}{\sqrt{\rho}}}^{n+1/2})d_x(A_y\overline{u}^{n+1/2}A_x v^{n+1/2})) \\
+\frac{1}{2}(\overline{v}^{n+1/2}D_y(\overline{\frac{1}{\sqrt{\rho}}}^{n+1/2}a_y v^{n+1/2}) + A_y(\overline{\frac{1}{\sqrt{\rho}}}^{n+1/2}d_y(\overline{v}^{n+1/2}v^{n+1/2}))) \\
= g_{v2}\Big\}|_{i,j+\frac{1}{2}}, i = 1,\cdots,N_x, j = 1,\cdots,N_y-1, \\
\\
\Big\{\delta_t q_1^{n+1/2} = \overline{\frac{\partial q_1}{\partial\rho_1}}^{n+1/2}\delta_t\rho_1^{n+1/2} + \overline{\frac{\partial q_1}{\partial\rho_2}}^{n+1/2}\delta_t\rho_2^{n+1/2}\Big\}|_{i,j}, \\
i = 1,\cdots,N_x, j = 1,\cdots,N_y,
\end{cases}
\tag{4.2.30}
$$

For any time step t_n, $\rho_i^n, \mu_i^n, i = 1, 2$ and q_1^n satisfy discrete homogeneous Neumann boundary conditions (4.2.8), u^n, v^n satisfy the discrete homogeneous Dirichlet

boundary conditions (4.2.9). The discrete Reynolds numbers are defined as follows

$$\begin{aligned}&\{\frac{1}{Re_s^{n+1/2}} = \overline{(\frac{\rho_1}{\rho})}^{n+1/2}\frac{1}{Re_{s1}} + \overline{(\frac{\rho_2}{\rho})}^{n+1/2}\frac{1}{Re_{s2}}\}|_{i,j}, i = 1, \cdots, N_x, j = 1, \cdots, N_y,\\ &\{\frac{1}{Re_v^{n+1/2}} = \overline{(\frac{\rho_1}{\rho})}^{n+1/2}\frac{1}{Re_{v1}} + \overline{(\frac{\rho_2}{\rho})}^{n+1/2}\frac{1}{Re_{v2}}\}|_{i,j}, i = 1, \cdots, N_x, j = 1, \cdots, N_y.\end{aligned} \tag{4.2.31}$$

Theorem 4.2.2. *Scheme (4.2.30) is unconditionally energy stable, and the discrete total energy satisfies the following identity*

$$\begin{aligned}&\frac{E_h^{n+1}-E_h^n}{\Delta t} = -2(\frac{1}{Re_s}, \boldsymbol{D}_h^{n+1/2} : \boldsymbol{D}_h^{n+1/2})_2 - (\frac{1}{Re_v}tr(\boldsymbol{D}_h^{n+1/2}), tr(\boldsymbol{D}_h^{n+1/2}))_2\\ &-M_1(\nabla(\mu_1^{n+1/2} - \mu_2^{n+1/2}), \nabla(\mu_1^{n+1/2} - \mu_2^{n+1/2}))_2 \le 0,\end{aligned} \tag{4.2.32}$$

where

$$\begin{aligned}&E_h^n = \tfrac{1}{2}[u^n, u^n]_{ew} + \tfrac{1}{2}[v^n, v^n]_{ns} + (q_1^n, q_1^n)_2 - (A, 1)_2\\ &+\tfrac{1}{2}\kappa_{\rho_1\rho_1}(\nabla\rho_1^n, \nabla\rho_1^n)_h + \tfrac{1}{2}\kappa_{\rho_2\rho_2}(\nabla\rho_2^n, \nabla\rho_2^n)_h + \kappa_{\rho_1\rho_2}(\nabla\rho_1^n, \nabla\rho_2^n)_h.\end{aligned} \tag{4.2.33}$$

and

$$\mathbf{D}_h^{n+1/2} = \begin{pmatrix} d_x(A_x(\overline{\frac{1}{\sqrt{\rho}}}^{n+1/2})u^{n+1/2})) & \frac{1}{2}S \\ \frac{1}{2}S & d_y(A_y(\overline{\frac{1}{\sqrt{\rho}}}^{n+1/2})v^{n+1/2})) \end{pmatrix} \tag{4.2.34}$$

where $S = D_x(A_y(\overline{\frac{1}{\sqrt{\rho}}}^{n+1/2})v^{n+1/2}) + D_y(A_x(\overline{\frac{1}{\sqrt{\rho}}}^{n+1/2})u^{n+1/2}))$.

Remark 4.2.2. We note that using lemmas (4.2.1)-(4.2.3), we could obtain identities as follows

$$\begin{aligned}&(u^{n+1/2}, \tfrac{1}{2}(\overline{u}^{n+1/2}D_x(\overline{\tfrac{1}{\sqrt{\rho}}}^{n+1/2}a_x u^{n+1/2}) + A_x(\overline{\tfrac{1}{\sqrt{\rho}}}^{n+1/2}d_x(\overline{u}^{n+1/2}u^{n+1/2})))\\ &+\tfrac{1}{2}(a_x(A_x\overline{v}^{n+1/2}D_y(A_x(\overline{\tfrac{1}{\sqrt{\rho}}}^{n+1/2})u^{n+1/2}))\\ &+A_x(\overline{\tfrac{1}{\sqrt{\rho}}}^{n+1/2})d_y(A_y u^{n+1/2}A_x(\overline{v}^{n+1/2})) = 0,\\ &(v^{n+1/2}, \tfrac{1}{2}(a_x(A_y\overline{u}^{n+1/2}D_x(A_y(\overline{\tfrac{1}{\sqrt{\rho}}}^{n+1/2})v^{n+1/2}))\\ &+A_y(\overline{\tfrac{1}{\sqrt{\rho}}}^{n+1/2})d_x(A_y\overline{u}^{n+1/2}A_x v^{n+1/2}))\\ &+\tfrac{1}{2}(\overline{v}^{n+1/2}D_y(\overline{\tfrac{1}{\sqrt{\rho}}}^{n+1/2}a_y v^{n+1/2}) + A_y(\overline{\tfrac{1}{\sqrt{\rho}}}^{n+1/2}d_y(\overline{v}^{n+1/2}v^{n+1/2})))) = 0.\end{aligned} \tag{4.2.35}$$

Proof: It follows from the definition of E_h^n that

$$\begin{aligned}
&\tfrac{E_h^{n+1}-E_h^n}{\Delta t} = [\tfrac{u^{n+1}+u^n}{2}, \tfrac{u^{n+1}-u^n}{\Delta t}]_{ew} + [\tfrac{v^{n+1}+v^n}{2}, \tfrac{v^{n+1}-v^n}{\Delta t}]_{ns} + 2(\tfrac{q_1^{n+1}+q_1^n}{2}, \tfrac{q_1^{n+1}-q_1^n}{\Delta t})_2 \\
&+\kappa_{\rho_1\rho_1}(\tfrac{\nabla\rho_1^{n+1}+\nabla\rho_1^n}{2}, \tfrac{\nabla\rho_1^{n+1}-\nabla\rho_1^n}{\Delta t})_h + \kappa_{\rho_2\rho_2}(\tfrac{\nabla\rho_2^{n+1}+\nabla\rho_2^n}{2}, \tfrac{\nabla\rho_2^{n+1}-\nabla\rho_2^n}{\Delta t})_h \\
&+\kappa_{\rho_1\rho_2}[(\tfrac{\nabla\rho_1^{n+1}+\nabla\rho_1^n}{2}, \tfrac{\nabla\rho_2^{n+1}-\nabla\rho_2^n}{\Delta t})_h + (\tfrac{\nabla\rho_2^{n+1}+\nabla\rho_2^n}{2}, \tfrac{\nabla\rho_1^{n+1}-\nabla\rho_1^n}{\Delta t})_h].
\end{aligned} \tag{4.2.36}$$

Taking the inner product of (4.2.30-3,4) with $u^{n+1/2}, v^{n+1/2}$ respectively and using identify (4.2.35), we obtain

$$\begin{aligned}
&[\tfrac{u^{n+1}+u^n}{2}, \tfrac{u^{n+1}-u^n}{\Delta t}]_{ew} + [\tfrac{v^{n+1}+v^n}{2}, \tfrac{v^{n+1}-v^n}{\Delta t}]_{ns} \\
&= -2(\tfrac{1}{Re_s}, \mathbf{D}_h^{n+1/2} : \mathbf{D}_h^{n+1/2})_2 - (\tfrac{1}{Re_v} tr(\mathbf{D}_h^{n+1/2}), tr(\mathbf{D}_h^{n+1/2}))_2 \\
&-[u^{n+1/2}, A_x(\overline{\rho_1}^{n+1/2}\overline{\tfrac{1}{\sqrt{\rho}}}^{n+1/2})D_x(\mu_1^{n+1/2}) + A_x(\overline{\rho_2}^{n+1/2}\overline{\tfrac{1}{\sqrt{\rho}}}^{n+1/2})D_x(\mu_2^{n+1/2})]_{ew} \\
&-[v^{n+1/2}, A_y(\overline{\rho_1}^{n+1/2}\overline{\tfrac{1}{\sqrt{\rho}}}^{n+1/2})D_y(\mu_1^{n+1/2}) + A_y(\overline{\rho_2}^{n+1/2}\overline{\tfrac{1}{\sqrt{\rho}}}^{n+1/2})D_y(\mu_2^{n+1/2})]_{ns},
\end{aligned} \tag{4.2.37}$$

Where we used lemmas (4.2.1) and (4.2.3). Taking the inner product of (4.2.30-5) with $2q_1^{n+1/2}$, and performing integration by parts, we obtain

$$\begin{aligned}
&2(\tfrac{q_1^{n+1}+q_1^n}{2}, \tfrac{q_1^{n+1}-q_1^n}{\Delta t})_2 = -M_1(\nabla(\mu_1^{n+1/2} - \mu_2^{n+1/2}), \nabla(\mu_1^{n+1/2} - \mu_2^{n+1/2}))_h \\
&+[A_x(\overline{\rho_1}^{n+1/2}\overline{\tfrac{1}{\sqrt{\rho}}}^{n+1/2})u^{n+1/2}, D_x(\mu_1^{n+1/2})]_{ew} \\
&+[A_y(\overline{\rho_1}^{n+1/2}\overline{\tfrac{1}{\sqrt{\rho}}}^{n+1/2})v^{n+1/2}, D_y(\mu_1^{n+1/2})]_{ns} \\
&+[A_x(\overline{\rho_2}^{n+1/2}\overline{\tfrac{1}{\sqrt{\rho}}}^{n+1/2})u^{n+1/2}, D_x(\mu_2^{n+1/2})]_{ew} \\
&+[A_y(\overline{\rho_2}^{n+1/2}\overline{\tfrac{1}{\sqrt{\rho}}}^{n+1/2})v^{n+1/2}, D_y(\mu_2^{n+1/2})]_{ns} \\
&-\kappa_{\rho_1\rho_1}(\tfrac{\nabla\rho_1^{n+1}+\nabla\rho_1^n}{2}, \tfrac{\nabla\rho_1^{n+1}-\nabla\rho_1^n}{\Delta t})_h - \kappa_{\rho_2\rho_2}(\tfrac{\nabla\rho_2^{n+1}+\nabla\rho_2^n}{2}, \tfrac{\nabla\rho_2^{n+1}-\nabla\rho_2^n}{\Delta t})_h \\
&-\kappa_{\rho_1\rho_2}[(\tfrac{\nabla\rho_1^{n+1}+\nabla\rho_1^n}{2}, \tfrac{\nabla\rho_2^{n+1}-\nabla\rho_2^n}{\Delta t})_h + (\tfrac{\nabla\rho_2^{n+1}+\nabla\rho_2^n}{2}, \tfrac{\nabla\rho_1^{n+1}-\nabla\rho_1^n}{\Delta t})_h],
\end{aligned} \tag{4.2.38}$$

where we used lemma (4.2.1). Combining (4.2.36), (4.2.37) and (4.2.38), we obtain

$$\begin{aligned}
&\tfrac{E_h^{n+1}-E_h^n}{\Delta t} = -2(\tfrac{1}{Re_s}, \mathbf{D}_h^{n+1/2} : \mathbf{D}_h^{n+1/2})_2 - (\tfrac{1}{Re_v} tr(\mathbf{D}_h^{n+1/2}), tr(\mathbf{D}_h^{n+1/2}))_2 \\
&-M_1(\nabla(\mu_1^{n+1/2} - \mu_2^{n+1/2}), \nabla(\mu_1^{n+1/2} - \mu_2^{n+1/2}))_2 \le 0,
\end{aligned} \tag{4.2.39}$$

provided $M_1 \ge 0$. Having established unconditional energy stability, we now turn to the solvability issue of the linear system of equations.

4.2.4 Unique Solvability of the Fully Discrete, Linear Numerical Scheme

The linear system resulting from scheme (4.2.30) can be written into

$$\mathcal{A} \cdot X = \mathcal{G}, \tag{4.2.40}$$

where $\mathcal{A}$ is the coefficient matrix of the system given in Appendix,
$X := (\mu_1, \mu_2, u, v, q_1, \rho_1, \rho_2)$ is the solution of the linear system and the right hand term $\mathcal{G} = (g_1, g_2, g_3, g_4, g_5, g_6, g_7)^T$ denotes all the terms at the nth time step.

Theorem 4.2.3. *Linear system (4.2.30) admits a unique solution.*

Proof: To prove the well-posedness of the system (4.2.30), we only need to prove the corresponding homogeneous system admits only the zero solution. We assume that there is a solution $X = (\mu_1, \mu_2, u, v, q_1, \rho_1, \rho_2)$ such that $\mathcal{A} \cdot X = 0$. Using (B.0.1), we have

$$\begin{aligned}
0 = (\mathcal{A} \cdot X, X)_2 &= M_1(\nabla(\mu_1 - \mu_2), \nabla(\mu_1 - \mu_2))_2 + \tfrac{2}{\Delta t}[u, u]_{ew} + \tfrac{2}{\Delta t}[v, v]_{ns} \\
&+ \tfrac{4}{\Delta t}(q_1, q_1)_2 + 2(\tfrac{1}{Re_s}, \mathbf{D}_h : \mathbf{D}_h)_2 + (\tfrac{1}{Re_v} tr(\mathbf{D}_h), tr(\mathbf{D}_h))_2 \\
&+ \tfrac{2}{\Delta t}[\kappa_{\rho_1\rho_1}(\nabla\rho_1, \nabla\rho_1)_h + \kappa_{\rho_2\rho_2}(\nabla\rho_2, \nabla\rho_2)_h] + \tfrac{4}{\Delta t}\kappa_{\rho_1\rho_2}(\nabla\rho_1, \nabla\rho_2)_h \\
&\geq C((\nabla\rho_1, \nabla\rho_2)_h + (\nabla\rho_2, \nabla\rho_2)_h + [u, u]_{ew} + [v, v]_{ns} + \|q_1\|_2^2),
\end{aligned} \tag{4.2.41}$$

where we used $\mathbf{K} > 0$, C is a positive constant and $\mathbf{D}_h$ is defined in (B.0.3). Thus, we obtain

$$D_x\rho_1 = D_y\rho_1 = 0, \quad D_x\rho_1 = D_y\rho_2 = 0, \quad u = v = 0, \quad q_1 = 0, \tag{4.2.42}$$

Based on linear system (B.0.1), we have

$$\mu_1 = \mu_2 = 0, \quad \rho_1 = \rho_2 = 0, \tag{4.2.43}$$

i.e. $X = \mathbf{0}$. Thus, linear system (4.2.30) admits an unique solution.

Remark 4.2.3. A second order in time, energy stable BDF scheme can be developed as well, which will not be presented here.

4.3 Accuracy Test

We conduct a mesh refinement test to verify the convergence rate of the numerical scheme by considering (4.0.1) with a double-well bulk free energy

$$h(\rho_1, \rho_2, T) = \rho_1^2(\rho_1 - 1)^2 + \rho_2^2(\rho_2 - 1)^2, \tag{4.3.1}$$

in a rectangular domain $\Omega = [0, 1] \times [0, 1]$. We use the following initial conditions

$$\begin{aligned} &\rho_1(x, y, t = 0) = 0.5 + 0.01cos(2\pi x), \\ &\rho_2(x, y, t = 0) = 0.5 - 0.01cos(2\pi x), \\ &\mathbf{v} = (0, 0). \end{aligned} \tag{4.3.2}$$

We denote the number of spatial grids as $N_x = N_y = N$, the time step as Δt. To test the convergence rate in time, we first fix $N = 256$ and vary the time step from 4×10^{-3} to 0.125×10^{-3} to calculate the l_2 norm of the difference between the numerical solutions obtained using consecutive step sizes at $T = 0.1$, i.e. $\|(\cdot)^{\Delta t}(T) - (\cdot)^{2\Delta t}(T)\|_2$. Then, we fix time step $\Delta t = 10^{-4}$, vary the spatial grid number from 8 to 256 and calculate the l_2 norm of the difference between the numerical solutions obtained using consecutive grid sizes at $T = 0.1$, i.e. $\|(\cdot)^h(T) - (\cdot)^{2h}(T)\|_2$. In both space and time, we calculate the convergence rate using $p = log_2\left(\frac{\|(\cdot)^{2h}(T) - (\cdot)^{4h}(T)\|_2}{\|(\cdot)^h(T) - (\cdot)^{2h}(T)\|_2}\right)$, where h is the mesh size in time or space. The refinement results are tabulated in Table 4.3 and Table 4.3, respectively. We observe that the proposed scheme is indeed second-order accurate in both time and space for all variables.

Table 4.1 Temporal refinement result for all variables. The model parameter values are chosen as $Re_s = 100, Re_v = 300, M_1 = 10^{-7}$, $\kappa_{\rho_1\rho_1} = \kappa_{\rho_2\rho_2} = 10^{-4}$, $\kappa_{\rho_1\rho_2} = \kappa_{\rho_2\rho_1} = 0$.

Δt	$\|{\rho_1}^h - {\rho_1}^{2h}\|$	order	$\|{\rho_2}^h - {\rho_2}^{2h}\|$	order	$\|\mathbf{u}^h - \mathbf{u}^{2h}\|$	order
0.004						
0.002	$0.5237{\cdot}10^{-8}$		$0.5240{\cdot}10^{-8}$		$0.1498{\cdot}10^{-7}$	
0.001	$0.1348{\cdot}10^{-8}$	1.96	$0.1349{\cdot}10^{-8}$	1.96	$0.3806{\cdot}10^{-8}$	1.98
0.0005	$0.3425{\cdot}10^{-9}$	1.98	$0.3428{\cdot}10^{-9}$	1.98	$0.9594{\cdot}10^{-9}$	1.99
0.00025	$0.8644{\cdot}10^{-10}$	1.99	$0.8651{\cdot}10^{-10}$	1.99	$0.2435{\cdot}10^{-9}$	1.98
0.000125	$0.2129{\cdot}10^{-10}$	2.02	$0.2130{\cdot}10^{-10}$	2.02	$0.5779{\cdot}10^{-10}$	2.08

Table 4.2 Spatial refinement result for all variables. The model parameter values are chosen as $Re_s = 1, Re_v = 3, M_1 = 10^{-3}$, $\kappa_{\rho_1\rho_1} = \kappa_{\rho_2\rho_2} = 10^{-4}$, $\kappa_{\rho_1\rho_2} = \kappa_{\rho_2\rho_1} = 0$.

N	$\|{\rho_1}^h - {\rho_1}^{2h}\|$	order	$\|{\rho_2}^h - {\rho_2}^{2h}\|$	order	$\|\mathbf{u}^h - \mathbf{u}^{2h}\|$	order
8						
16	$0.2281{\cdot}10^{-5}$		$0.2282{\cdot}10^{-5}$		$0.2676{\cdot}10^{-7}$	
32	$0.3417{\cdot}10^{-6}$	1.74	$0.3421{\cdot}10^{-6}$	1.74	$0.3487{\cdot}10^{-8}$	1.85
64	$0.4452{\cdot}10^{-7}$	1.94	$0.4457{\cdot}10^{-7}$	1.93	$0.4607{\cdot}10^{-9}$	1.88
128	$0.5623{\cdots}10^{-8}$	1.98	$0.5631{\cdot}10^{-8}$	1.99	$0.5898{\cdot}10^{-10}$	1.95
256	$0.7050{\cdot}10^{-9}$	2.00	$0.7059{\cdot}10^{-9}$	2.00	$0.7444{\cdot}10^{-11}$	1.98

Chapter 5

Phase separation in binary compressible viscous fluids

5.1 Introduction

When the curvature of the bulk free energy is negative, the mixtures are thermodynamically unstable. Perturbation with a range of wave numbers will lead to the phase separation of the mixtures into distinct phases with distinctly different chemical compositions and physical properties. This mechanism is the well-known spinodal decomposition. In this chapter, we investigate the phase separation due to the spinodal decomposition in a binary compressible fluid flow.

5.2 Free Energy and Linear Stability Analysis

The choice of free energy function can have a significant effect on the physical behavior of the interface, and should be selected with care. The double-well function represents an approximation of the Van der Waals EOS near the critical point, and has historically been used for its simplicity of implementation when the phase field model is employed solely for interface tracking purposes.

To demonstrate stability and efficiency of the new scheme, we simulate phase separation dynamics using system (4.0.1) with the Flory-Huggins mixing energy

$$h(\rho_1, \rho_2, T) = \frac{k_B T}{m}\rho f(c) = \frac{k_B T}{m}\rho(\frac{1}{N_1}\frac{\rho_1}{\rho}ln\frac{\rho_1}{\rho} + \frac{1}{N_2}\frac{\rho_2}{\rho}ln\frac{\rho_2}{\rho} + \chi\frac{\rho_1\rho_2}{\rho^2}), \tag{5.2.1}$$

where $f(c)$ is a function of mass fraction of component 1, i.e. $c = \frac{\rho_1}{\rho}$. We choose the

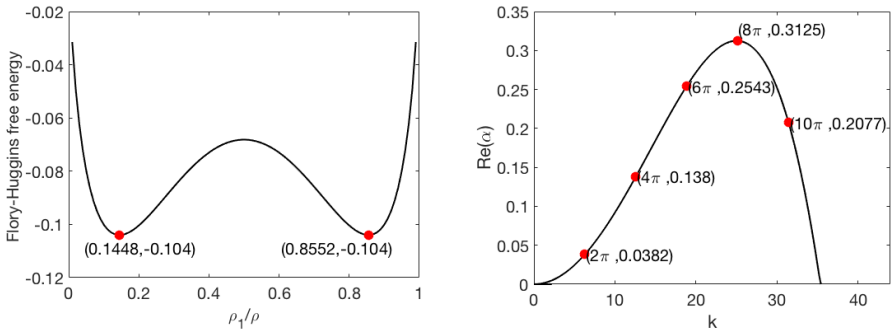

(a) Flory-Huggins mixing energy density function with respect to $\frac{\rho_1}{\rho}$

(b) Unstable mode

Figure 5.1 (a) Flory-Huggins mixing energy density function with respect to the mass density fraction $\frac{\rho_1}{\rho}$ at the chosen parameter values. The two minima are labeled by dots in the curve. (b) The unstable mode with parameter values: $N_1 = N_2 = 1, \chi = 2.5$, $M_1 = 10^{-3}, Re_s = 100, Re_v = 300$, $\kappa_{\rho_1\rho_1} = \kappa_{\rho_2\rho_2} = 0.0004$, $\kappa_{\rho_1\rho_2} = 0$.

characteristic scales so that $\frac{k_B T}{m} = 1$ in the simulation, N_1, N_2 are the polymerization indices and χ is the mixing coefficient, which are given by

$$N_1 = N_2 = 1, \qquad \chi = 2.5. \tag{5.2.2}$$

The plot of this energy density with the chosen parameter values as a function of $\frac{\rho_1}{\rho}$ is shown in 5.1-(a). The other dimensionless model parameters are chosen as follows

$$\begin{aligned} &M_1 = 10^{-3}, \quad Re_s = 100, \quad Re_v = 300, \\ &\kappa_{\rho_1\rho_1} = \kappa_{\rho_2\rho_2} = 4 \times 10^{-4}, \quad \kappa_{\rho_1\rho_2} = 0. \end{aligned} \tag{5.2.3}$$

In order to identify the spinodal decomposition that drives the phase separation in the binary polymer blend, we conduct a simple linear stability analysis on the hydrodynamic phase field model. We note that this compressible model admits a family of constant solutions:

$$\mathbf{v} = \mathbf{0}, \quad \rho_1 = \rho_1^0, \quad \rho_2 = \rho_2^0, \tag{5.2.4}$$

where ρ_1^0, ρ_2^0 are constants. We perturb the constant solutions with a normal mode as follows:

$$\mathbf{v} = \epsilon e^{\alpha t + i\mathbf{k}\cdot\mathbf{x}}\mathbf{v}^c, \quad \rho_1 = \rho_1^0 + \epsilon e^{\alpha t + i\mathbf{k}\cdot\mathbf{x}}{\rho_1}^c, \quad \rho_2 = \rho_2^0 + \epsilon e^{\alpha t + i\mathbf{k}\cdot\mathbf{x}}{\rho_2}^c, \tag{5.2.5}$$

where ϵ is a small parameter, representing the magnitude of the perturbation, and $\mathbf{v}^c, \rho_1^c, \rho_2^c$ are constants, α is the growth rate, and $\mathbf{k}$ is the wave number of the perturbation. Without loss of generality, we limit our study to 1 dimensional perturbation in $\mathbf{k}$ in the (x, y) plane. Substituting these perturbations into the equations in (4.0.1) and truncating the equations at order $O(\epsilon)$, we obtain the linearized equations. The dispersion equation of the linearized equation system of the compressible model [72] is given by an algebraic equation of α:

$$\begin{aligned}
&(\eta^0 k^2 + \alpha\rho^0)\{\alpha^3\rho_0 + \alpha^2 k^2[\eta + \rho^0 M_1(h_{\rho_1\rho_1} + \kappa_{\rho_1\rho_1}k^2) + \rho^0 M_1(h_{\rho_2\rho_2} + \kappa_{\rho_2\rho_2}k^2)] \\
&-\alpha^2 k^2[2\rho^0 M_1(h_{\rho_1\rho_2} + \kappa_{\rho_1\rho_2}k^2)] + \alpha[\mathbf{p}^T\cdot\mathbf{C}\cdot\mathbf{p} + \mathbf{p}^T\cdot\mathbf{K}\cdot\mathbf{p}k^2]k^2 \\
&+\alpha\eta M_1[(h_{\rho_1\rho_1} + \kappa_{\rho_1\rho_1}k^2) + (h_{\rho_2\rho_2} + \kappa_{\rho_2\rho_2}k^2) - 2(h_{\rho_1\rho_2} + \kappa_{\rho_1\rho_2}k^2)]k^4 \\
&+k^4 M_1(\rho_1^0 + \rho_2^0)^2[(h_{\rho_1\rho_1} + \kappa_{\rho_1\rho_1}k^2)(h_{\rho_2\rho_2} + \kappa_{\rho_2\rho_2}k^2) - (h_{\rho_1\rho_2} + \kappa_{\rho_1\rho_2}k^2)^2]\} = 0,
\end{aligned} \tag{5.2.6}$$

where $\eta = 2\eta^0 + \overline{\eta}^0$, $\mathbf{p} = (\rho_1^0, \rho_2^0)^T$. In the following, we set $\rho_1^0 = \rho_2^0 = 0.5$. $\mathbf{K}$ is the coefficient matrix of the conformational entropy and $\mathbf{C}$ is the Hessian of bulk energy $h(\rho_1, \rho_2, T)$ with respect to ρ_1 and ρ_2,

$$\mathbf{K} = \begin{pmatrix} \kappa_{\rho_1\rho_1} & \kappa_{\rho_1\rho_2} \\ \kappa_{\rho_1\rho_2} & \kappa_{\rho_2\rho_2} \end{pmatrix}, \mathbf{C} = \begin{pmatrix} h_{\rho_1\rho_1} & h_{\rho_1\rho_2} \\ h_{\rho_1\rho_2} & h_{\rho_2\rho_2} \end{pmatrix}. \tag{5.2.7}$$

Obviously, $\alpha = -\frac{\eta^0}{\rho^0}k^2 < 0$ is a solution of the dispersion equation (5.2.6), which contributes a stable mode. To resolve the other modes, we use numerical calculations. Based on the model parameters listed above, we obtain only one unstable mode, shown in Figure 5.1-(b). This unstable mode is dominated by the mixing energy of the model, independent of hydrodynamics of the model. Next, we will numerically simulate phase separation phenomena due to the unstable perturbation on the constant steady state without and with hydrodynamics to show how hydrodynamics can affect the path of phase separation and its outcome.

5.3 Phase separation without hydrodynamics

Based on unstable mode shown in Figure (5.1-b), we add a 1D perturbation with wave number $k = 10\pi$ to the steady state and observe its ensuing nonlinear dynamics. Since the eigenvector corresponding to the unstable mode shown in Figure (5.1-b) is $(\rho_1^c, \rho_2^c) = (1, -1)$, we impose the initial conditions specifically as follows

$$\begin{aligned} \rho_1(x, y, t = 0) &= 0.5 + 0.005 \times cos(10\pi y), \\ \rho_2(x, y, t = 0) &= 0.5 - 0.005 \times cos(10\pi y). \end{aligned} \tag{5.3.1}$$

Since $\rho_1 + \rho_2 = 1$ in the thermodynamic model without hydrodynamics, we show the phase behavior of ρ_1 only. The time evolution of ρ_1 at a few selected times are depicted in Figure 5.1. Firstly, we observe that the growth rate of the numerical solutions ρ_1 near the equilibrium state is $\alpha = 0.2077$, which matches with the linear stability analysis result shown in Figure (5.1-b). In the long-time behavior, we observe that ρ_1 develops small-scale structures and then coarsens to large-scale structures eventually. In Figure 5.1, we show numerical solutions at several time slots and the corresponding total energy up to $t = 3000$. The system goes through two coarsening events which are captured by the phase morphology at different times shown as well as the total energy evolution in Figure 5.1. The outcome at the end of the computation is a five-band structure.

5.4 Phase separation with hydrodynamics

When hydrodynamics is coupled with the thermodynamical phase evolution, its role must show up somewhere. Here, we investigate how hydrodynamic impact on phase separation dynamics. Since the eigenvector corresponding to the unstable mode shown in Figure (5.1-b) is $(\rho_1^c, \rho_2^c) = (1, -1, 0)$, we adopt the same initial conditions

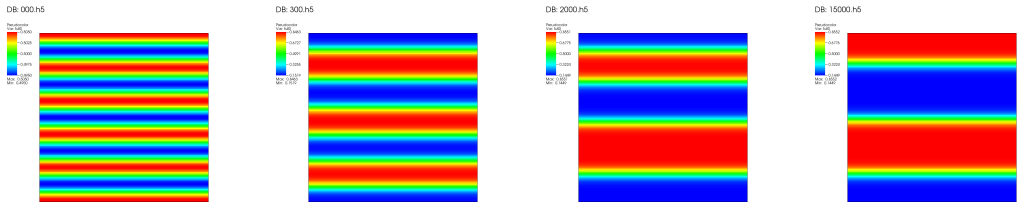

(a) ρ_1 at t = 0 (b) ρ_1 at t = 300 (c) ρ_1 at t = 2000 (d) ρ_1 at t = 15000

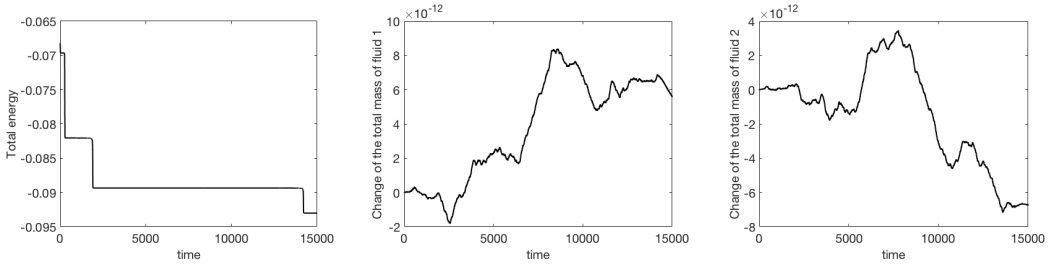

(e) Total Energy (f) Difference of total mass of the component 1 with its initial total mass (g) Difference of total mass of the component 2 with its initial total mass

Figure 5.1 (a-d) Snapshots of ρ_1 at different times as solutions of system (4.0.1) with the Flory-Huggins mixing energy (5.2.1) without hydrodynamics. (e) The total free energy of system (4.0.1). Two major coarsening events bring the phase of the binary system into the final state shown in (d). ρ_2 is given by $1 - \rho_1$. The total mass of both phases are conserved as shown in (f-g).

for ρ_1 and ρ_2 as before and a zero velocity condition:

$$\begin{aligned} \rho_1(x, y, 0) &= 0.5 + 0.005 \times cos(10\pi y), \\ \rho_2(x, y, 0) &= 0.5 - 0.005 \times cos(10\pi y), \\ \mathbf{v}(x, y, 0) &= (0, 0). \end{aligned} \tag{5.4.1}$$

When hydrodynamics is considered, the local total mass density ρ and the bulk area of the ρ_1 and ρ_2 are no longer spatially homogeneous anymore which are shown in Figure 5.1 and 5.2. However, phase separation goes on as shown in Figure 5.3. In Figure 5.1, we observe that the total energy of the system is dissipative and the total mass of component 1 and 2 are conserved in the domain globally. The velocity field in the domain is plotted at the selected times. Some vorticities form and disperse eventually as the phase morphology approaches a steady state. The induced nontrivial velocity

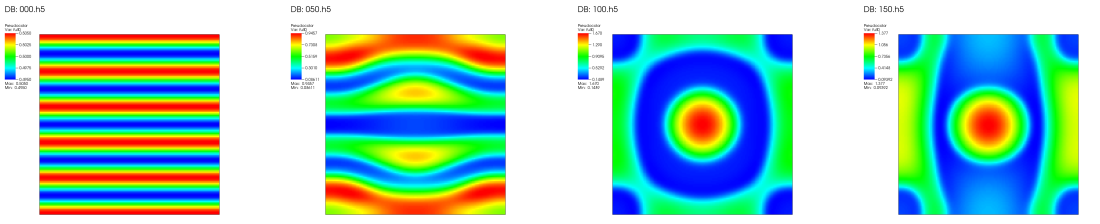

(a) ρ_1 at t = 0 (b) ρ_1 at t = 50 (c) ρ_1 at t = 100 (d) ρ_1 at t = 150

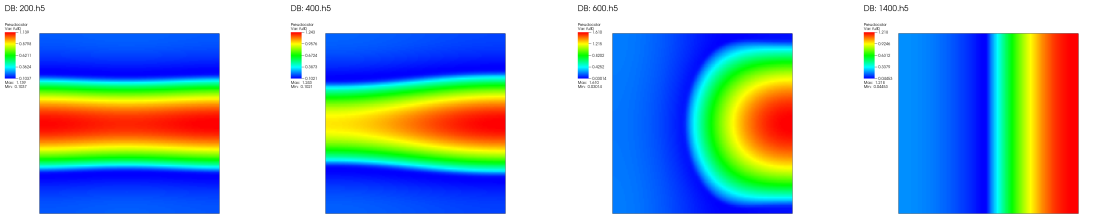

(e) ρ_1 at t = 200 (f) ρ_1 at t = 400 (g) ρ_1 at t = 600 (h) ρ_1 at t = 1400

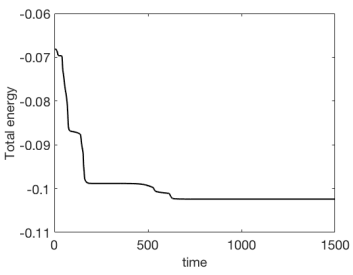

(i) Total Energy

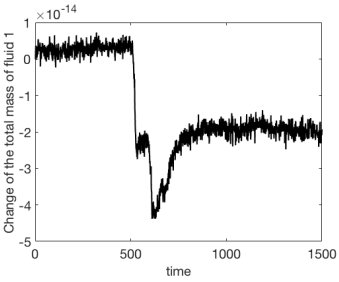

(j) Difference of total mass of the component 1 with its initial total mass

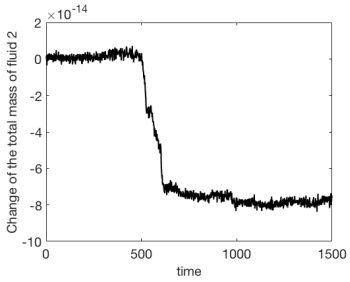

(k) Difference of total mass of the component 2 with its initial total mass

Figure 5.1 (a-h) Snapshots of ρ_1 at different times as a solution of system (4.0.1) with the Flory-Huggins mixing energy (5.2.1) and hydrodynamic interaction. (i) Total energy of the system (4.0.1) with the Flory-Huggins bulk free energy (5.2.1); (j, k) Difference of the total mass of component 1 and 2 compared with the initial mass, indicating mass conservation of both phases in the simulation.

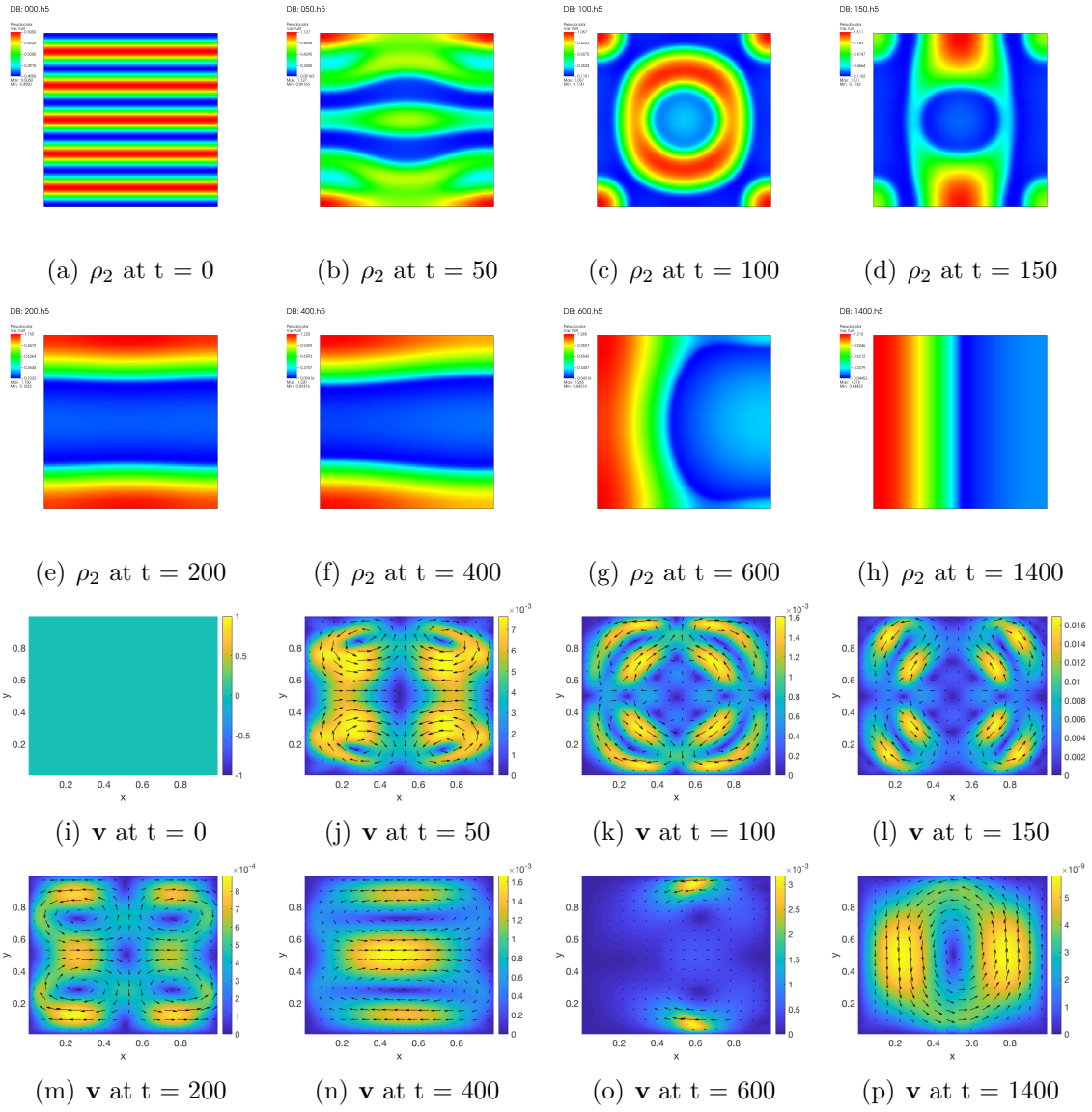

(a) ρ_2 at t = 0 (b) ρ_2 at t = 50 (c) ρ_2 at t = 100 (d) ρ_2 at t = 150

(e) ρ_2 at t = 200 (f) ρ_2 at t = 400 (g) ρ_2 at t = 600 (h) ρ_2 at t = 1400

(i) $\mathbf{v}$ at t = 0 (j) $\mathbf{v}$ at t = 50 (k) $\mathbf{v}$ at t = 100 (l) $\mathbf{v}$ at t = 150

(m) $\mathbf{v}$ at t = 200 (n) $\mathbf{v}$ at t = 400 (o) $\mathbf{v}$ at t = 600 (p) $\mathbf{v}$ at t = 1400

Figure 5.2 (a-h) Snapshots of ρ_2 at different times as a solution of system (4.0.1) with the Flory-Huggins mixing energy given in (5.2.1) and hydrodynamic interaction. (i-p) Snapshots for velocity field $\mathbf{v} = (v_1, v_2)$ at different times. Weak flows are present due to hydrodynamic effect during the phase evolution. The nontrivial velocity leads to different phase morphology in the end compared to the case without hydrodynamic interaction at the end of our simulation.

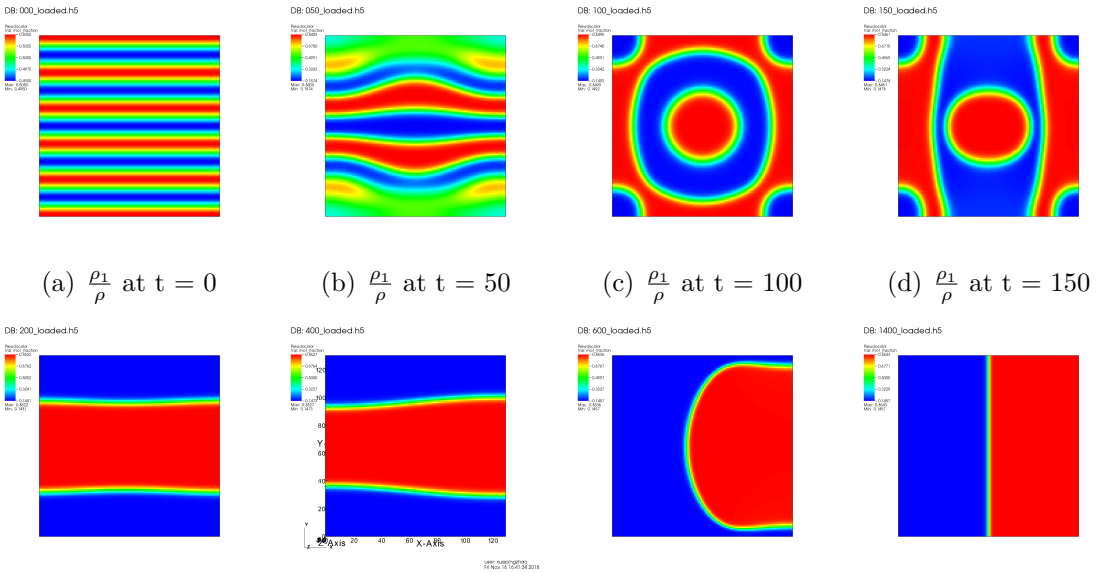

(a) $\frac{\rho_1}{\rho}$ at t = 0 (b) $\frac{\rho_1}{\rho}$ at t = 50 (c) $\frac{\rho_1}{\rho}$ at t = 100 (d) $\frac{\rho_1}{\rho}$ at t = 150

(e) $\frac{\rho_1}{\rho}$ at t = 200 (f) $\frac{\rho_1}{\rho}$ at t = 400 (g) $\frac{\rho_1}{\rho}$ at t = 600 (h) $\frac{\rho_1}{\rho}$ at t = 1400

(i) $\frac{\rho_2}{\rho}$ at t = 0 (j) $\frac{\rho_2}{\rho}$ at t = 50 (k) $\frac{\rho_2}{\rho}$ at t = 100 (l) $\frac{\rho_2}{\rho}$ at t = 150

(m) $\frac{\rho_2}{\rho}$ at t = 200 (n) $\frac{\rho_2}{\rho}$ at t = 400 (o) $\frac{\rho_2}{\rho}$ at t = 600 (p) $\frac{\rho_2}{\rho}$ at t = 1400

Figure 5.3 (a-h) Snapshots of $\frac{\rho_1}{\rho}$ at different times as a solution of system (4.0.1) with the Flory-Huggins mixing energy given in (5.2.1) and hydrodynamic interaction. (i-p) Snapshots of $\frac{\rho_1}{\rho}$ at different times.

field promotes the transport of materials and mixing across the domain leading to a two-band structure phase morphology eventually, which is a global energy stable state. In contrast, the final phase morphology developed in the phase separation without hydrodynamics may have only reached a local energy stable state, which can be explained by the comparison of the total energy evolutions shown in Figure (5.1-e) and Figure (5.1-i), respectively. This tells us that hydrodynamics indeed changes local densities, the path of phase evolution and even the final energy steady states of fluid mixtures. This is alarming, indicating that hydrodynamic effects are instrumental in determining the correct spatial phase diagram for the binary fluid mixture. The total energy in the solution with hydrodynamics is smaller than that without it. So, hydrodynamics in a binary compressible fluid flow promotes fluid mixing and thereby speeds up phase separation.

Chapter 6

Dynamics of gas-liquid Mixtures

6.1 Introduction

The compressible fluid model has many applications in the petroleum industry, where mixtures of non-hydrocarbons and hydrocarbons are abundant, such as in petroleum reservoirs or natural gas pipelines. Understanding their thermodynamic and hydrodynamic properties can help one to improve petroleum quality and yield significantly.

In the past, several equations of state had been developed to describe the relation among state variables (e.g. the volume, pressure and temperature) under a given set of physical conditions for compressible fluids. The Peng-Robinson equation of state (PR-EOS) [48] is one of the popular ones, which has been successfully applied to thermodynamic and volumetric calculations in both industries and academics. Specifically, PR-EOS provides a reasonable accuracy near the critical point, which makes it a good choice for gas-condensate systems in the petroleum industry. For this reason, we adopt it in a hydrocarbon mixture of methane and n-decane to show the performance of our model and numerical scheme in simulating hydrodynamics of the hydrocarbon mixtures. Many properties of the mixture can be studied by our mathematical model, such as mass adsorption of one component in the mixture on the interface between two phases near the equilibrium state, surface tension and even verification of mixing rules in the mixture. In this example, we will focus on hydrodynamics of a hydrocarbon mixture with an unstable gas-liquid interface and

study the mass adsorption phenomena at the interface from the point of view of the free energy at the equilibrium states.

6.2 Gas-Liquid Interface Dynamics of the Hydrocarbon Mixtures

In this example, we use molar densities n_i as the fundamental variables in the model $i = 1, 2$, hydrodynamic phase field models of binary compressible mixtures can be rewritten as follows

$$\begin{cases} m_1(\frac{\partial n_1}{\partial t} + \nabla \cdot (n_1 \mathbf{v})) = \nabla \cdot M_1 \cdot \nabla(\frac{1}{m_1}\mu_{n1} - \frac{1}{m_2}\mu_{n2}), \\ m_2(\frac{\partial n_2}{\partial t} + \nabla \cdot (n_2 \mathbf{v})) = -\nabla \cdot M_1 \cdot \nabla(\frac{1}{m_1}\mu_{n1} - \frac{1}{m_2}\mu_{n2}), \\ \frac{\partial(\rho \mathbf{v})}{\partial t} + \nabla \cdot (\rho \mathbf{v}\mathbf{v}) = 2\nabla \cdot (\eta \mathbf{D}) + \nabla(\overline{\eta}\nabla \cdot \mathbf{v}) - n_1 \nabla \mu_{n1} - n_2 \nabla \mu_{n2}, \end{cases} \tag{6.2.1}$$

where $n_i = \frac{\rho_i}{m_i}$, m_i is the molar mass of the ith component and $\mu_{ni} = \frac{\delta f}{\delta n_i} = \frac{\delta f}{\delta \rho_i} m_i$, i = 1, 2. Correspondingly, The shear and volumetric viscosities are given respectively by $\eta = \sum_{i=1}^{2} \frac{n_i m_i}{n_1 m_1 + n_2 m_2} \eta_i$ and $\overline{\eta} = \sum_{i=1}^{2} \frac{n_i m_i}{n_1 m_1 + n_2 m_2} \overline{\eta_i}$.

The free energy density function derived from PR-EOS reads

$$f = f_b + h(\mathbf{n}, T), \tag{6.2.2}$$

where $f_b = \frac{1}{2} \sum_{i,j=1}^{N} c_{i,j} \nabla n_i \cdot \nabla n_j$ is the conformational energy. The bulk free energy density function $h(\mathbf{n}, T)$ is given by [33],

$$h(n_1, n_2, T) = f^{ideal} + f^{repulsion} + f^{attraction}, \tag{6.2.3}$$

where

$$\begin{aligned} f^{ideal} &= RT \sum_{i=1}^{2} n_i (ln(n_i) - 1), \\ f^{repulsion} &= -nRTln(1 - bn), \\ f^{attraction} &= \frac{a(T)n}{2\sqrt{2}b} ln\Big(\frac{1 + (1 - \sqrt{2})bn}{1 + (1 + \sqrt{2})bn}\Big). \end{aligned} \tag{6.2.4}$$

Here $n = \sum_{i=1}^{2} n_i$ is the total molar density. The corresponding chemical potential of the ith component is given by

$$\begin{aligned}
&\mu_{ni} = \tfrac{\partial h}{\partial n_i} - \nabla \cdot \tfrac{\partial h}{\partial \nabla n_i} = RT\Big(ln(n_i) + \tfrac{b_i n}{1-bn} - ln(1-bn)\Big) \\
&+\tfrac{ab_i n}{b((\sqrt{2}-1)bn-1)(1+(1+\sqrt{2})bn)} - \kappa_{n_i n_i}\Delta n_i - \kappa_{n_i n_j}\Delta n_j \\
&+\tfrac{1}{2\sqrt{2}}\big(\tfrac{2\sum_{j=1}^{2} n_j (a_i a_j)^{1/2}(1-k_{ij})}{bn} - \tfrac{ab_i}{b^2}\big) ln\big(\tfrac{1+(1-\sqrt{2})bn}{1+(1+\sqrt{2})bn}\big), \qquad j \neq i,
\end{aligned} \tag{6.2.5}$$

where $b(n_1, n_2)$ is the volume parameter and $a(n_1, n_2, T)$ is the interaction parameter.

Remark 6.2.1. Since f^{ideal} changes rapidly near the origin which may introduce singularity in numerical simulations, we regularize this term near the origin as follows

$$f^{ideal} = \begin{cases} RTn_i(ln(\epsilon) - 1) + RT(\tfrac{1}{2\epsilon}n_i^2 - \tfrac{\epsilon}{2}), & if \quad n_i < \epsilon, \\ RTn_i(ln(n_i) - 1), \text{otherwise}, \end{cases} \tag{6.2.6}$$

where $\epsilon > 0$. Corresponding to the modification, the chemical potential is changed to

$$\mu^{ideal} = \begin{cases} RT(ln(\epsilon) - 1) + RT(\tfrac{1}{\epsilon}n_i), & if \quad n_i < \epsilon, \\ RTln(n_i), \text{otherwise}. \end{cases} \tag{6.2.7}$$

Using characteristic molar density n_0 $(mol \cdot m^{-d})$, characteristic mass density $\rho_0 = n_0 m_2 (kg \cdot m^{-d}, d = 3)$ and characteristic temperature T_0 (Kelvin), we nondimensionalize the physical variables and parameters as follows

$$\begin{aligned}
&\tilde{t} = \tfrac{t}{t_0}, \quad \tilde{x} = \tfrac{x}{l_0}, \quad \tilde{\rho} = \tfrac{\rho}{\rho_0}, \quad \tilde{n} = \tfrac{n}{n_0}, \quad \tilde{T} = \tfrac{T}{T_0}, \quad \tfrac{1}{Re_s} = \tilde{\eta} = \tfrac{t_0}{\rho_0 l_0^2}\eta, \quad \tilde{m_1} = \tfrac{m_1 n_0}{\rho_0}, \\
&\tilde{m_2} = \tfrac{m_2 n_0}{\rho_0}, \quad \tfrac{1}{Re_v} = \tilde{\overline{\eta}} = \tfrac{t_0}{\rho_0 l_0^2}\overline{\eta}, \quad \tilde{\mu}_{ni} = \tfrac{n_0 t_0^2}{\rho_0 l_0^2}\mu_{ni}, \quad i = 1, 2, \quad \tilde{M}_1 = \tfrac{M_1}{t_0 \rho_0}, \\
&\tilde{\kappa_{n_i n_j}} = \kappa_{n_i n_j}\tfrac{n_0^2 t_0^2}{\rho_0 l_0^4}, \quad i, j = 1, 2.
\end{aligned} \tag{6.2.8}$$

Dropping ˜s for simplicity, we rewrite the dimensionless governing equations as follows

$$\begin{cases} m_1(\tfrac{\partial n_1}{\partial t} + \nabla \cdot (n_1 \mathbf{v})) = \nabla \cdot M_1 \cdot \nabla(\tfrac{1}{m_1}\mu_{n1} - \mu_{n2}), \\ (\tfrac{\partial n_2}{\partial t} + \nabla \cdot (n_2 \mathbf{v})) = -\nabla \cdot M_1 \cdot \nabla(\tfrac{1}{m_1}\mu_{n1} - \mu_{n2}), \\ \tfrac{\partial(\rho \mathbf{v})}{\partial t} + \nabla \cdot (\rho \mathbf{v}\mathbf{v}) = 2\nabla \cdot (\eta \mathbf{D}) + \nabla(\overline{\eta}\nabla \cdot \mathbf{v}) - n_1 \nabla \mu_{n1} - n_2 \nabla \mu_{n2}. \end{cases} \tag{6.2.9}$$

Table 6.1 Dimensional critical parameters

Symbol	$T_c(K)$	$P_c(MPa)$	w	m (kg $\cdot mol^{-1}$)
n-decane ($C_{10}H_{22}$)	617.7	2.103	0.4884	0.14228
methane (CH_4)	190.564	4.5992	0.01142	0.0160428

where we set $\tilde{m_2} = \frac{m_2 n_0}{\rho_0} = 1$, i.e. m_1 is the ratio of the specific masses, a dimensionless model parameter. The dimensionless chemical potentials are given by

$$\mu_{n1} = \frac{\partial h}{\partial n_1} - \kappa_{n_1 n_1}\Delta n_1 - \kappa_{n_1 n_2}\Delta n_2, \tag{6.2.10}$$

$$\mu_{n2} = \frac{\partial h}{\partial n_2} - \kappa_{n_1 n_2}\Delta n_1 - \kappa_{n_2 n_2}\Delta n_2. \tag{6.2.11}$$

We consider a mixture of methane and n-decane in a square domain with the length of 80 nm on each side. We denote the molar density of n-decane as n_1 and that of methane as n_2, respectively. In Table 6.1, we list the dimensional parameters related to these two components. Other parameter values [13] are chosen as follows

$$\begin{aligned} &\eta_1 = \eta_2 = 1 \times 10^{-4} Pa \cdot s, \quad \overline{\eta}_1 = \overline{\eta}_2 = 0.33 \times 10^{-4} Pa \cdot s, \\ &M_1 = 1 \times 10^{-12} m^2 \cdot s^{-1}, \kappa_{n_1 n_1} = 1.1246 \times 10^{-18}, \\ &\kappa_{n_2 n_2} = 2.8649 \times 10^{-20}, \quad \kappa_{n_1 n_2} = 8.9748 \times 10^{-20}. \end{aligned} \tag{6.2.12}$$

The gas constant is $R = 8.3144598 J \cdot mol^{-1} \cdot K^{-1}$, the temperature $T = 330K$. The initial conditions are given by

$$n_i = \begin{cases} n_i^{liquid}, & (x^2 + y^2) \leq (r_1 + r_2 \times cos(n \times arctan(\frac{x}{y})))^2 \\ in \quad [-4 \times 10^{-8} m, 4 \times 10^{-8} m]^2, & \\ n_i^{gas}, & otherwise \quad in \quad [-4 \times 10^{-8} m, 4 \times 10^{-8} m]^2, \end{cases} \tag{6.2.13}$$

where $r_1 = 1$, $r_2 = 0.2$, $n = 8$ and

$$\begin{aligned} n_1^{liquid} &= 3814.6 mol \cdot m^{-3}, \qquad n_1^{gas} = 26.5 mol \cdot m^{-3}, \\ n_2^{liquid} &= 3513.2 mol \cdot m^{-3}, \qquad n_2^{gas} = 7133.9 mol \cdot m^{-3}. \end{aligned} \tag{6.2.14}$$

Table 6.2 Dimensionless critical parameters

Symbol	T_c	P_c	w	m
n-decane ($C_{10}H_{22}$)	2.2626	1.3495	0.4884	8.8688
methane (CH_4)	0.6980	2.9513	0.01142	1

If we take characteristic molar density $n_0 = 10^3 mol \cdot m^{-3}$, characteristic density $\rho_0 = n_0 m_2 = 16.0428 kg \cdot m^{-3}$, characteristic length $h = 2 \times 10^{-8} m$, characteristic time $t_0 = 6.4171 \times 10^{-11} s$, and characteristic temperature $T_0 = 273K$, we obtain dimensionless parameter values as follows

$$\begin{aligned} &Re_{1s} = Re_{2s} = 1, \quad Re_{1v} = Re_{2v} = 3, \quad M_1 = 9.7136 \times 10^{-4}, \\ &\kappa_{n_1 n_1} = 0.0018, \quad \kappa_{n_2 n_2} = 4.5961 \times 10^{-5}, \quad \kappa_{n_1 n_2} = 1.4398 \times 10^{-4}. \end{aligned} \tag{6.2.15}$$

Other dimensionless critical parameters of the methane and n-decane are given in table 6.2. Through the non-dimensionalization, the gas constant R results in a constant $R_0 = 1.4566$, the dimensionless temperature $T = 1.2088$. The corresponding dimensionless initial conditions become

$$n_i = \begin{cases} n_i^{liquid}, & (x^2 + y^2) \leq (r_1 + r_2 \times cos(n \times arctan(\frac{x}{y})))^2 \\ in \quad [-2, 2] \times [-2, 2], & \\ n_i^{gas}, & otherwise \quad in \quad [-2, 2] \times [-2, 2], \end{cases} \tag{6.2.16}$$

where $r_1 = 1$, $r_2 = 0.2$, $n = 8$ and

$$n_1^{liquid} = 3.8146, \quad n_1^{gas} = 0.0265, \quad n_2^{liquid} = 3.5132, \quad n_2^{gas} = 7.1339. \tag{6.2.17}$$

Shown in Figure 6.1, we perturb the initial condition with certain roughness on the interface, which is unstable due to the surface tension. As time elapses, the roughness vanishes, leading to a surface with the minimal surface tension on it, shown in Figure (6.3-b). The corresponding time evolution of velocities are depicted in Figure 6.2, which show that hydrodynamics indeed speed up the evolution of the system to the steady states.

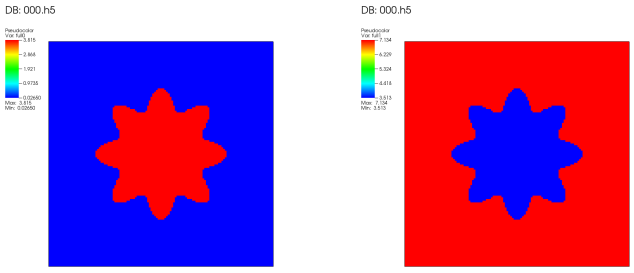

(a) Initial condition of n-decane ($C_{10}H_{22}$)

(b) Initial condition of methane (CH_4)

Figure 6.1 Initial conditions of two components in gas-liquid mixture

6.3 Mass absorption at the interface

Near equilibrium ($t = 6000$), we show the density profiles of the two fluid components at $y = 0$ in Figure (6.4-a) and observe mass absorption of methane at the interface. At the equilibrium of co-existing phases, two (or more) bulk phases have equal chemical potentials, i.e. the corresponding bulk free energies lie on the same tangent line (or surface). For the Peng-Robinson free energy, it is not straightforward to find the equilibrium states by observing the graph of the free energy function directly. Following the work reported in [42, 50], we subtract the tangent line (or surface) from the Helmoholtz free energy density function to make the equilibrium states as the minimum points, which are then easily observed,

$$h_m(\mathbf{n}, T) = h(\mathbf{n}, T) - \textstyle\sum_{i=1}^{2} \mu_i^0 n_i, \tag{6.3.1}$$

where $\mu_i^0, i = 1, 2$ represent the chemical potential of the ith component at the bulk equilibrium state. We show the modified free energy contour in Figure (6.4-b). The circled curve represents the energy path of density profiles at the equilibrium state. To avoid high free energy, n-decane and methane change from one equilibrium state (Gas) to another equilibrium state (Liquid) through the saddle point of the free energy surface. Thus, the methane has a higher density on the interface than in the bulk

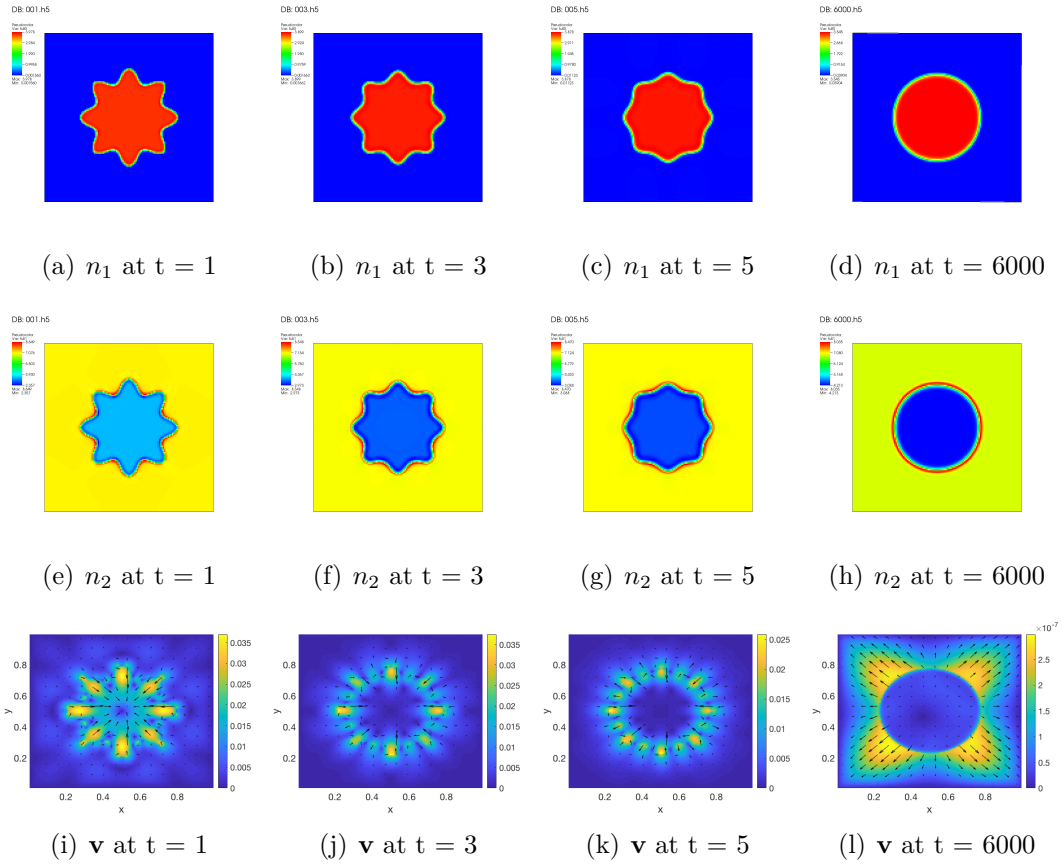

(a) n_1 at t = 1 (b) n_1 at t = 3 (c) n_1 at t = 5 (d) n_1 at t = 6000

(e) n_2 at t = 1 (f) n_2 at t = 3 (g) n_2 at t = 5 (h) n_2 at t = 6000

(i) $\mathbf{v}$ at t = 1 (j) $\mathbf{v}$ at t = 3 (k) $\mathbf{v}$ at t = 5 (l) $\mathbf{v}$ at t = 6000

Figure 6.2 (a-d) Snapshots of n_1 at t = 1, 3, 5, 6000. (e-h) Snapshots of n_2. (i-l) The corresponding velocity fields.

states, leading to the mass absorption phenomena at the interface.

The total energy and total mass difference with the initial condition for each component are shown in Figure 6.3, which verifies energy stability and mass conservation of our numerical scheme.

This numerical experiment not only demonstrates that our mathematical model can be applied to study thermodynamic and hydrodynamic properties of the fluid mixture in an application relevant to the petroleum industry, but also showcases that our numerical scheme can handle the Navier-Stokes-Cahn-Hilliard equation system with a highly nonlinear free energy (6.2.2).

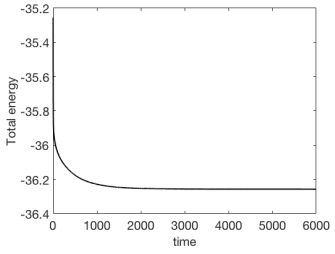

(a) Total Energy

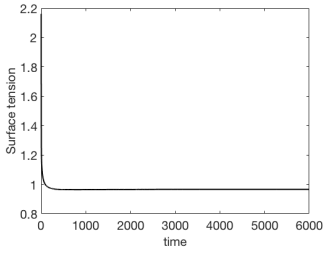

(b) Surface tension

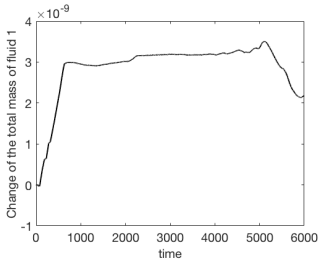

(c) The difference of total mass of the component 2 with its initial total mass

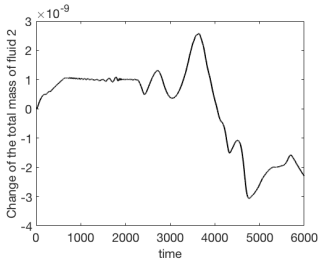

(d) The difference of total mass of the component 2 with its initial total mass

Figure 6.3 (a) Total energy of the system (6.2.9) with the Peng-Robinson bulk free energy (6.2.2); (b) Surface tension of the mixture; (c, d) Total mass of the component 1 and 2 on the rectangular domain $\Omega = [-2, 2] \times [-2, 2]$, solved in the system (6.2.9) with the Peng-Robinson bulk free energy (6.2.2). (e) Density profiles of n-decane and methane (y = 0) at the equilibrium state; (f) Free energy contour. Green points represent the densities of n-decane and methane at bulk area and red circles represent their densities on the interface at equilibrium state.

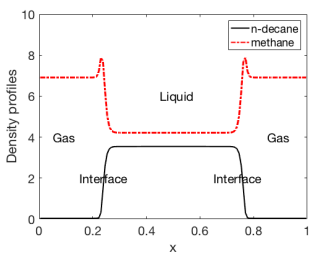

(a) Density profiles at the equilibrium state (t = 6000)

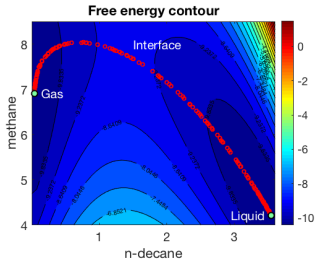

(b) Free energy contour at the equilibrium state (t = 6000)

Figure 6.4 (a) Density profiles of n-decane and methane (y = 0) at the equilibrium state; (b) Free energy contour. Green points represent the densities of n-decane and methane at bulk area and red circles represent their densities on the interface at equilibrium state.

Chapter 7

Conclusion

We have presented a systematic way to derive hydrodynamic phase field models for multi-component fluid mixtures of compressible fluids as well as incompressible fluids. The governing equations in the models are composed of the mass and momentum conservation law as well as the constitutive equations, which are derived using the generalized Onsager Principle to warrant an energy dissipation in time. By relaxing or enforcing local mass conservation law while keeping the total mass conserved, we obtain two classes of compressible models, one conserves the local mass while the other does not. Via a Lagrange multiplier approach, we reduce the compressible model with the local mass conservation law to a quasi-incompressible model when the constituent fluids are all incompressible. The quasi-incompressible model further reduces to the incompressible model. In addition, the derivation of the compressible models and its reduction to quasi-incompressible models have be extended to compressible fluid mixtures of N-component.

We then study linear stability of all the models. The properties of linear stability are studied and differences of the models in the linear regime are identified: there exist three types of growth/decay rates among the models. The first type is dominated by the viscous property of the fluid, known as the viscous mode. The second type is the thermodynamic mode, which is dominated by the mobility and Hessian of the bulk free energy density. The third type is the coupled mode among the phase variables and hydrodynamic variables. When more constraints are enforced to reduce the models from the compressible, to the quasi-incompressible and then to the

incompressible model, the number of coupled modes reduces accordingly, indicating that these constraints weaken the coupling of the equations in the model. This study not only develops a general framework for the derivation of compressible models and their reduction to quasi-incompressible models, but also identifies differences between compressible and incompressible models in near equilibrium dynamics. It provides an easy to use theoretical tool for studying hydrodynamics of multiphasic fluids.

In this thesis, we present a second order, fully-discrete, linear and unconditionally energy stable numerical scheme for the hydrodynamic phase field model of compressible fluid flow. Firstly, we reformulate the model by introducing a couple of intermediate variables, based on the Energy Quadratization approach. Using the reformulated model equations, we develop a second order, energy stable, semi-discrete numerical scheme in time. Then, we obtain a fully discrete numerical scheme applying the finite difference method on the staggered grid, which preserves a fully discrete energy dissipation law. In addition, the well-posedness of the linear system resulting from the linear numerical scheme is proved rigorously. Several numerical experiments are presented to verify the accuracy, stability and efficiency of our numerical scheme. The comparison between the simulations with and without hydrodynamics is used to demonstrate the mixing role played by hydrodynamics in phase separation phenomena in binary compressible fluid flows. The scheme can be readily extended to models N-component compressible fluid flows with $N > 2$.

Bibliography

[1] Helmut Abels. On a diffuse interface model for two-phase flows of viscous, incompressible fluids with matched densities. *Archive for Rational Mechanics and Analysis*, 194(2):463–506, Nov 2009.

[2] S. Aland, S. Egerer, J. Lowengrub, and A. Voigt. Diffuse interface models of locally inextensible vesicles in a viscous fluid. *Journal of Computational Physics*, 277:32–47, 2014.

[3] S. Aland, J. Lowengrub, and A. Voigt. Particles at fluid-fluid interfaces: a new Navier-Stokes-Cahn-Hilliard surface-phase-field model. *Physical Review E*, 86(4), 2012.

[4] Nicolas Auffray, Francesco dell'Isola, Victor Eremeyev, Angela Madeo, and Giuseppe Rosi. Analytical continuum mechanics *à* la hamilton-piola least action principle for second gradient continua and capillary fluids. *Mathematics and Mechanics of Solids*, 20(4):375–417, 2015.

[5] A. N. Beris and B. Edwards. *Thermodynamics of Flowing Systems*. Ocford Science Publications, New York, 1994.

[6] A. Bertozzi, S. Esedoglu, and A. Gillette. Inpainting of binary images using the cahn-hilliard equation. *IEEE Trans Image Process.*, 16(1):285–291, 2007.

[7] M. Borden, C. Verhoosej, M. Scott, T. Hughes, and C. Landis. A phase-field description of dynamic brittle fracture. *Computer Methods in Applied Mechanics and Engineering*, 217(220):77–95, 2012.

[8] B. Camley, Y. Zhao, Bo Li, H. Levine, and W. Rappel. Crawling and turning in a minimal reaction-diffusion cell motility model: coupling cell shape and biochemistry. *Physical Review E*, 95(012401), 2017.

[9] L. Q. Chen and W. Yang. Computer simulation of the dynamics of a quenched system with large number of non-conserved order parameters. *Phys. Rev. B*, 60:15752–15756, 1994.

[10] Wenbin Chen, Wenqiang Feng, Yuan Liu, Cheng Wang, and Steven M. Wise. A second order energy stable scheme for the cahn-hilliard-hele-shaw equations. *Discrete & Continuous Dynamical Systems - B*, 22:1, 2018.

[11] Y. Chen and J. Shen. Efficient adaptive energy stable schemes for the incompressible cahn-hilliard navier-stokes phase-field models. *Journal of Computational Physics*, 308:40–56, 2016.

[12] Kelong Cheng, Wenqiang Feng, Cheng Wang, and Steven M. Wise. An energy stable fourth order finite difference scheme for the cahn-hilliard equation. *Journal of Computational and Applied Mathematics*, 2018.

[13] Alvin S. Cullick and Melwyn L. Mathis. Densities and viscosities of mixtures of carbon dioxide and n-decane from 310 to 403 k and 7 to 30 mpa. *Journal of Chemical & Engineering Data*, 29(4):393–396, 1984.

[14] H. C. Öttinger. Beyond equilibrium thermodynamics. *Wiley, Hoboken*, 2005.

[15] H. C. Öttinger and M. Grmela. Dynamics and thermodynamics of complex fluids. II. illustrations of a general formalism. *Phys. Rev. E*, 56(6), 1997.

[16] Francesco dell'Isola, Angela Madeo, and Pierre Seppecher. Boundary conditions at fluid-permeable interfaces in porous media: A variational approach. *International Journal of Solids and Structures*, 46(17):3150 – 3164, 2009.

[17] Masao Doi. Onsager's variational principle in soft matter. *Journal of Physics: Condensed Matter*, 23:284118, 2011.

[18] Q. Du, C. Liu, R. Ryham, and X. Wang. A phase field formulation of the willmore problem. *Nonlinearity*, 18:1249–1267, 2005.

[19] C. M. Elliott and A. M. Stuart. The global dynamics of discrete semilinear parabolic equations. *SIAM Journal of Numerical Analysis*, 30:1622–1663, 1993.

[20] D. Eyre. Unconditionally gradient stable time marching the Cahn-Hilliard equation. *Computational and mathematical models of microstructural evolution (San Francisco, CA, 1998)*, 529:39–46, 1998.

[21] Nir Gavish, Gurgen Hayrapetyan, Keith Promislow, and Li Yang. Curvature driven flow of bilayer interfaces. *Physica D.: Nonlinear Phenomena*, 240:675–693, 2011.

[22] Sergey Gavrilyuk and Henri Gouin. A new form of governing equations of fluids arising from hamilton's principle. *International Journal of Engineering Science*, 37(12):1495 – 1520, 1999.

[23] Sergey Gavrilyuk, Henri Gouin, and Yurii Perepechko. Hyperbolic models of homogeneous two-fluid mixtures. *Meccanica*, 33(2):161–175, 1998.

[24] Yuezheng Gong, Jia Zhao, and Qi Wang. An energy stable algorithm for a quasi-incompressible hydrodynamic phase-field model of viscous fluid mixtures with variable densities and viscosities. *Computer Physics Communications*, 219:20 – 34, 2017.

[25] Yuezheng Gong, Jia Zhao, and Qi Wang. Second order fully discrete energy stable methods on staggered grids for hydrodynamic phase field models of binary viscous fluids. *SIAM Journal on Scientific Computing*, 40(2):B528–B553, 2018.

[26] Yuezheng Gong, Jia Zhao, Xiaogang Yang, and Qi Wang. Fully discrete second-order linear schemes for hydrodynamic phase field models of binary viscous fluid flows with variable densities. *SIAM Journal on Scientific Computing*, 40(1):B138–B167, 2018.

[27] Henri Gouin. Variational theory of mixtures in continuum mechanics. *European Journal of Mechanics - B/Fluids*, 9(5):469–491, 1990.

[28] Henri Gouin and Sergey Gavrilyuk. Hamilton's principle and rankine-hugoniot conditions for general motions of mixtures. *Meccanica*, 34(1):39–47, 1999.

[29] M. Grmela and H. C. Öttinger. Dynamics and thermodynamics of complex fluids. I. development of a general formalism. *Phys. Rev. E*, 56(6), 1997.

[30] Edouard Hannezo, Alice Coucke, and Jean-François Joanny. Interplay of migratory and division forces as a generic mechanism for stem cell patterns. *Phys. Rev. E*, 93:022405, Feb 2016.

[31] P. C. Hohenberg and B. I. Halperin. Theory of dynamic critical phenomena. *Reviews of Modern Physics*, 49(3):435–479, 1977.

[32] Maryna Kapustina, Denis Tsygankov, Jia Zhao, Timothy Wessler, Xiaofeng Yang, Alex Chen, Nathan Roach, Timothy C. Elston, Qi Wang, Ken Jacobson, and M. Gregory Forest. Modeling the excess cell surface stored in a complex morphology of bleb-like protrusions. *PLOS Computational Biology*, 12(3):1–25, 03 2016.

[33] Jisheng Kou and Shuyu Sun. Thermodynamically consistent modeling and simulation of multi-component two-phase flow model with partial miscibility. *Computer Methods in Applied Mechanics and Engineering*, 331:623 – 649, 2018.

[34] Jisheng Kou, Shuyu Sun, and Xiuhua Wang. Linearly decoupled energy-stable numerical methods for multi-component two-phase compressible flow. *arXiv preprint arXiv:1712.02222*, 2017.

[35] Jun Li and Qi Wang. A class of conservative phase field models for multiphase fluid flows. *Journal of Applied Mechanics*, 81(2):021004, 2014.

[36] Y. Li and J. Kim. Multiphase image segmentation using a phase-field model. *Computers and Mathematics with Applications*, 62:737–745, 2011.

[37] Hong Lin and Yuan-Yuan Duan. Surface tension measurements of propane (r-290) and isobutane (r-600a) from (253 to 333) k. *Journal of Chemical & Engineering Data*, 48(5):1360–1363, 2003.

[38] C. Liu and J. Shen. A phase field model for the mixture of two incompressible fluids and its approximation by a fourier-spectral method. *Physica D*, 179:211–228, 2003.

[39] J. Lober, F. Ziebert, and I. S. Aranson. Modeling crawling cell movement on soft engineered substrates. *Soft Matter*, 10:1365, 2014.

[40] J. Lowengrub, A. Ratz, and A. Voigt. Phase field modeling of the dynamics of multicomponent vesicles spinodal decomposition coarsening budding and fission. *Physical Review E*, 79(3), 2009.

[41] J. S. Lowengrub and L. Truskinovsky. Quasi incompressible Cahn-Hilliard fluids and topological transitions. *Proceedings of the Royal Society A*, 454:2617–2654, 1998.

[42] Xiaoqun Mu, Florian Frank, Faruk O. Alpak, and Walter G. Chapman. Stabilized density gradient theory algorithm for modeling interfacial properties of pure and mixed systems. *Fluid Phase Equilibria*, 435:118 – 130, 2017.

[43] S. Najem and M. Grant. Phase-field model for collective cell migration. *Physical Review E*, 93(052405), 2016.

[44] M. Nonomura. Study on multicellular systems using a phase field model. *PLoS One*, 7(4):0033501, 2012.

[45] Hossein Nourozieh, Bita Bayestehparvin, Mohammad Kariznovi, and Jalal Abedi. Equilibrium properties of (carbon dioxide + n-decane + n-octadecane) systems: Experiments and thermodynamic modeling. *Journal of Chemical & Engineering Data*, 58(5):1236–1243, 2013.

[46] L. Onsager. Reciprocal relations in irreversible processes I. *Physical Review*, 37:405–426, 1931.

[47] L. Onsager. Reciprocal relations in irreversible processes II. *Physical Review*, 38:2265–2279, 1931.

[48] Ding-Yu Peng and Donald B. Robinson. A new two-constant equation of state. *Ind. Eng. Chem. Fundamen.*, 15(1):59–64, 1976.

[49] Jonas Ranft, Markus Basan, Jens Elgeti, Jean-François Joanny, Jacques Prost, and Frank Jülicher. Fluidization of tissues by cell division and apoptosis. *Proceedings of the National Academy of Sciences*, 107(49):20863–20868, 2010.

[50] J. S. Rowlinson and B. Widom. *Molecular Theory of Capillarity*. Clarendon Press, Oxford, 1989.

[51] D. Shao, H. Levine, and W. Pappel. Coupling actin flow, adhesion, and morphology in a computational cell motility model. *PNAS*, 109(18):6855, May 2012.

[52] D. Shao, W. Pappel, and H. Levine. Computational model for cell morphodynamics. *Physical Review Letters*, 105, September 2010.

[53] J. Shen, C. Wang, X. Wang, and S. M. Wise. Second-order convex splitting schemes for gradient flows with ehrlichâÂĂÂŞschwoebel type energy: Application to thin film epitaxy. *SIAM Journal on Numerical Analysis*, 50(1):105–125, 2012.

[54] J. Shen and X. Yang. Numerical approximations of Allen-Cahn and Cahn-Hilliard equations. *Disc. Conti. Dyn. Sys.-A*, 28:1669–1691, 2010.

[55] Jie Shen, Jie Xu, and Jiang Yang. The scalar auxiliary variable (sav) approach for gradient flows. *Journal of Computational Physics*, 353:407 – 416, 2018.

[56] S. Torabi, J. Lowengrub, A. Voigt, and S. Wise. A new phase-field model for strongly anisotropic systems. *Proceedings of the Royal Society A*, 265:1337–1359, 2009.

[57] X. Wang and Q. Du. Modeling and simulations of multi-component lipid membranes and open membranes via diffuse interface approaches. *Journal of Mathematical Biology*, 56:347–371, 2008.

[58] S. Wise, J. Kim, and J. Lowengrub. Solving the regularized strongly anisotropic cahn-hilliard equation by an adaptive nonlinear multigrid method. *Journal of Computational Physics*, 226(1):414–446, 2007.

[59] S. Wise, J. Lowengrub, H. Frieboes, and B. Cristini. Three dimensional multispecies nonlinear tumor growth i: model and numerical method. *Journal of Theoretical Biology*, 253(3):524–543, 2008.

[60] T. Witkowski, R. Backofen, and A. Voigt. The influence of membrane bound proteins on phase separation and coarsening in cell membranes. *Physical Chemistry Chemical Physics*, 14(42):14403–14712, 2012.

[61] X. Yang. Linear, first and second order and unconditionally energy stable numerical schemes for the phase field model of homopolymer blends. *J. Comput. Phys.*, 327:294–316, 2016.

[62] X. Yang, J. Li, G. Forest, and Q. Wang. Hydrodynamic theories for flows of active liquid crystals and the generalized onsager principle. *Entropy*, 18(6):202, 2016.

[63] P. Yue, J. J. Feng, C. Liu, and J. Shen. A diffuse-interface method for simulating two-phase flows of complex fluids. *J. Fluid Mech*, 515:293–317, 2004.

[64] J. Zhao, P. Seeluangsawat, and Q. Wang. Modeling antimicrobial tolerance and treatment of heterogeneous biofilms. *Mathematical Biosciences*, 282:1–15, 2016.

[65] J. Zhao, Y. Shen, M. Happasalo, Z. J. Wang, and Q. Wang. A 3d numerical study of antimicrobial persistence in heterogeneous multi-species biofilms. *Journal of Theoretical Biology*, 392:83–98, 2016.

[66] J. Zhao and Q. Wang. Three-dimensional numerical simulations of biofilm dynamics with quorum sensing in a flow cell. *Bulletin of Mathematical Biology*, 79(4):884–919, 2017.

[67] J. Zhao, X. Yang, Y. Gong, and Q. Wang. A novel linear second order unconditionally energy-stable scheme for a hydrodynamic q tensor model for liquid crystals. *Computer Methods in Applied Mechanics and Engineering*, In Press, 2017.

[68] J. Zhao, X. Yang, Y. Gong, and Q. Wang. A novel linear second order unconditionally energy stable scheme for a hydrodynamic q-tensor model of liquid crystals. *in press, DOI: 10.1016/j.cma.2017.01.031, Comput. Meth. Appl. Mech. Engrg.*, 2017.

[69] Jia Zhao and Qi Wang. Modeling cytokinesis of eukaryotic cells driven by the actomyosin contractile ring. *International Journal for Numerical Methods in Biomedical Engineering*, 32(12), 2016.

[70] Jia Zhao, Xiaofeng Yang, Yuezheng Gong, Xueping Zhao, Xiaogang Yang, Jun Li, and Qi Wang. A general strategy for numerical approximations of non-equilibrium models-part i: Thermodynamical systems. *International Journal of Numerical Analysis & Modeling*, 15(6):884–918, 2018.

[71] Jia Zhao, Xiaofeng Yang, Jun Li, and Qi Wang. Energy stable numerical schemes for a hydrodynamic model of nematic liquid crystals. *SIAM. J. Sci. Comput.*, 38:A3264–A3290, 2016.

[72] Xueping Zhao, Tiezheng Qian, and Qi Wang. Thermodynamically consistent phase field models of multi-component compressible fluid flows. *Continuum Mechanics and Thermodynamics, in revision*, 2018.

[73] L. Zhornitskaya and A. Bertozzi. Positivity-preserving numerical schemes for lubrication-type equations. *SIAM Journal of Numerical Analysis*, 37(2):523–555, 2000.

[74] Jingzhi Zhu, Longqing Chen, Jie Shen, and Veena Tikare. Coarsening kinetics from a variable-mobility cahn-hilliard equation: application of a semi-impliciit fourier spectral method. *Physical Review E*, 60:3564, 1999.

[75] F. Ziebert and I. S. Aranson. Effects of adhesion dynamics and substrate compliance on the shape and motility of crawling cells. *PLOS One*, 8(5):e64511, 2013.

[76] F. Ziebert, S. Swaminathan, and I. S. Aranson. Model for self-polarization and motility of keratocyte fragments. *Journal of The Royal Society Interface*, 9:1084–1092, 2012.

[77] D. Zwicker, R. Seyboldt, C. Weber, A. Hyman, and F. Julicher. Growth and division of active droplets provides a model for protocells. *Nature Physics*, 13:408–413, 2017.

Appendix A

Dispersion equation of the compressible models

We list the dispersion equations in determinant forms of all hydrodynamic models derived in this study in 2 space dimension in the appendix.

A.1 Dispersion equation of the compressible model with the global mass conservation

The dispersion equation of the linearized equation system of the compressible model with the global mass conservation is given by a 4×4 determinant as follows

$$det\begin{pmatrix} \alpha + A_{11} & A_{12} & i\rho_1^0 k & 0 \\ A_{21} & \alpha + A_{22} & i\rho_2^0 k & 0 \\ B_1 & B_2 & \alpha\rho^0 + \frac{1}{Re}k^2 & 0 \\ 0 & 0 & 0 & \alpha\rho^0 + \frac{1}{Re_s}k^2 \end{pmatrix} = 0, \tag{A.1.1}$$

where $B_1 = ik(\rho_1^0 D_{11} + \rho_2^0 D_{12})$, $B_2 = ik(\rho_2^0 D_{22} + \rho_1^0 D_{12})$, $A_{11} = k^2(M_{11}D_{11} + M_{12}D_{12})$, $A_{12} = k^2(M_{11}D_{12} + M_{12}D_{22})$, $A_{21} = k^2(M_{12}D_{11} + M_{22}D_{12})$, $A_{22} = k^2(M_{12}D_{12} + M_{22}D_{22})$ and $D_{11} = h_{\rho_1\rho_1} + k^2\kappa_{\rho_1\rho_1}$, $D_{22} = h_{\rho_2\rho_2} + k^2\kappa_{\rho_2\rho_2}$, $D_{12} = h_{\rho_1\rho_2} + k^2\kappa_{\rho_1\rho_2}$, $\frac{1}{Re} = 2\frac{1}{Re_s} + \frac{1}{Re_v}$. The growth/decay rate in the hydrodynamic mode associated to the viscous stress is given explicitly by $\alpha = -\frac{1}{Re_s}\frac{1}{\rho^0}k^2$, which decouples from the rest of the modes. This decoupling is inherited by all its limiting models given below.

A.2 Dispersion equation of the compressible model with local mass conservation

The dispersion equation of the linearized equation system of this model is given by a 4×4 determinant as follows

$$det\begin{pmatrix} \alpha & 0 & i\rho^0 k & 0 \\ (k^2 M_{11})D_{12} & \alpha + (k^2 M_{11})D_{22} & i\rho_1^0 k & 0 \\ B_1 & B_2 & \alpha\rho^0 + \frac{1}{Re}k^2 & 0 \\ 0 & 0 & 0 & \alpha\rho^0 + \frac{1}{Re_s}k^2 \end{pmatrix} = 0, \quad \text{(A.2.1)}$$

where $B_1 = ik(\rho_1^0 D_{12} + \rho^0 D_{11})$, $B_2 = ik(\rho_1^0 D_{22} + \rho^0 D_{12})$, $D_{11} = \tilde{h}_{\rho\rho} + k^2\tilde{\kappa}_{\rho\rho}$, $D_{22} = \tilde{h}_{\rho_1\rho_1} + k^2\tilde{\kappa}_{\rho_1\rho_1}$, $D_{12} = \tilde{h}_{\rho\rho_1} + k^2\tilde{\kappa}_{\rho\rho_1}$, and $\frac{1}{Re} = 2\frac{1}{Re_s} + \frac{1}{Re_v}$.

A.3 Dispersion equation of the quasi-incompressible model

The resulting dispersion equation of the linearized system of this model is given by a 4×4 determinant as follows

$$det\begin{pmatrix} 0 & -\alpha(1 - \frac{\hat{\rho_1}}{\hat{\rho_2}}) & ik - ik\phi^0(1 - \frac{\hat{\rho_1}}{\hat{\rho_2}}) & 0 \\ B_1 & B_2 & ik\phi^0 & 0 \\ ik & ik\phi^0 D_\phi & \alpha\rho^0 + \frac{1}{Re}k^2 & 0 \\ 0 & 0 & 0 & \alpha\rho^0 + \frac{1}{Re_s}k^2 \end{pmatrix} = 0, \quad \text{(A.3.1)}$$

where $B_1 = \frac{1}{\hat{\rho_1}^2}M_{11}k^2(1 - \frac{\hat{\rho_1}}{\hat{\rho_2}})$, $B_2 = \alpha + \frac{1}{\hat{\rho_1}^2}M_{11}k^2 D_\phi$, $D_\phi = \hat{h}_{\phi\phi} + \hat{\kappa}_{\phi\phi}k^2$, $\hat{h}_{\phi\phi} = \frac{\partial^2 h}{\partial\phi^2}$ is the second order derivative of the bulk free energy density function h with respect to volume fraction ϕ at the constant solution, and $\hat{\kappa}_{\phi\phi}$ is the coefficient of the conformational entropy. If we multiply $(1 - \frac{\hat{\rho_1}}{\hat{\rho_2}})$ by the second row and add it to the

first row of the dispersion relation matrix, we obtain

$$det\begin{pmatrix} B_1 & (1-\frac{\hat{\rho_1}}{\hat{\rho_2}})\frac{1}{\hat{\rho_1}^2}M_{11}k^2D_\phi & ik & 0 \\ B_2 & \alpha+\frac{1}{\hat{\rho_1}^2}M_{11}k^2D_\phi & ik\phi^0 & 0 \\ ik & ik\phi^0D_\phi & \alpha\rho^0+\frac{1}{Re}k^2 & 0 \\ 0 & 0 & 0 & \alpha\rho^0+\frac{1}{Re_s}k^2 \end{pmatrix}=0, \qquad \text{(A.3.2)}$$

Where $B_1=\frac{1}{\hat{\rho_1}^2}M_{11}(1-\frac{\hat{\rho_1}}{\hat{\rho_2}})^2k^2$, and $B_2=\frac{1}{\hat{\rho_1}^2}M_{11}(1-\frac{\hat{\rho_1}}{\hat{\rho_2}})k^2$.

A.4 Dispersion equation of the incompressible model

The dispersion equation of the linearized system of the incompressible model is given by

$$det\begin{pmatrix} 0 & 0 & ik & 0 \\ 0 & \alpha+\frac{1}{\hat{\rho_1}^2}M_{11}k^2D_\phi & ik\phi^0 & 0 \\ ik & ik\phi^0D_\phi & \alpha\rho^0+\frac{1}{Re}k^2 & 0 \\ 0 & 0 & 0 & \alpha\rho^0+\frac{1}{Re_s}k^2 \end{pmatrix}=0. \qquad \text{(A.4.1)}$$

This can be obtain from that in the quasi-incompressible model by equating $\hat{\rho}_1=\hat{\rho}_2$ in (A.3.2).

Appendix B

Linear system resulting from the numerical scheme

We summarize the linear system resulting from the numerical scheme as follows:

$$
\begin{cases}
\Big\{2\frac{\rho_1}{\Delta t} + d_x(A_x(\overline{\rho}_1^{n+1/2}\overline{\frac{1}{\sqrt{\rho}}}^{n+1/2})u) + d_y(A_y(\overline{\rho}_1^{n+1/2}\overline{\frac{1}{\sqrt{\rho}}}^{n+1/2})v) = \\
M_1\Delta_h\mu_1 - M_1\Delta_h\mu_2 + g_1\Big\}|_{i,j}, i = 1,\cdots,N_x, j = 1,\cdots,N_y, \\
\\
\Big\{2\frac{\rho_2}{\Delta t} + d_x(A_x(\overline{\rho}_2^{n+1/2}\overline{\frac{1}{\sqrt{\rho}}}^{n+1/2})u) + d_y(A_y(\overline{\rho}_2^{n+1/2}\overline{\frac{1}{\sqrt{\rho}}}^{n+1/2})v) = \\
-M_1\Delta_h\mu_1 + M_1\Delta_h\mu_2 + g_2\Big\}|_{i,j}, i = 1,\cdots,N_x, j = 1,\cdots,N_y, \\
\\
\Big\{ -\frac{2}{\Delta t}\mu_1 = -4q_1\frac{1}{\Delta t}\overline{\frac{\partial q_1}{\partial\rho_1}}^{n+1/2} + \frac{2}{\Delta t}\kappa_{\rho_1\rho_1}\Delta_h\rho_1 + \frac{2}{\Delta t}\kappa_{\rho_1\rho_2}\Delta_h\rho_2 + g_6,\Big\}|_{i,j}, \\
i = 1,\cdots,N_x, j = 1,\cdots,N_y, \\
\\
\Big\{ -\frac{2}{\Delta t}\mu_2 = -4q_1\frac{1}{\Delta t}\overline{\frac{\partial q_1}{\partial\rho_2}}^{n+1/2} + \frac{2}{\Delta t}\kappa_{\rho_2\rho_2}\Delta_h\rho_2 + \frac{2}{\Delta t}\kappa_{\rho_1\rho_2}\Delta_h\rho_1 + g_7,\Big\}|_{i,j}, \\
i = 1,\cdots,N_x, j = 1,\cdots,N_y, \\
\\
\Big\{4\frac{q_1}{\Delta t} = 4\overline{\frac{\partial q_1}{\partial\rho_1}}^{n+1/2}\frac{\rho_1}{\Delta t} + 4\overline{\frac{\partial q_1}{\partial\rho_2}}^{n+1/2}\frac{\rho_2}{\Delta t} + g_5\Big\}|_{i,j}, \\
i = 1,\cdots,N_x, j = 1,\cdots,N_y,
\end{cases}
\tag{B.0.1}
$$

$$
\begin{cases}
\Big\{2\frac{u}{\Delta t}+\frac{1}{2}(\overline{u}^{n+1/2}D_x(\overline{\frac{1}{\sqrt{\rho}}}^{n+1/2}a_xu)+A_x(\overline{\frac{1}{\sqrt{\rho}}}^{n+1/2}d_x(\overline{u}^{n+1/2}u)))\\
+\frac{1}{2}(a_x(A_x\overline{v}^{n+1/2}D_y(A_x(\overline{\frac{1}{\sqrt{\rho}}}^{n+1/2})u))\\
+A_x(\overline{\frac{1}{\sqrt{\rho}}}^{n+1/2})d_y(A_yuA_x(\overline{v}^{n+1/2}))\\
=A_x(\overline{\frac{1}{\sqrt{\rho}}}^{n+1/2})(D_x(\frac{1}{Re_s}d_x(A_x(\overline{\frac{1}{\sqrt{\rho}}}^{n+1/2})u))\\
+d_y(A_x(A_y\frac{1}{Re_s})D_y(A_x(\overline{\frac{1}{\sqrt{\rho}}}^{n+1/2})u)))\\
+A_x(\overline{\frac{1}{\sqrt{\rho}}}^{n+1/2})D_x(\frac{1}{Re_s}d_x(A_x(\overline{\frac{1}{\sqrt{\rho}}}^{n+1/2})u))\\
+A_x(\overline{\frac{1}{\sqrt{\rho}}}^{n+1/2})d_y(A_x(A_y\frac{1}{Re_s})D_x(A_y(\overline{\frac{1}{\sqrt{\rho}}}^{n+1/2})v))\\
+A_x(\overline{\frac{1}{\sqrt{\rho}}}^{n+1/2})D_x(\frac{1}{Re_v}d_x(A_x(\overline{\frac{1}{\sqrt{\rho}}}^{n+1/2})u))\\
+A_x(\overline{\frac{1}{\sqrt{\rho}}}^{n+1/2})D_x(\frac{1}{Re_v}d_y(A_y(\overline{\frac{1}{\sqrt{\rho}}}^{n+1/2})v))-A_x(\overline{\rho_1}^{n+1/2}\overline{\frac{1}{\sqrt{\rho}}}^{n+1/2})D_x(\mu_1)\\
-A_x(\overline{\rho_2}^{n+1/2}\overline{\frac{1}{\sqrt{\rho}}}^{n+1/2})D_x(\mu_2)+g_3\Big\}|_{i+\frac{1}{2},j},\\
i=1,\cdots,N_x-1,j=1,\cdots,N_y,\\
\\
\Big\{2\frac{v}{\Delta t}+\frac{1}{2}(a_x(A_y\overline{u}^{n+1/2}D_x(A_y(\overline{\frac{1}{\sqrt{\rho}}}^{n+1/2})v))\\
+A_y(\overline{\frac{1}{\sqrt{\rho}}}^{n+1/2})d_x(A_y\overline{u}^{n+1/2}A_xv^{n+1/2}))\\
+\frac{1}{2}(\overline{v}^{n+1/2}D_y(\overline{\frac{1}{\sqrt{\rho}}}^{n+1/2}a_yv^{n+1/2})+A_y(\overline{\frac{1}{\sqrt{\rho}}}^{n+1/2}d_y(\overline{v}^{n+1/2}v^{n+1/2})))\\
=A_y(\overline{\frac{1}{\sqrt{\rho}}}^{n+1/2})(d_x(A_x(A_y\frac{1}{Re_s})D_x(A_y(\overline{\frac{1}{\sqrt{\rho}}}^{n+1/2})v))\\
+D_y(\frac{1}{Re_s}d_y(A_y(\overline{\frac{1}{\sqrt{\rho}}}^{n+1/2})v)))\\
+A_y(\overline{\frac{1}{\sqrt{\rho}}}^{n+1/2})d_x(A_x(A_y\frac{1}{Re_s})D_y(A_x(\overline{\frac{1}{\sqrt{\rho}}}^{n+1/2})u))\\
+A_y(\overline{\frac{1}{\sqrt{\rho}}}^{n+1/2})D_y(\frac{1}{Re_s}d_y(A_y(\overline{\frac{1}{\sqrt{\rho}}}^{n+1/2})v))\\
+A_y(\overline{\frac{1}{\sqrt{\rho}}}^{n+1/2})D_y(\frac{1}{Re_v}d_x(A_x(\overline{\frac{1}{\sqrt{\rho}}}^{n+1/2})u))\\
+A_y(\overline{\frac{1}{\sqrt{\rho}}}^{n+1/2})D_y(\frac{1}{Re_v}d_y(A_y(\overline{\frac{1}{\sqrt{\rho}}}^{n+1/2})v))-A_y(\overline{\rho_1}^{n+1/2}\overline{\frac{1}{\sqrt{\rho}}}^{n+1/2})D_y(\mu_1)\\
-A_y(\overline{\rho_2}^{n+1/2}\overline{\frac{1}{\sqrt{\rho}}}^{n+1/2})D_y(\mu_2)+g_4\Big\}|_{i,j+\frac{1}{2}},\\
i=1,\cdots,N_x,j=1,\cdots,N_y-1.
\end{cases}
\tag{B.0.2}
$$

where $\rho_i, \mu_i, i = 1, 2$ and q_1 satisfy discrete homogeneous Neumann boundary conditions (4.2.8), u, v the discrete homogeneous Dirichlet boundary conditions (4.2.9). We define $\mathbf{D}_h$ as

$$\begin{pmatrix} d_x(A_x(\overline{\frac{1}{\sqrt{\rho}}}^{n+1/2})u)) & S \\ S & d_y(A_y(\overline{\frac{1}{\sqrt{\rho}}}^{n+1/2})v)) \end{pmatrix} \tag{B.0.3}$$

Where $S = \frac{1}{2}(D_x(A_y(\overline{\frac{1}{\sqrt{\rho}}}^{n+1/2})v) + D_y(A_x(\overline{\frac{1}{\sqrt{\rho}}}^{n+1/2})u)))$.